RADIATION AND RESONANCES OF ELECTROACOUSTIC AND IONACOUSTIC WAVES IN COMPRESSIBLE PLASMAS

Dissertation for the Degree of Ph. D.

MICHIGAN STATE UNIVERSITY

KAM - CHI LI

1974

This is to certify that the

thesis entitled

RADIATION AND RESONANCES OF ELECTROACOUSTIC

AND IONACOUSTIC WAVES IN COMPRESSIBLE PLASMAS

presented by

Kam-Chi Li

has been accepted towards fulfillment
of the requirements for

Ph. D. degree in Electrical Engineering

Kun-Mu Chen
Major professor

Date November 4, 1974

O-7639

ABSTRACT

RADIATION AND RESONANCES

OF ELECTROACOUSTIC AND IONACOUSTIC

WAVES IN COMPRESSIBLE PLASMA

By

Kam-Chi Li

The present study consists mainly of two major parts. The first part is the study on the basic properties of the electroacoustic and ionacoustic waves excited by an electromagnetic source or field in an infinite, homogeneous, isotropic, compressible and lossy plasma. A two-fluid plasma model is employed and this leads to the formulation of the generalized electroacoustic and ionacoustic waves. The electron-ion compositions, as well as the propagation constants of the generalized electroacoustic and ionacoustic waves with various collision frequencies and under various electron and ion temperatures, are obtained.

The radiation patterns of the generalized electroacoustic and ionacoustic waves excited by simple antennas, such as Hertzian dipole, disk monopole, disk dipole and cylindrical antennas, are studied. They agree very closely

with the results of some recent experimental studies.

The second part is the investigation of the excitation of an electroacoustic wave in the plasma sheath surrounding a cylindrical antenna, the excitation of electroacoustic resonances in various plasma geometries, and the reflection behavior of electroacoustic waves on various surfaces. A new diagnostic scheme for measuring the plasma density directly has been developed. In this scheme, a cylindrical antenna immersed in a compressible plasma is driven by a frequency-sweeping electromagnetic wave, and its d.c. bias voltage is varied. Based on the information on the electroacoustic wave excited in the plasma sheath surrounding the antenna, the plasma density can be read directly on the oscilloscope.

The behaviors of electroacoustic resonances excited in the plasma sheaths at the boundaries of various plasma geometries which include cylindrical, rectangular and single-slope density profile plasma columns were studied. The technique of exciting electroacoustic resonances was then applied to study the reflection behavior of electroacoustic waves on dielectric and metallic surfaces.

RADIATION AND RESONANCES
OF ELECTROACOUSTIC AND IONACOUSTIC
WAVES IN COMPRESSIBLE PLASMAS

By

Kam-Chi Li

A DISSERTATION

Submitted to
Michigan State University
in partial fulfillment of the requirements
for the degree of

DOCTOR OF PHILOSOPHY

Department of Electrical Engineering and Systems Science

1974

To my parents

Mr. & Mrs. Chung-Wah Li

ACKNOWLEDGMENTS

The author is sincerely grateful to his major professor, Dr. K. M. Chen, for his guidance, wisdom and encouragement during the course of this research.

He also wishes to thank his committee members, Dr. B. Ho, Dr. J. Asmussen, Dr. J. S. Frame and Dr. D. P. Nyquist, for their time and interest in this work.

Finally, the author thanks his wife, Joyce Pui-Ping, for the typing of the manuscript, and especially for the love and understanding shown by her during the entire course of this study.

TABLE OF CONTENTS

Page

LIST OF FIGURES

Figure		Page

Figure | Page

Figure | Page

Figure		Page

Figure | Page

Figure		Page

Figure Page

LIST OF TABLES

Table		Page
C-12	k_1a versus f. (V_A = 1.05 x 10^3 m/sec, T_e = T_i ≈ 1200°K, Re[$k_1/(\omega/V_i)$] = 0.7071 for (T_e/T_i) = 1, a = 2.25 cm)	164
C-13	k_2a versus T_e. (f = 17.5 MHz, Re[$k_2/(\omega/V_e)$] = 0.2235 for ($\omega_e{}^2/\omega^2$) = 0.95 and (T_e/T_i) = 1 to 10^4, a = 7.2 cm)	165
C-14	k_2a versus f. (T_e = 2000°K, Re[$k_2/(\omega/V_e)$] = 0.2235 for ($\omega_e{}^2/\omega^2$) = 0.95 and (T_e/T_i) = 1 to 10^4, a = 7.2 cm)	165
C-15	k_1h versus T_e. (f = 30 kHz, Re[$k_1/(\omega/V_i)$] = 0.3016 for (T_e/T_i) = 10)	166
C-16	k_1h versus T_e/T_i. (f = 30 kHz, T_e = 6000°K)	167
C-17	k_1h versus f. (T_e = 6000°K, Re[$k_1/(\omega/V_i)$] = 0.3016 for (T_e/T_i) = 10, h = 5 cm)	166
C-18	k_2h and k_e/k_2 versus T_e. (f = 5.5 MHz, f_p = 4.5 MHz, (T_e/T_i) = 1 to 10^4, Re[$k_2/(\omega/V_e)$] ≈ 0.57 and k_e ≈ 0.066 for ($\omega_e{}^2/\omega^2$) = 0.67, h = 6 cm)	168
C-19	k_2h and k_e/k_2 versus f. (T_e = 6000°K, (T_e/T_i) = 1 to 10^4, f_p = 4.5 MHz, h = 8.5 cm)	169
C-20	k_2h and k_e/k_2 versus f. (T_e = 5150°K, (T_e/T_i) = 1 to 10^4, f_p = 4.5 MHz)	169
C-21	k_eh versus f. (f_p = 4.5 MHz, h = 8.5 cm)	168

CHAPTER 1

INTRODUCTION

The research described in this dissertation deals with the interaction of the electromagnetic radiation with a plasma. The first part of the dissertation studies the radiation of various antennas imbedded in an infinite, homogeneous, isotropic, compressible and lossy plasma. A two-fluid model is used to describe the plasma. The second part of the dissertation investigates the excitation of an electroacoustic wave in the plasma sheath surrounding a cylindrical antenna, the excitation of electroacoustic resonances in various plasma geometries, and the reflection behavior of electroacoustic waves on various surfaces.

The excitation and radiation of the electroacoustic and ionacoustic waves from various simple antennas imbedded in a plasma medium is a subject that has received a great deal of attention from researchers. As to the excitation and propagation properties of the electroacoustic and ionacoustic waves, theoretical and experimental investigations have been done by the researchers such as Cohen [1], Hessel and Shmoys [2], Kuehl [3], Barrett and Little [4], Jones and Alexeff [5,6],

Malmberg and Wharton [7], Chen and Lin [8], Doucet [9], Lonngren et al.[10] and Alexeff, Jones and Montgomery [11]. More recently, Nakamura et al.[12], Ishizone et al.[13] and Shen et al.[14] have detected the electroacoustic and ion-acoustic waves excited by some simple antennas, and their radiation patterns have also been measured. In treating the plasma, most of the workers, including Majumdar [15], Cohen [1], Hessel amd Shmoys [2] and Seshadri [16], have idealized the plasma to be a homogeneous, collisionless and compressive electron fluid with stationary ions that neutralize the electrons on the average. Recently, Kuehl [3] has studied the excitation of waves in a warm plasma by an electric dipole wherein the motion of the ion has been included. Seshadri [17] studied the radiation from electric current sources in a two-component finite temperature plasma and Maxam and Chen [18] decoupled electroacoustic and ionacoustic wave equations based on a two-fluid plasma model using macroscopic approach.

It is the purpose of this research to apply the decoupled equations of electroacoustic and ionacoustic waves, with the consideration of various collision frequencies and under various electron and ion temperatures, to investigate in detail the electron-ion compositions and the propagation constants of the so-called generalized electroacoustic and ionacoustic waves. The radiation patterns of the generalized electroacoustic and ionacoustic waves excited by some simple antennas including Hertzian dipole, disk monopole, disk dipole and cylindrical antennas are calculated. Theoretical radiation patterns are then compared with recent experimental results by Nakamura et al.[12], Ishizone et al.[13] and Shen et al.[14]. A good agreement is obtained between the present theory and experimental results.

The excitation of an electroacoustic wave in an inhomogeneous compressible plasma and the resonance of the electroacoustic wave in a plasma sheath leading to the so-called Tonks-Dattner's resonance, or thermal resonance, have been studied by numerous workers including Tonks [19], Dattner [20], Crowford [21], Parker et al.[22], Vandenplas [23], Tutter [24], Van Hoven [25], Derfler and Simonen [26] and Golddan and Yadlowsky [27]. Recently, Baldwin [28] and Parbhakar and Gregory [29], through their theoretical and experimental studies, proposed a new physical mechanism for the electroacoustic resonance in the plasma sheath of a cylindrical plasma column. The mechanism implies that in order to excite an electroacoustic wave, an electromagnetic wave is required to interact with the plasma at the critical density point where the plasma frequency is equal to the frequency of the electromagnetic wave. If no critical density point exists in the plasma, an electroacoustic wave may not be excited.

In the second part of this research, experimental studies have been conducted to study (1) the excitation of the electroacoustic wave in the plasma sheath surrounding a cylindrical antenna imbedded in a compressible plasma, (2) the excitation of electroacoustic resonances in various plasma geometries which include cylindrical, rectangular and single-slope density profile plasma columns, and (3) the reflection behavior of electroacoustic waves on dielectric and metallic surfaces based on the technique of exciting electroacoustic resonances. Baldwin's mechanism [28] was used to explain some experimental results.

In this part of the experimental study, a new diagnostic scheme for plasma density measurement was developed. A cylindrical antenna immersed in a compressible plasma is driven by a frequency-sweeping electromagnetic wave and a variable d.c. bias voltage is applied to the antenna. By observing the effect of the d.c. bias voltage on the excitation of the electroacoustic wave in the plasma sheath surrounding the antenna, the plasma density at the location of the antenna can be directly read on the oscilloscope.

Throughout the study, the macroscopic approach is used. The problem was solved based on the hydrodynamic equations and Maxwell's equations. Chapter 2 studies the generalized electroacoustic and ionacoustic waves, their electron-ion compositions, propagation constants, the effects due to the collision frequency and electron and ion temperatures. Chapter 3 applies the results of Chapter 2 to calculate the radiation patterns of generalized electroacoustic and ionacoustic waves excited by four different types of antennas.

Theoretical results are then compared with some recent experimental results. Chapter 4 studies the excitation of an electroacoustic wave in the plasma sheath surrounding a cylindrical antenna. A new diagnostic method for the plasma density measurement is described in this chapter. The excitation of electroacoustic waves in various plasma geometries and the reflection behavior of electroacoustic waves on various surfaces are investigated in Chapter 5.

CHAPTER 2

ELECTROACOUSTIC WAVE AND IONACOUSTIC WAVE EXCITED IN AN INFINITE, HOMOGENEOUS, ISOTROPIC, COMPRESSIBLE AND LOSSY PLASMA BY AN ELECTROMAGNETIC SOURCE

2.1 Geometry and the Related Equations

We consider a system in which an electromagnetic source with current density $\vec{J}^S$ and charge density ρ^S is immersed in an infinite, homogeneous, isotropic, compressible and lossy plasma. The plasma is assumed to consist of two fluids, the electrons and the ions. The neutral particles of the plasma contribute to the dynamics of the plasma by collisions with the charged particles. The electromagnetic source excited a longitudinal electroacoustic wave and a longitudinal ionacoustic wave in addition to the usual electromagnetic wave. Since the excitation and propagation of the electromagnetic wave in the plasma are well known, only the electroacoustic wave and ionacoustic wave are investigated in detail in this study.

A macroscopic approach is used to describe this system. It is assumed that the perturbation of the plasma due to the source is small, so that the linearized equations are applicable.

Under these assumptions, the basic equations which govern this system are Maxwell's equations and the hydrodynamic equations.

Maxwell's equations:

$$\nabla \times \vec{E} = - \frac{\partial \vec{B}}{\partial t} \tag{2.1.1}$$

$$\nabla \times \vec{B} = \mu_o \vec{J}^S + \mu_o e(n_{oi}\vec{U}_i - n_{oe}\vec{U}_e) + \mu_o \varepsilon_o \frac{\partial \vec{E}}{\partial t} \tag{2.1.2}$$

$$\nabla \cdot \vec{E} = \frac{\rho^S}{\varepsilon_o} + \frac{e}{\varepsilon_o}(n_i - n_e) \tag{2.1.3}$$

$$\nabla \cdot \vec{B} = 0 \tag{2.1.4}$$

where n_{oi} and n_{oe} are the unperturbed ion and electron densities which can be assumed to be equal and uniform throughout the system, that is,

$$n_{oi} = n_{oe} = n_o \quad . \tag{2.1.5}$$

n_i and n_e are the perturbed ion and electron densities such that $n_i << n_o$; $n_e << n_o$. n_i and n_e are functions of both position and time. $\vec{U}_i$ and $\vec{U}_e$ are the average velocities of the ions and electrons induced by the external force. $\vec{E}$ and $\vec{B}$ are the electric and the magnetic fields. $\vec{J}^S$ and ρ^S are the current and charge density of the source and are related by the equation of continuity as

$$\nabla \cdot \vec{J}^S + \frac{\partial \rho^S}{\partial t} = 0 \quad . \tag{2.1.6}$$

μ_o and ε_o are the permeability and permittivity of free space respectively.

Hydrodynamic equations:

The linearized equations of motion for the electrons are

$$\frac{\partial n_e}{\partial t} + n_o(\nabla \cdot \vec{U}_e) = 0 \tag{2.1.7}$$

$$\frac{\partial \vec{U}_e}{\partial t} + \gamma_e \vec{U}_e = - \frac{e}{m_e} \vec{E} - \frac{V_e^{\,2}}{n_o} \nabla n_e \quad . \tag{2.1.8}$$

The linearized equations of motion for the ions are

$$\frac{\partial n_i}{\partial t} + n_o(\nabla \cdot \vec{U}_i) = 0 \tag{2.1.9}$$

$$\frac{\partial \vec{U}_i}{\partial t} + \gamma_i \vec{U}_i = \frac{e}{m_i} \vec{E} - \frac{V_i^{\,2}}{n_o} \nabla n_i \tag{2.1.10}$$

where γ_e and γ_i are the mean electron-neutral particle collision frequency and mean ion-neutral particle collision frequency respectively. V_e and V_i are the thermal velocities of electrons and of ions, and are defined as

$$V_e^{\,2} = \frac{3kT_e}{m_e} \tag{2.1.11}$$

$$V_i^{\,2} = \frac{3kT_i}{m_i} \tag{2.1.12}$$

where m_e and m_i are the electron and ion masses. T_e and T_i are the electron and ion temperatures. e is the magnitude of electron charge and k is the Boltzmann's constant.

It is assumed that the electromagnetic source oscillates with a constant frequency ω, consequently, all quantities vary with time as $e^{j\omega t}$. The phaser analysis method is then applied in the following development.

2.2 Equations for Electroacoustic and Ionacoustic Waves

To establish equations for the electroacoustic wave, n_e, and the ionacoustic wave, n_i, equation (2.1.8) is written as

$$(j\omega + \gamma_e)\vec{U}_e = -\frac{e}{m_e}\vec{E} - \frac{V_e^{\,2}}{n_o}\nabla n_e \quad . \qquad (2.2.1)$$

Taking the divergence of equation (2.2.1) yields

$$(j\omega + \gamma_e)\nabla \cdot \vec{U}_e = -\frac{e}{m_e}\nabla \cdot \vec{E} - \frac{V_e^{\,2}}{n_o}\nabla^2 n_e \quad . \qquad (2.2.2)$$

$\nabla \cdot \vec{U}_e$ can be obtained from equation (2.1.7) as

$$\nabla \cdot \vec{U}_e = -\frac{j\omega}{n_o} n_e \quad . \qquad (2.2.3)$$

Also from equation (2.1.9), we obtain

$$\nabla \cdot \vec{U}_i = -\frac{j\omega}{n_o} n_i \quad . \qquad (2.2.4)$$

$\nabla \cdot \vec{E}$ can be obtained by taking the divergence of equation (2.1.2);

$$0 = \nabla \cdot \vec{J}^S + en_o(\nabla \cdot \vec{U}_i - \nabla \cdot \vec{U}_e) + j\omega\varepsilon_o \nabla \cdot \vec{E} \quad . \tag{2.2.5}$$

Substituting equations (2.2.3) and (2.2.4) into equation (2.2.5) gives

$$\nabla \cdot \vec{E} = \frac{j}{\omega\varepsilon_o}[\nabla \cdot \vec{J}^S - je\omega(n_i - n_e)] \quad . \tag{2.2.6}$$

Substituting equations (2.2.6) and (2.2.3) into equation (2.2.2), we have

$$\nabla^2 n_e + \frac{\omega^2}{V_e^2}\left(1 - \frac{\omega_e^2}{\omega^2} - j\,\frac{\gamma_e}{\omega}\right)n_e + \frac{\omega_e^2}{V_e^2}\,n_i$$
$$= - j\,\frac{\omega_e^2}{V_e^2 e\omega}\,\nabla \cdot \vec{J}^S \tag{2.2.7}$$

where the electron plasma frequency is

$$\omega_e = \left(\frac{n_o e^2}{m_e \varepsilon_o}\right)^{\frac{1}{2}} \quad . \tag{2.2.8}$$

Using $\nabla \cdot \vec{J}^S = - j\omega\rho^S$ from the equation of continuity and defining

$$\beta_e^2 = \frac{\omega^2}{V_e^2}\left(1 - \frac{\omega_e^2}{\omega^2} - j\,\frac{\gamma_e}{\omega}\right) \quad , \tag{2.2.9}$$

equation (2.2.7) can be rewritten as

$$\nabla^2 n_e + \beta_e^{\,2} n_e + \frac{\omega_e^{\,2}}{V_e^{\,2}}\, n_i = -\frac{\omega_e^{\,2}}{V_e^{\,2}}\left(\frac{\rho^S}{e}\right) \quad . \qquad (2.2.10)$$

Similarly, we can get an equation for n_i as

$$\nabla^2 n_i + \beta_i^{\,2} n_i + \frac{\omega_i^{\,2}}{V_i^{\,2}}\, n_e = \frac{\omega_i^{\,2}}{V_i^{\,2}}\left(\frac{\rho^S}{e}\right) \qquad (2.2.11)$$

where the ion plasma frequency is

$$\omega_i = \left(\frac{n_o e^2}{m_i \varepsilon_o}\right)^{\frac{1}{2}} \qquad (2.2.12)$$

and

$$\beta_i^{\,2} = \frac{\omega^2}{V_i^{\,2}}\left(1 - \frac{\omega_i^{\,2}}{\omega^2} - j\,\frac{\gamma_i}{\omega}\right) \quad . \qquad (2.2.13)$$

2.3 Decoupling of n_e and n_i Waves

Equations (2.2.10) and (2.2.11) can be decoupled mathematically into two independent wave equations [18] as

$$(\nabla^2 + k_1^{\,2}) n_1 = S_1\, \frac{\rho^S}{e} \qquad (2.3.1)$$

$$(\nabla^2 + k_2^{\,2}) n_2 = S_2\, \frac{\rho^S}{e} \qquad (2.3.2)$$

where n_1 and n_2 are linear combinations of n_e and n_i; namely,

$$n_1 = \left(\frac{V_i}{\omega_i} T_{12}\right) n_i - \left(\frac{V_e}{\omega_e} T_{22}\right) n_e \tag{2.3.3}$$

$$n_2 = \left(\frac{V_e}{\omega_e} T_{21}\right) n_e - \left(\frac{V_i}{\omega_i} T_{11}\right) n_i \tag{2.3.4}$$

which represent two new waves of perturbation densities. On the other hand, n_e and n_i can be written in terms of n_1 and n_2 as

$$n_e = \frac{\omega_e}{V_e}(T_{11}n_1 + T_{12}n_2) \tag{2.3.5}$$

$$n_i = \frac{\omega_i}{V_i}(T_{21}n_1 + T_{22}n_2) \quad . \tag{2.3.6}$$

The propagation constants, k_1 and k_2, for the n_1 wave and the n_2 wave are given by

$$k_1^2 = \frac{1}{2}\left\{\beta_e^2 + \beta_i^2 + \left[(\beta_i^2 - \beta_e^2)^2 + 4\,\frac{\omega_e^2\omega_i^2}{V_e^2V_i^2}\right]^{\frac{1}{2}}\right\} \tag{2.3.7}$$

$$k_2^2 = \frac{1}{2}\left\{\beta_e^2 + \beta_i^2 - \left[(\beta_i^2 - \beta_e^2)^2 + 4\,\frac{\omega_e^2\omega_i^2}{V_e^2V_i^2}\right]^{\frac{1}{2}}\right\} \quad . \tag{2.3.8}$$

The constants S_1, S_2, T_{11}, T_{21} and T_{22} are expressed as functions of plasma parameters as

$$S_1 = T_{22}\frac{\omega_e}{V_e} + T_{12}\frac{\omega_i}{V_i} \qquad (2.3.9)$$

$$S_2 = -T_{21}\frac{\omega_e}{V_e} - T_{11}\frac{\omega_i}{V_i} \qquad (2.3.10)$$

$$T_{11} = \frac{1}{\left[1 + \frac{1}{4}\frac{V_e^2 V_i^2}{\omega_e^2\omega_i^2}(\beta_e^2 - \beta_i^2 - A_o)^2\right]^{\frac{1}{2}}} \qquad (2.3.11)$$

$$T_{21} = -\frac{1}{2}\frac{V_e V_i}{\omega_e\omega_i}\frac{\beta_e^2 - \beta_i^2 - A_o}{\left[1 + \frac{1}{4}\frac{V_e^2 V_i^2}{\omega_e^2\omega_i^2}(\beta_e^2 - \beta_i^2 - A_o)^2\right]^{\frac{1}{2}}}$$

$$(2.3.12)$$

$$T_{12} = \frac{1}{\left[1 + \frac{1}{4}\frac{V_e^2 V_i^2}{\omega_e^2\omega_i^2}(\beta_e^2 - \beta_i^2 + A_o)^2\right]^{\frac{1}{2}}} \qquad (2.3.13)$$

$$T_{22} = -\frac{1}{2}\frac{V_e V_i}{\omega_e\omega_i}\frac{\beta_e^2 - \beta_i^2 + A_o}{\left[1 + \frac{1}{4}\frac{V_e^2 V_i^2}{\omega_e^2\omega_i^2}(\beta_e^2 - \beta_i^2 + A_o)^2\right]^{\frac{1}{2}}}$$

$$(2.3.14)$$

where

$$A_o = \left[(\beta_i^2 - \beta_e^2)^2 + 4\frac{\omega_e^2\omega_i^2}{V_e^2 V_i^2}\right]^{\frac{1}{2}} . \qquad (2.3.15)$$

Physically, n_1 and n_2 represent two separate longitudinal plasma waves each consisting of electrons and ions and propagating with a particular velocity. For convenience, we will call n_1 the generalized ionacoustic wave and n_2 the generalized electroacoustic wave.

2.4 Electron-ion Composition Ratios of the Generalized Ionacoustic Wave (n_1 Wave) and the Generalized Electroacoustic Wave (n_2 Wave)

The electron-ion composition ratios for the n_1 wave and the n_2 wave are studied for various collision frequencies and various ratios of electron temperature to ion temperature.

From equation (2.3.3), we have

$$n_1 = -\left(\frac{V_e}{\omega_e} T_{22}\right) n_e + \left(\frac{V_i}{\omega_i} T_{12}\right) n_i \quad . \tag{2.4.1}$$

Let R_1 be the electron-ion composition ratio for the n_1 wave such that

$$R_1 = -\left(\frac{V_e \omega_i T_{22}}{V_i \omega_e T_{12}}\right) \quad . \tag{2.4.2}$$

Using equations (2.3.13) and (2.3.14), equation (2.4.2) can be written as

$$R_1 = \frac{1}{2}\left(\frac{V_e}{\omega_e}\right)^2 \left(\beta_e{}^2 - \beta_i{}^2 + A_o\right) \quad . \tag{2.4.3}$$

Similarly, from equation (2.3.4), we calculate R_2, the electron-ion composition ratio for the n_2 wave, as

$$R_2 = -\left(\frac{V_e \omega_i T_{21}}{V_i \omega_e T_{11}}\right) \quad . \tag{2.4.4}$$

Using equations (2.3.11) and (2.3.14) in equation (2.4.4), we have

$$R_2 = \frac{1}{2}\left(\frac{V_e}{\omega_e}\right)^2 (\beta_e{}^2 - \beta_i{}^2 - A_o) \quad . \qquad (2.4.5)$$

R_1 and R_2 are numerically calculated for various collision frequencies, various T_e/T_i and various source frequencies. A hydrogen gas plasma is assumed in the numerical example. The detail of this calculation is shown in Appendix A.

The numerical calculation of R_1 and R_2 for various parameters was carried out on the CDC 6500 computer in five programs. In each program, we assign one of the T_e/T_i ratios (1, 10, 100, 1000, 10000) and consider six different collision frequency ratios γ_e/ω (0, 0.001, 0.01, 0.1, 1.0 and 10).

Figures 2.1 and 2.2 plot the electron-ion composition ratios of the n_1 wave and n_2 wave respectively for $\gamma_e/\omega = 0$, 0.001, 0.01, 0.1, 1.0 and 10 with $T_e/T_i = 1$, 10, 100, 1000, 10000 as a function of the plasma frequency square over the frequency square. The range of $\omega_e{}^2/\omega^2$ considered in these figures is from 1×10^{-4} to 1×10^6 which corresponds to a hgih frequency region and a low frequency region respectively.

It can be seen in Figure 2.1 that at the high frequency limit, the n_1 wave consists mainly of ions regardless of the γ_e/ω and T_e/T_i values. At the low frequency limit, electron composition is T_e/T_i times higher than the ion composition; in the case of $T_e = T_i$, the n_1 wave consists of equal amount of ions and electrons. In Figure 2.2, at the high frequency limit, the n_2 wave consists mainly of electrons; the higher the T_e/T_i values, the higher is the composition of electrons. At the low frequency limit, the n_2 wave consists of equal amount of electrons and ions regardless of the γ_e/ω and T_e/T_i values. It should be noted that the n_2 wave is evanescent at the low frequency. In both figures, the effect due to the γ_e/ω value is not very obvious.

The numerical output of the computer can be checked analytically for the simple case where $T_e = T_i$ and $\gamma_e/\omega = 0$.

In the low frequency limit, we have $\omega < \omega_i << \omega_e$, and we can assume $(\omega_e^2/\omega^2) \rightarrow \infty$; $(\omega_i^2/\omega^2) \rightarrow \infty$.

Under these conditions, equations (2.2.9), (2.2.13) and (2.3.15) are reduced to

$$\beta_e^2 = \frac{\omega^2}{V_e^2}\left(-\frac{\omega_e^2}{\omega^2}\right)$$

$$\beta_i^2 = \frac{\omega^2}{V_i^2}\left(-\frac{\omega_i^2}{\omega^2}\right)$$

$$A_o = \frac{\omega_i^2}{V_i^2} + \frac{\omega_e^2}{V_e^2} \quad ,$$

and thus equation (2.4.3) becomes

$$R_1 = \left(\frac{V_e^2}{V_i^2}\right)\left(\frac{\omega_i^2}{\omega_e^2}\right) \quad .$$

Using equations (2.1.11), (2.1.12), (2.2.8) and (2.2.12), we have

$$R_1 = \frac{T_e}{T_i} \tag{2.4.6}$$

which is reduced to 1 when $T_e = T_i$. This result is consistent with Figure 2.1. Similarly, equation (2.4.5) becomes $R_2 = -1$. Since R_1 and R_2 are ratios of two waves, we are interested only in their absolute values, that is, the ratio of their magnitudes. Therefore we have $|R_2| = 1$. This result is consistent with Figure 2.2.

In the high frequency limit, we have $\omega > \omega_e >> \omega_i$, and we can assume $(\omega_e^2/\omega^2) \to 0$; $(\omega_i^2/\omega^2) \to 0$.

Equations (2.2.9), (2.2.13) and (2.3.15) are reduced to

$$\beta_e^2 = \frac{\omega^2}{V_e^2} \tag{2.4.7}$$

$$\beta_i^2 = \frac{\omega^2}{V_i^2} \tag{2.4.8}$$

$$A_o = \left[\left(\frac{\omega^2}{V_i^2} - \frac{\omega^2}{V_e^2}\right)^2 + 4\,\frac{\omega_e^2\omega_i^2}{V_e^2V_i^2}\right]^{\frac{1}{2}} . \tag{2.4.9}$$

Since $\omega > \omega_e >> \omega_i$, it is true that $4\,\frac{\omega_e^2\omega_i^2}{V_e^2V_i^2} << 2\,\frac{\omega^4}{V_e^2V_i^2}$.

After omitting the term $4\,\frac{\omega_e^2\omega_i^2}{V_e^2V_i^2}$ in equation (2.4.9), we have

$$A_o = \beta_i^2 - \beta_e^2 \quad . \tag{2.4.10}$$

Substituting equations (2.4.7), (2.4.8) and (2.4.10) into equation (2.4.3), we have $R_1 = 0$. This result implies that the n_1 wave in the high frequency region consists mainly of positive ions. This phenomenon is shown in Figure 2.1.

Substituting equation (2.4.10) into equation (2.4.5), we have

$$R_2 = \left(\frac{V_e}{\omega_e}\right)^2 (\beta_e^2 - \beta_i^2) \quad . \tag{2.4.11}$$

Using equations (2.4.7) and (2.4.8) in equation (2.4.11), we have

$$R_2 = \left(\frac{\omega}{\omega_e}\right)^2 \left(1 - \frac{V_e^2}{V_i^2}\right) \quad .$$

With $T_e/T_i = 1$ and for hydrogen gas plasma model, $V_e^2/V_i^2 = m_i/m_e = 1836$, thus, we have $|R_2| = \infty$. This result indicates that the n_2 wave in the high frequency region consists mainly of electrons. This fact is shown in Figure 2.2.

Furthermore, since R_1 at the low frequency limit is equal to T_e/T_i as given in equation (2.4.6), it can easily be seen that in the cases of $T_e = 10\ T_i$, $T_e = 100\ T_i$, $T_e = 1000\ T_i$ and $T_e = 10000\ T_i$, the ratios of n_e to n_i are 10, 100, 1000 and 10000 respectively. These results are shown in Figure 2.1.

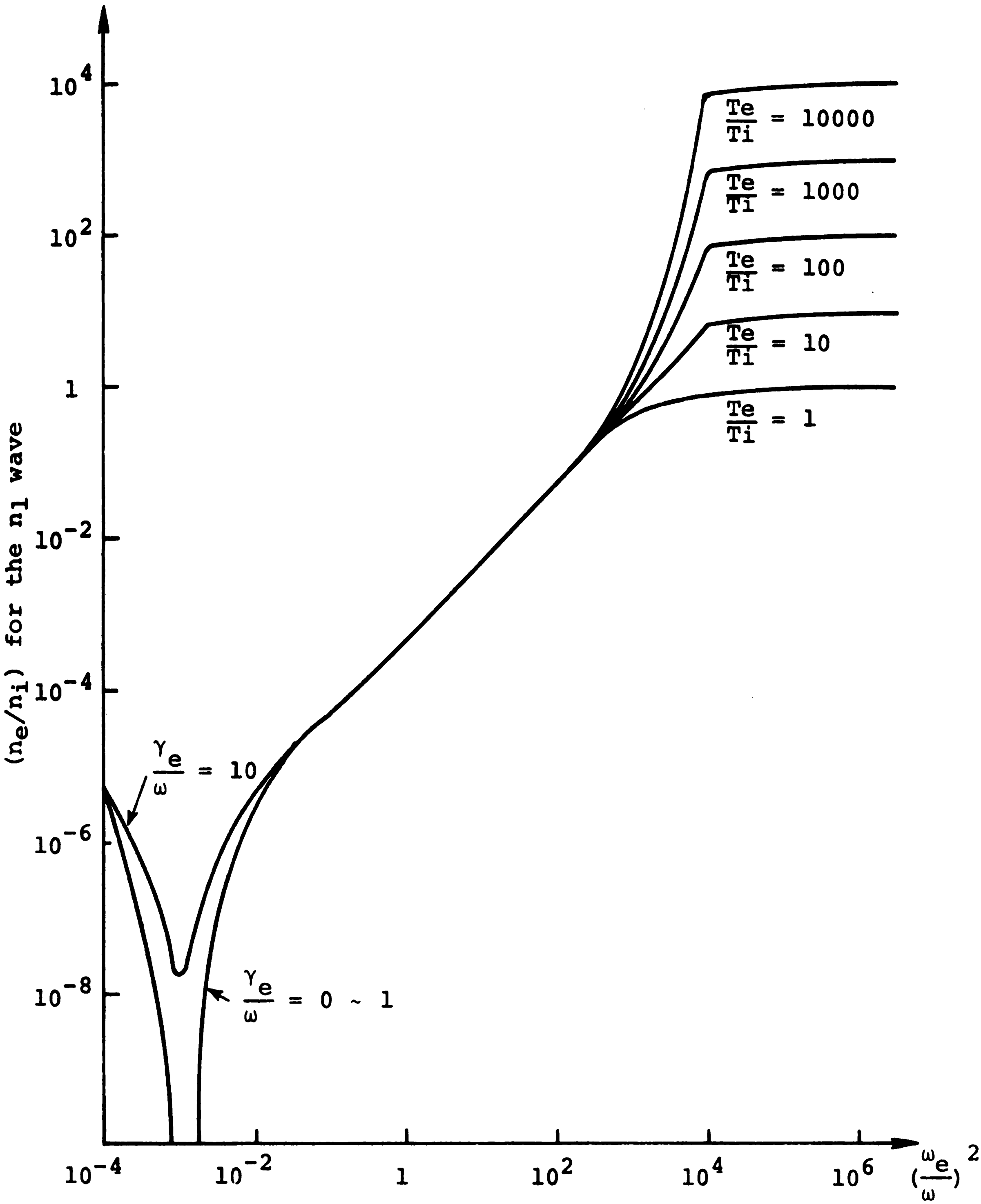

Figure 2.1 Electron-ion composition ratio of the generalized ionacoustic wave (n_1 wave) as a function of $(\omega_e/\omega)^2$ for various ratios of electron temperature to ion temperature.

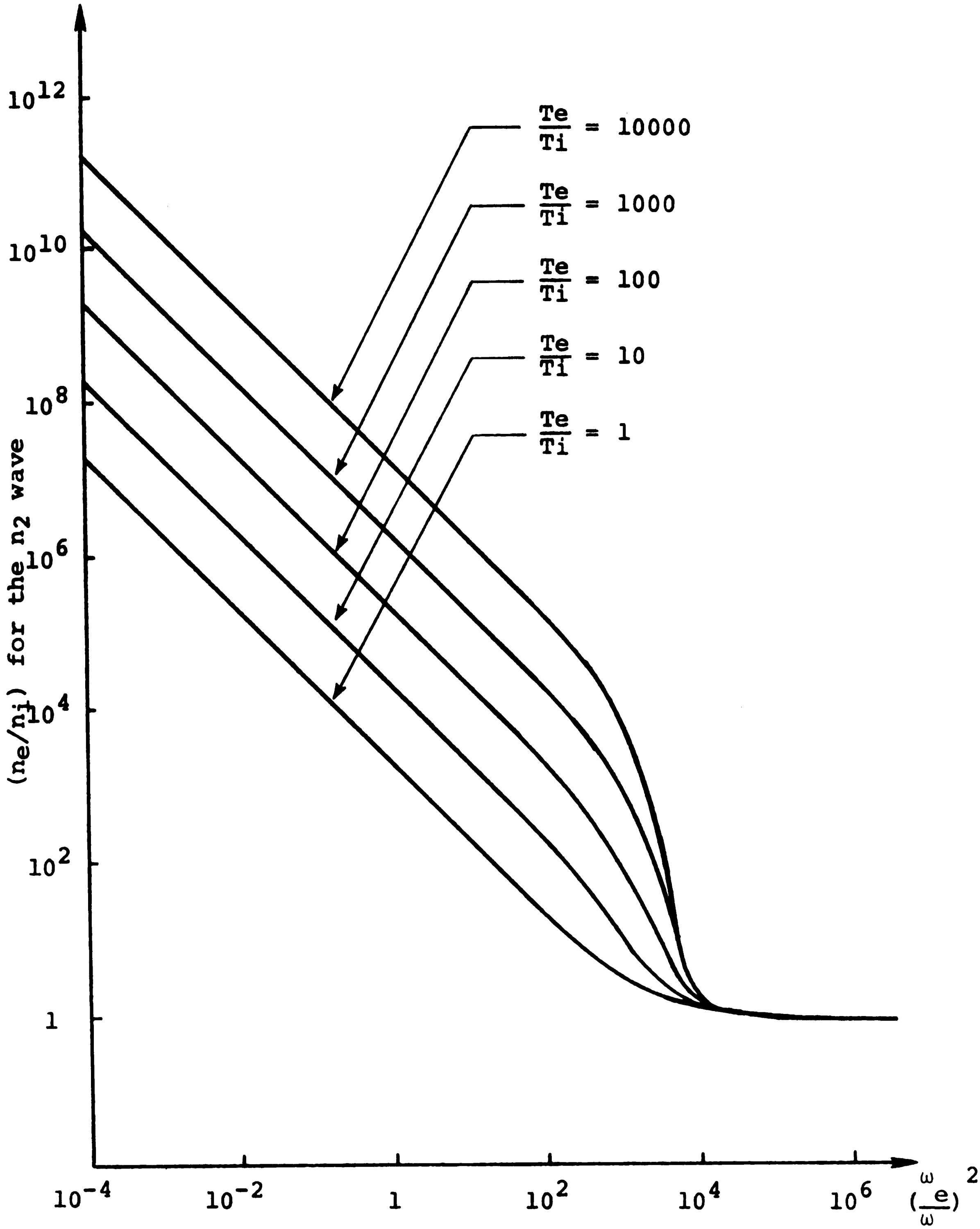

Figure 2.2 Electron-ion composition ratio of the generalized electroacoustic wave (n_2 wave) as a function of $(\omega_e/\omega)^2$ for various ratios of electron temperature to ion temperature.

2.5 Propagation Constants of the Generalized Ionacoustic Wave and the Generalized Electroacoustic Wave

The propagation constants of the generalized ionacoustic wave and the generalized electroacoustic wave, k_1 and k_2, for the cases of various collision frequencies and various ratios of electron temperature to ion temperature are studied in this section. k_1 and k_2 are given by equations (2.3.7), (2.3.8) and (2.3.15) as

$$k_1^2 = \frac{1}{2}(\beta_e^2 + \beta_i^2 + A_o) \tag{2.5.1}$$

$$k_2^2 = \frac{1}{2}(\beta_e^2 + \beta_i^2 - A_o) \quad . \tag{2.5.2}$$

It is shown in Appendix B that equations (2.5.1) and (2.5.2) are reduced to two sets of equations; one set for hydrogen gas and another set for xenon gas, such that $k_1/(\omega/V_i)$ and $k_2/(\omega/V_e)$ for each gas assumption can be calculated numerically by using CDC 6500 computer in five programs. In each program, we assign one of the T_e/T_i ratios (1, 10, 100, 1000, 10000) and consider six different collision frequency ratios γ_e/ω (0, 0.001, 0.01, 0.1, 1 and 10). The numerical results for the hydrogen gas are drawn in Figures 2.3 to 2.7. The numerical results for the xenon gas are used in the electroacoustic wave and the ionacoustic wave radiation pattern calculations.

Figure 2.3 plots the real part of $k_1/(\omega/V_i)$, or the phase constant of the n_1 wave, for the cases of $\gamma_e/\omega = 0$, 0.001, 0.01, 0.1, 1.0 and 10 with T_e/T_i = 1, 10, 100, 1000 and 10000 as a function of the plasma frequency square over the frequency square. The range of ω_e^2/ω^2 considered in these figures is from 1×10^{-4} to 1×10^6 which corresponds to a high frequency region and a low frequency region respectively. The effect due to the collision frequency is not very evident so that it is not shown in the figure. However, the temperature ratio, T_e/T_i, has a big effect in the low frequency region. It should be noted that $k_1/(\omega/V_i)$ does not vanish at any frequency range. This implies that the n_1 wave propagates under all conditions. The phase velocity of the n_1 wave, V_{ph1}, can also be observed in this figure, since it is given as $\omega/[\mathrm{Re}(k_1)]$. At the high frequency limit, we have $\mathrm{Re}[k_1/(\omega/V_i)] = 1$, or $\mathrm{Re}(\omega/k_1) = V_i$. This implies that at the high frequency limit, or in the low plasma density region, the phase velocity of the n_1 wave approaches to the thermal velocity of ions. Also, it can be seen in the figure that at the low frequency region or as the plasma density increases, the phase velocity becomes greater and then approaches to the value of $V_i\sqrt{(T_e + T_i)/T_i}$, which is called V_A, the phase velocity of the pseudosonic wave.

Figures 2.4 and 2.5 plot the negative imaginary part of $k_1/(\omega/V_i)$, the attenuation constant, of the n_1 wave. In Figure 2.4, the cases for $T_e = T_i$, $\gamma_e/\omega = 1$ and $T_e = T_i$, $\gamma_e/\omega = 10$ are plotted. In Figure 2.5, the cases for $T_e = 100\ T_i$ with γ_e/ω = 0.001, 0.01, 0.1 and 1 are plotted.

It is noted that for the case of $\gamma_e/\omega = 0$, the attenuation constant is zero.

From Figures 2.4 and 2.5, the most striking phenomenon is that the attenuation constant of the n_1 wave decreases drastically once ω becomes smaller than ω_i. It is also seen that the attenuation of the n_1 wave is reduced as the collision frequency becomes smaller or the temperature ratio T_e/T_i becomes higher. It should be noted that the Landau damping is very high for the n_1 wave at high frequency range where V_{ph1} approaches to V_i.

Figure 2.6 plots the real part of $[k_e/(\omega/V_e)]$, or the phase constant of the n_2 wave, as a function of $(\omega_e/\omega)^2$ for various collision frequencies.

The effect due to the collision frequency is significant. For the collisionless case, it is seen that the real part of $[k_e/(\omega/V_e)]$ changes from one in the high frequency region to zero abruptly as ω approaches ω_e. It is understood that as the phase constant of a wave goes to zero, the wave becomes evanescent. Therefore, it can be seen that the n_2 wave is cut off when $\omega < \omega_e$. The phase velocity of the n_2 wave, V_{ph2}, in the high frequency region is $\mathrm{Re}(\omega/k_2)$ which is equal to V_e.

As the collision frequency becomes higher, the region in which the n_2 wave propagates is extended further to the lower frequency region, though it can be seen in Figure 2.7 that the wave in this region will suffer a very high attenuation. When ω is around ω_i, a peak appears in the curve, this peak probably corresponds to the oscillation of ions at this frequency.

The ratio T_e/T_i affects the phase constant curve of the n_2 wave only slightly on the low frequency region, therefore, it will not be plotted.

Figure 2.7 plots the negative imaginary part of $k_e/(\omega/V_e)$, that is, the attenuation constant of the n_2 wave. It is seen in the figure that the higher the collision frequency, the higher is the attenuation factor. Once ω becomes smaller than ω_e, the attenuation constant becomes extremely large implying that the n_2 wave is nearly cut off. It is noted that our theory based on the macroscopic approach does not predict the Landau damping which occurs at the high frequency region where V_{ph2} approaches to V_e.

The numerical results for the propagation constants, k_1 and k_2, can also be checked analytically for the case where $T_e = T_i$ and $\gamma_e/\omega = 0$.

In the low frequency limit, we have $\omega < \omega_i << \omega_e$. Using equation (2.2.9) with $\gamma_e/\omega = 0$, we have

$$\beta_e^{\,2} = \frac{\omega^2}{V_e^{\,2}} - \frac{\omega_e^{\,2}}{V_e^{\,2}} \quad . \qquad (2.5.3)$$

Using equations (2.2.13), (A-12) with $\gamma_e/\omega = 0$, we have

$$\beta_i^{\,2} = \frac{\omega^2}{V_i^{\,2}} - \frac{\omega_i^{\,2}}{V_i^{\,2}} \quad . \qquad (2.5.4)$$

Then $(\beta_i^2 - \beta_e^2)^2 = \beta_e^4 - 2\beta_e^2\beta_i^2 + \beta_i^4$ becomes

$$(\beta_i^2 - \beta_e^2)^2 = \left(\frac{\omega_e^2}{V_e^2} - \frac{\omega_i^2}{V_i^2}\right)^2 - 2\omega^2\left(\frac{\omega_e^2}{V_e^4} - \frac{\omega_e^2 + \omega_i^2}{V_e^2V_i^2} + \frac{\omega_i^2}{V_i^4}\right)$$

$$+ \omega^4\left(\frac{1}{V_e^2} - \frac{1}{V_i^2}\right)^2 \quad .$$

Noting that $\omega < \omega_i << \omega_e$, we drop the term containing ω^4 and neglect the term ω_i^2 in comparison with ω_e^2, thus, this equation reduces to

$$(\beta_i^2 - \beta_e^2)^2 \simeq \left(\frac{\omega_e^2}{V_e^2} - \frac{\omega_i^2}{V_i^2}\right)^2 - 2\omega^2\left(\frac{\omega_e^2}{V_e^4} - \frac{\omega_e^2}{V_e^2V_i^2} + \frac{\omega_i^2}{V_i^4}\right) \; . \tag{2.5.5}$$

Using equation (2.5.5) in equation (2.3.15), we have

$$A_o \simeq \frac{\omega_e^2V_i^2 + \omega_i^2V_e^2}{V_e^2V_i^2}\left(1 - 2\omega^2A_4\right)^{\frac{1}{2}} \quad , \tag{2.5.6}$$

where

$$A_4 = \frac{\omega_e^2V_i^4 - \omega_e^2V_i^2 + \omega_i^2V_e^4}{(\omega_e^2V_i^2 + \omega_i^2V_e^2)^2} \quad .$$

A_4 can be expressed in terms of T_i and T_e by using equations (2.1.11), (2.1.12), (2.2.8) and (2.2.12);

$$A_4 = \frac{1}{\omega_i^2}\,\frac{T_e^2 - T_iT_e + T_i^2(m_e/m_i)}{(T_e + T_i)^2} \quad . \tag{2.5.7}$$

Because $T_i = T_e$ and $m_i >> m_e$, then $T_i^2(m_e/m_i) << T_e^2$. After neglecting $T_i^2(m_e/m_i)$ in the numerator of equation (2.5.7) and recognizing that $(T_e + T_i)^2 >> (T_e^2 - T_iT_e)$, the inequality becomes $A_4 < (1/\omega_i^2)$, or $2\omega^2 A_4 < (2\omega^2/\omega_i^2)$. Since $(\omega^2/\omega_i^2) << 1$, then $2\omega^2 A_4 << 1$. Using binomial expansion in equation (2.5.6) and keeping the first two terms, we have

$$A_o \simeq \frac{\omega_e^2 V_i^2 + \omega_i^2 V_e^2}{V_e^2 V_i^2}\left[1 - \omega^2 \frac{\omega_e^2 V_i^4 - \omega_e^2 V_e^2 V_i^2 + \omega_i^2 V_e^4}{(\omega_e^2 V_i^2 + \omega_i^2 V_e^2)^2} + \cdots\right] \tag{2.5.8}$$

Substituting equations (2.5.3), (2.5.4) and (2.5.8) into equation (2.5.1), we have

$$k_1^2 = \frac{\omega^2}{V_i^2}\left[\frac{1}{1 + (\omega_i/\omega_e)^2 (V_e/V_i)^2}\right]$$

where $(\omega_i/\omega_e)^2 (V_e/V_i)^2 = 1$ for $T_e = T_i$.

Thus,

$$\frac{k_1}{(\omega/V_i)} = \frac{1}{\sqrt{2}} \quad . \tag{2.5.9}$$

This result is confirmed in Figure 2.3. Putting equations (2.5.3), (2.5.4) and (2.5.8) into equation (2.5.2), we drop terms with ω^2 since $\omega < \omega_i << \omega_e$, then

$$k_2^2 \simeq -\left(\frac{\omega_e^2}{V_e^2} + \frac{\omega_i^2}{V_i^2}\right) \tag{2.5.10}$$

which is a negative value.

Since k_2 is purely imaginary, the n_2 wave will not propagate in the low frequency limit.

In the high frequency limit, we have $\omega > \omega_e >> \omega_i$. Using equation (2.2.9) with $\gamma_e/\omega = 0$, we have

$$\beta_e^2 = \frac{\omega^2}{V_e^2}\left(1 - \frac{\omega_e^2}{\omega^2}\right) . \qquad (2.5.11)$$

Using equations (2.2.13), (A-12) with $\gamma_e/\omega = 0$ and $\omega_i << \omega$, we have

$$\beta_i^2 = \frac{\omega^2}{V_i^2} . \qquad (2.5.12)$$

Thus, equation (2.3.15) reduces to

$$A_o \simeq \frac{\omega^2}{V_i^2} - \frac{\omega^2}{V_e^2} + \frac{\omega_e^2}{V_e^2}$$

and finally, $k_1^2 \simeq \omega^2/V_i^2$ or $k_1/(\omega/V_i) \simeq 1$. This result is shown in Figure 2.3. Similarly,

$$k_2^2 \simeq \frac{\omega^2}{V_e^2}\left(1 - \frac{\omega_e^2}{\omega^2}\right) .$$

The last term in the bracket can be dropped, because $\omega > \omega_e$. Therefore, $k_2^2 \simeq \omega^2/V_e^2$, or $k_2/(\omega/V_e) \simeq 1$. This result is shown in Figure 2.6.

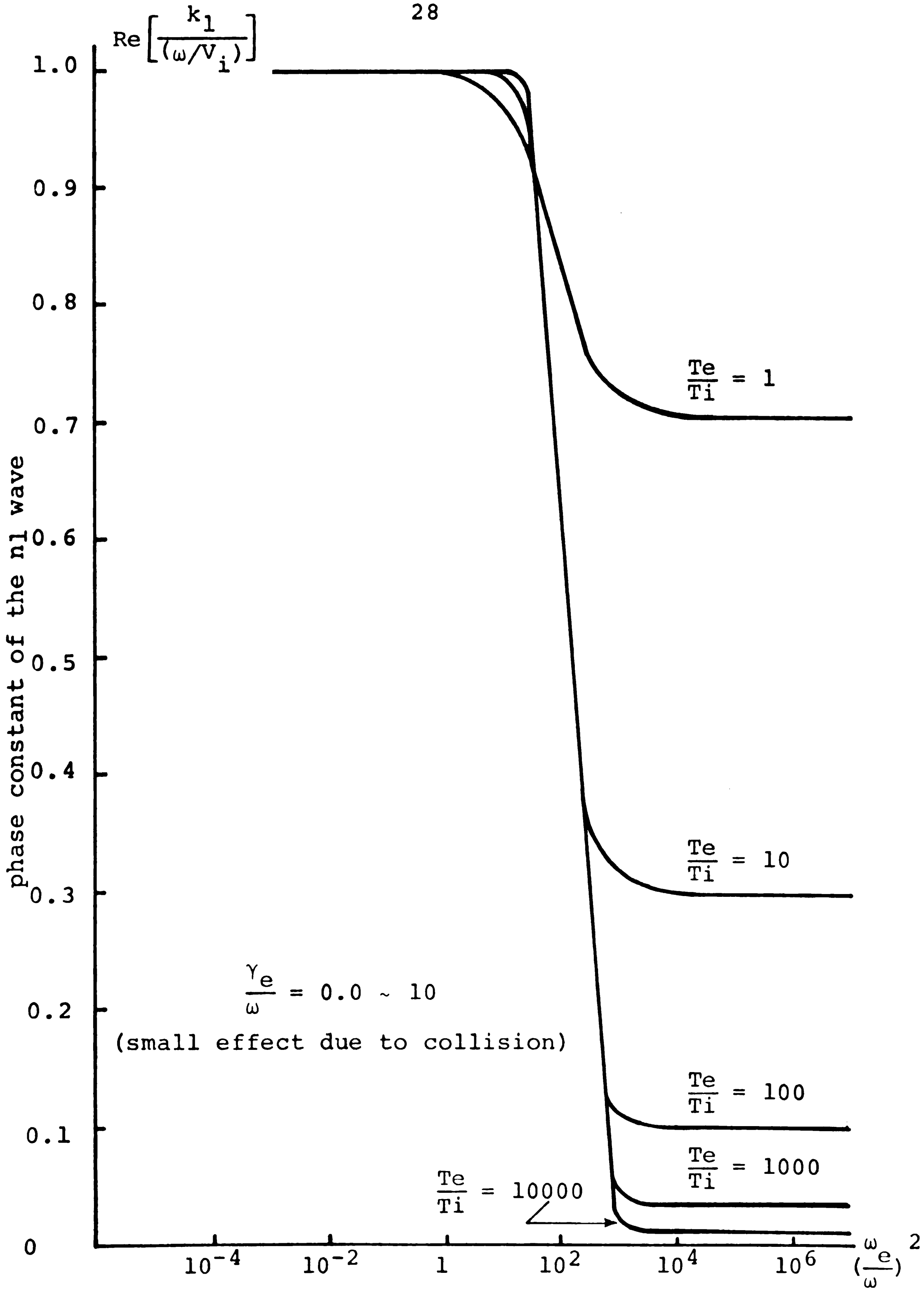

Figure 2.3 Phase constant of the generalized ionacoustic wave (n_1 wave) as a function of $(\omega_e/\omega)^2$ for various ratios of electron temperature to ion temperature in a hydrogen plasma.

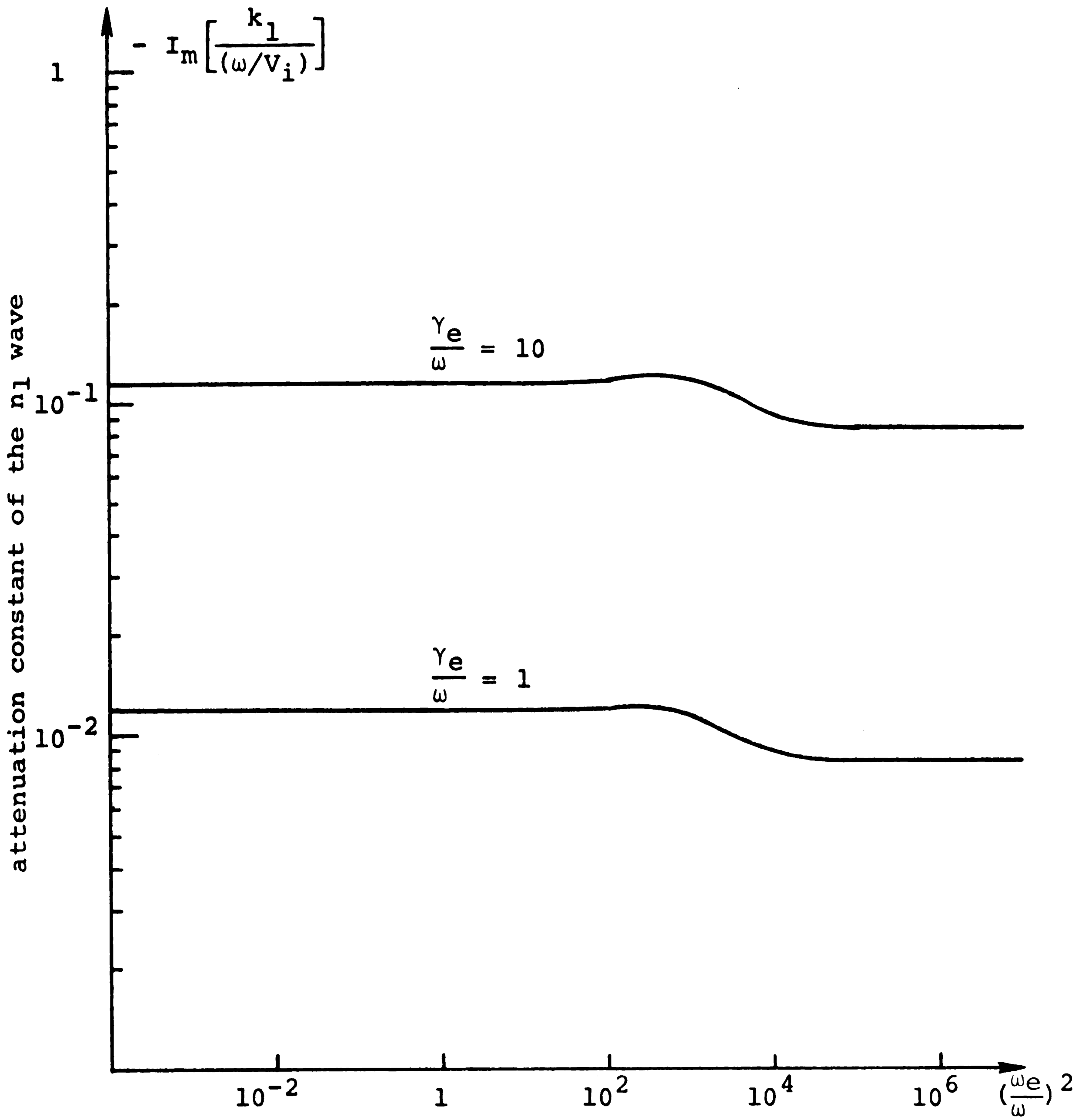

Figure 2.4 Attenuation constant of the generalized ionacoustic wave (n_1 wave) as a function of $(\omega_e/\omega)^2$ for various collision frequencies in a hydrogen plasma. ($T_e/T_i = 1$)

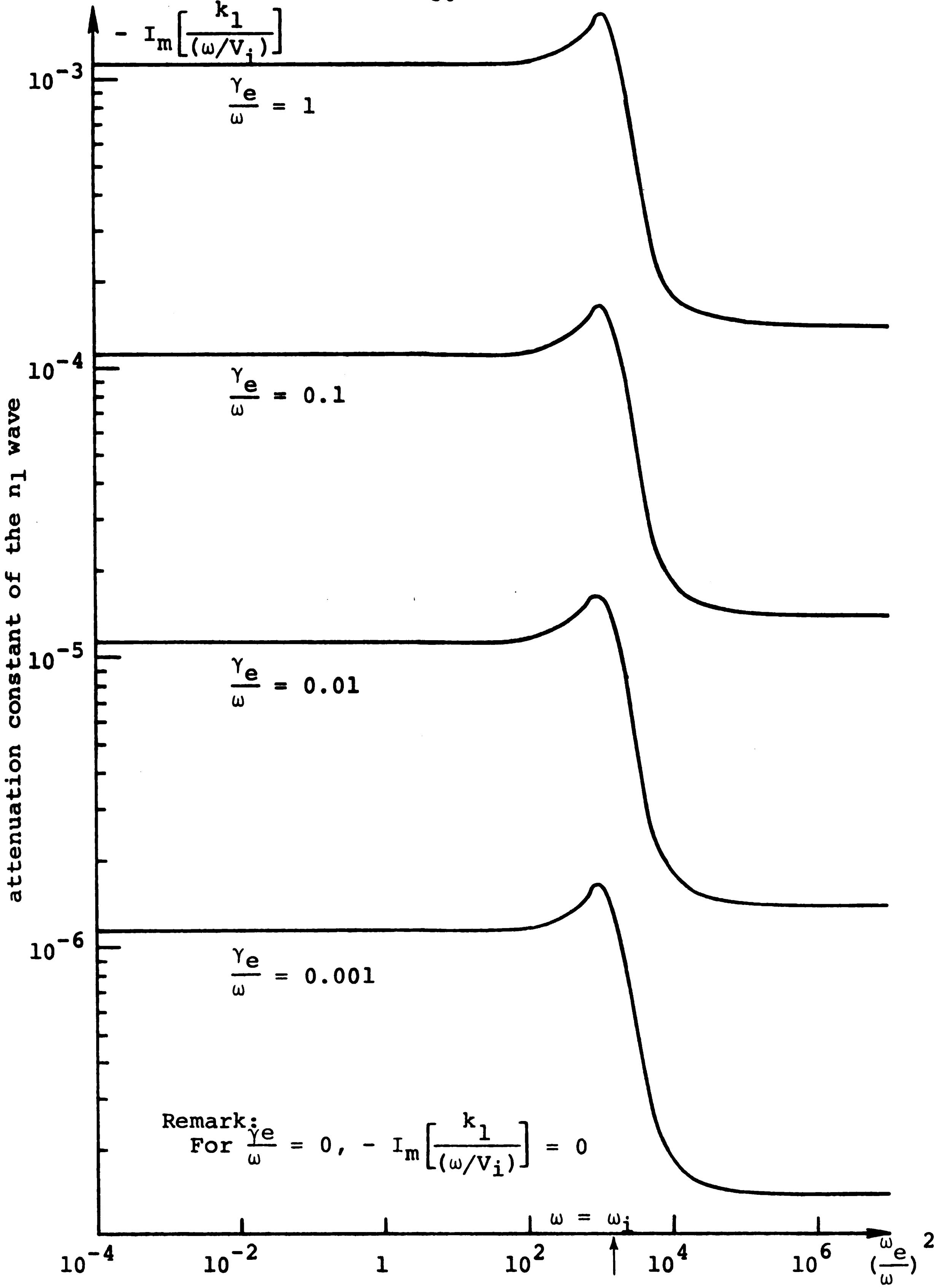

Figure 2.5 Attenuation constant of the generalized ionacoustic wave (n_1 wave) as a function of $(\omega_e/\omega)^2$ for various collision frequencies in a hydrogen plasma. ($T_e/T_i = 100$)

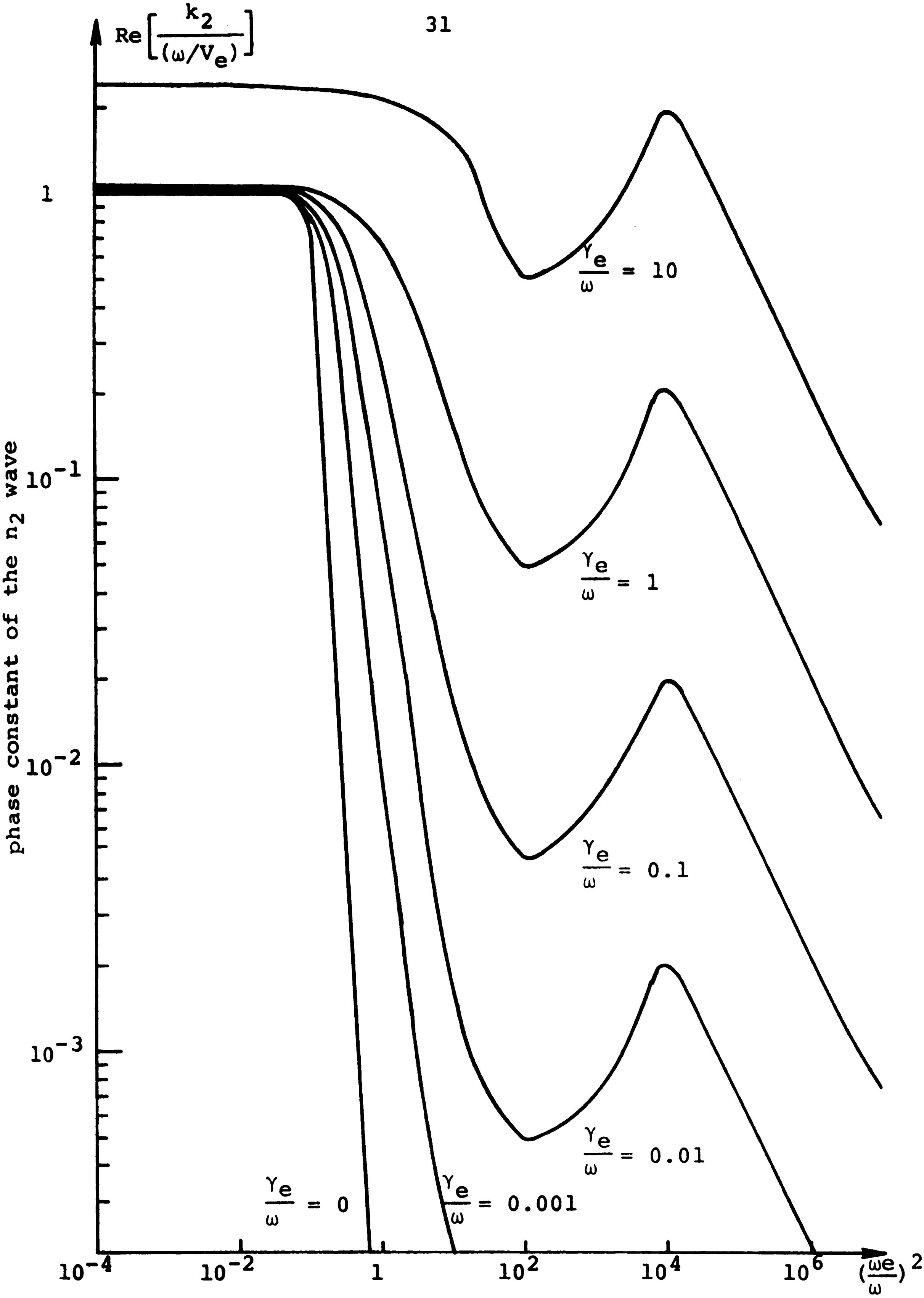

Figure 2.6 Phase constant of the generalized electro-acoustic wave (n_2 wave) as a function of $(\omega_e/\omega)^2$ for various collision frequencies. (T_e/T_i = 100)

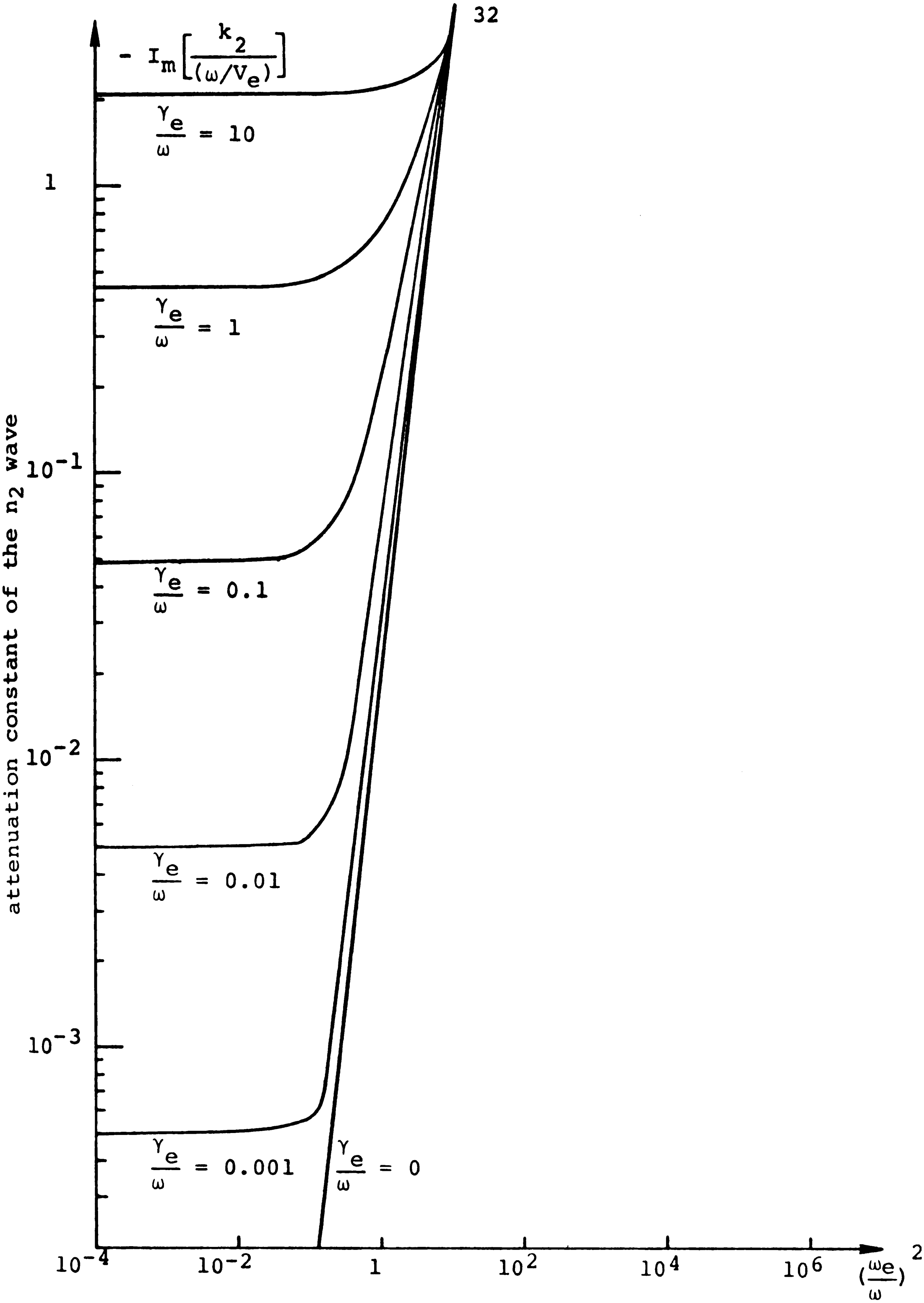

Figure 2.7 Attenuation constant of the generalized electroacoustic wave (n_2 wave) as a function of $(\omega_e/\omega)^2$ for various collision frequencies. $(T_e/T_i = 100)$

2.6 Differential Equations of the Magnetic Field

The magnetic field excited by the electric source in the plasma can be found as follows:

From equation (2.1.2), with the assumption of periodic time dependence and using the relation of equation (2.1.5), we have

$$\nabla \times \vec{B} = \mu_o \vec{J}^S + \mu_o e n_o (\vec{U}_i - \vec{U}_e) + j\omega\mu_o\varepsilon_o \vec{E} \quad . \tag{2.6.1}$$

Taking the curl of equation (2.6.1), we get

$$\begin{aligned} \nabla \times \nabla \times \vec{B} = {} & \mu_o \nabla \times \vec{J}^S + \mu_o e n_o (\nabla \times \vec{U}_i - \nabla \times \vec{U}_e) \\ & + j\omega\mu_o\varepsilon_o \nabla \times \vec{E} \end{aligned} \tag{2.6.2}$$

where

$$\nabla \times \vec{E} = - j\omega\vec{B} \tag{2.6.3}$$

is given by equation (2.1.1), $\nabla \times \vec{U}_e$ and $\nabla \times \vec{U}_i$ can be obtained by taking the curl of equations (2.1.8)and (2.1.10) and using equation (2.6.3), thus,

$$\nabla \times \vec{U}_e = \frac{j\omega e\vec{B}}{m_e(\gamma_e + j\omega)} \tag{2.6.4}$$

$$\nabla \times \vec{U}_i = - \frac{j\omega e\vec{B}}{m_i(\gamma_i + j\omega)} \quad . \tag{2.6.5}$$

Substituting equations (2.6.3), (2.6.4) and (2.6.5) into equation (2.6.2), we have

$$\nabla \times \nabla \times \vec{B} = \mu_o \nabla \times \vec{J}^S - j\omega\mu_o\varepsilon_o\left[\frac{\omega_i^{\,2}}{(\gamma_i + j\omega)} + \frac{\omega_e^{\,2}}{(\gamma_e + j\omega)}\right]\vec{B}$$

$$+ \omega^2\mu_o\varepsilon_o\vec{B} \quad . \tag{2.6.6}$$

Since $\nabla \times \nabla \times \vec{B} = \nabla(\nabla \cdot \vec{B}) - \nabla^2\vec{B}$ and $\nabla \cdot \vec{B} = 0$, equation (2.6.6) can be rewritten as

$$\nabla^2\vec{B} + \omega^2\mu_o\varepsilon_o\left[1 + \frac{\omega_e^{\,2}}{j\omega(\gamma_e + j\omega)} + \frac{\omega_i^{\,2}}{j\omega(\gamma_i + j\omega)}\right]\vec{B}$$

$$= - \mu_o\nabla \times \vec{J}^S \quad . \tag{2.6.7}$$

Let $k_e^{\,2} = \omega^2\mu_o\varepsilon$, where

$$\varepsilon = \varepsilon_o\left[1 + \frac{\omega_e^{\,2}}{j\omega(\gamma_e + j\omega)} + \frac{\omega_i^{\,2}}{j\omega(\gamma_i + j\omega)}\right]$$

$$= \varepsilon_o\left[1 - \frac{\omega_e^{\,2}}{\omega^2 + \gamma_e^{\,2}} - \frac{\omega_i^{\,2}}{\omega^2 + \gamma_i^{\,2}} - j\left(\frac{\omega_e^{\,2}\gamma_e}{\omega(\omega^2 + \gamma_e^{\,2})}\right.\right.$$

$$\left.\left. + \frac{\omega_i^{\,2}\gamma_i}{\omega(\omega^2 + \gamma_i^{\,2})}\right)\right] \tag{2.6.8}$$

= the equivalent complex permittivity in the plasma, equation (2.6.7) can be written as

$$(\nabla^2 + k_e^{\,2})\vec{B} = - \mu_o\nabla \times \vec{J}^S \tag{2.6.9}$$

which is an inhomogeneous wave equation and its solution can be expressed as

$$\vec{B}(\vec{r}) = \frac{\mu_o}{4\pi} \nabla \times \int_{v'} \vec{J}^S(\vec{r}') \frac{e^{-jk_eR}}{R} dv' \qquad (2.6.10)$$

where $R = |\vec{r} - \vec{r}'|$.

2.7 The Electric Field in the Plasma

The electric field in the plasma can be derived from the equation of magnetic fields, equations of the n_1 wave and n_2 wave. It will be shown later in this section that the electric field in the plasma consists of three components; one of which is electromagnetic in nature, while the other two components, which are due to the presence of the electro-acoustic and ionacoustic waves, are longitudinal in nature.

Let us consider the source free Maxwell's equation in the plasma:

$$\nabla \times \vec{B} = \mu_o e n_o (\vec{U}_i - \vec{U}_e) + j\omega\mu_o\varepsilon_o\vec{E} \qquad (2.7.1)$$

where $\vec{U}_e$ and $\vec{U}_i$ can be found from equations of momentum conservation for electrons and ions. That is,from equations (2.1.8) and (2.1.10), we have

$$\vec{U}_e = - \frac{e}{m_e(\gamma_e + j\omega)} \vec{E} - \frac{3kT_e}{n_o m_e(\gamma_e + j\omega)} \nabla n_e \qquad (2.7.2)$$

$$\vec{U}_i = \frac{e}{m_i(\gamma_i + j\omega)} \vec{E} - \frac{3kT_i}{n_o m_i(\gamma_i + j\omega)} \nabla n_i \quad . \qquad (2.7.3)$$

It is seen that these average velocities of electrons and ions are proportional to the electric field in the plasma and the pressure gradient of the particles. Using equations (2.7.2) and (2.7.3) in equation (2.7.1) and after rearrangement, we have

$$\nabla \times \vec{B} = \left[j\omega\mu_o\varepsilon_o + \frac{\mu_o\varepsilon_o\omega_e^2}{(\gamma_e + j\omega)} + \frac{\mu_o\varepsilon_o\omega_i^2}{(\gamma_i + j\omega)} \right] \vec{E}$$

$$+ \frac{3\mu_o ekT_e \nabla n_e}{m_e(\gamma_e + j\omega)} - \frac{3\mu_o ekT_i \nabla n_i}{m_i(\gamma_i + j\omega)}$$

which yields

$$\nabla \times \vec{B} = \frac{P}{(\gamma_e + j\omega)(\gamma_i + j\omega)} \vec{E} + \frac{3\mu_o ekT_e \nabla n_e}{m_e(\gamma_e + j\omega)}$$

$$- \frac{3\mu_o ekT_i \nabla n_i}{m_i(\gamma_i + j\omega)} \tag{2.7.4}$$

where

$$P = j\omega\mu_o\varepsilon_o(\gamma_e + j\omega)(\gamma_i + j\omega) + \mu_o\varepsilon_o\omega_e^2(\gamma_i + j\omega)$$

$$+ \mu_o\varepsilon_o\omega_i^2(\gamma_e + j\omega)$$

$$= \mu_o\varepsilon_o\{[\gamma_i(\omega_e^2 - \omega^2) + \gamma_e(\omega_i^2 - \omega^2)]$$

$$+ j\omega[\omega_e^2 + \omega_i^2 - \omega^2 + \gamma_e\gamma_i]\} \quad . \tag{2.7.5}$$

Express $\vec{E}$ in terms of $\vec{B}$, n_e and n_i in equation (2.7.4), we have

$$\vec{E} = \frac{1}{P}\left[(\gamma_e + j\omega)(\gamma_i + j\omega)(\nabla \times \vec{B}) + \frac{3\mu_o ekT_i(\gamma_e + j\omega)\nabla n_i}{m_i} - \frac{3\mu_o ekT_e(\gamma_i + j\omega)\nabla n_e}{m_e}\right] . \tag{2.7.6}$$

Using equations (2.3.5) and (2.3.6) which express n_e, n_i in terms of n_1 and n_2, we can obtain $\vec{E}$ in terms of $\vec{B}$, n_1 and n_2 as follows:

$$\begin{aligned}\vec{E} = {} & \frac{1}{P}[(\gamma_e\gamma_i - \omega^2) + j\omega(\gamma_e + \gamma_i)](\nabla \times \vec{B}) \\ & + \frac{3\mu_o ek}{P}\left\{\left[\left(\frac{\gamma_e\omega_i T_i T_{21}}{m_i V_i} - \frac{\gamma_i\omega_e T_e T_{11}}{m_e V_e}\right) + j\omega\left(\frac{\omega_i T_i T_{21}}{m_i V_i} - \frac{\omega_e T_e T_{11}}{m_e V_e}\right)\right]\nabla n_1 + \left[\left(\frac{\gamma_e\omega_i T_i T_{22}}{m_i V_i} - \frac{\gamma_i\omega_e T_e T_{12}}{m_e V_e}\right)\right.\right. \\ & \left.\left. + j\omega\left(\frac{\omega_i T_i T_{22}}{m_i V_i} - \frac{\omega_e T_e T_{12}}{m_e V_e}\right)\right]\nabla n_2\right\} .\end{aligned} \tag{2.7.7}$$

It is seen in this equation that the electric field in the plasma has three components. The first term on the right hand side of the equation is electromagnetic in nature, because $\vec{B}$ field is entirely electromagnetic. The second and third terms, which are due to the presence of the electro-acoustic and ionacoustic waves, are longitudinal in nature.

2.8 Average Velocities of Electrons and Ions in the Plasma

The average velocities of electrons and ions in the plasma can be obtained from equations (2.7.2) and (2.7.3) with equations (2.3.5) and (2.3.6) as

$$\vec{U}_e = \frac{1}{\gamma_e + j\omega}\left[-\frac{e\vec{E}}{m_e} - \frac{3kT_e\omega_e}{m_e n_o V_e(\gamma_e + j\omega)}(T_{11}\nabla n_1 + T_{12}\nabla n_2)\right] \tag{2.8.1}$$

$$\vec{U}_i = \frac{1}{\gamma_i + j\omega}\left[\frac{e\vec{E}}{m_i} - \frac{3kT_i\omega_i}{m_i n_o V_i(\gamma_i + j\omega)}(T_{21}\nabla n_1 + T_{22}\nabla n_2)\right] . \tag{2.8.2}$$

n_1 and n_2 can be found by solving equations (2.3.1) and (2.3.2) and $\vec{E}$ is given by equation (2.7.7). It is observed that $\vec{U}_e$ and $\vec{U}_i$ also possess both electromagnetic and longitudinal natures.

CHAPTER 3

RADIATION PATTERNS OF ELECTROACOUSTIC AND IONACOUSTIC WAVES EXCITED BY VARIOUS ANTENNAS

3.1 Introduction

Our objective in this chapter is to calculate the radiation patterns of electroacoustic and ionacoustic waves excited by four different types of antennas; namely, Hertzian dipole antenna, disk monopole antenna, disk dipole antenna and cylindrical antenna. The antennas are assumed to be immersed in an infinite, homogeneous, isotropic and compressible plasma.

In Chapter 2, the generalized ionacoustic and electroacoustic waves which are excited by an electromagnetic source are given in equations (2.3.1) and (2.3.2) as

$$(\nabla^2 + k_1{}^2)n_1 = S_1 \frac{\rho^S}{e} \tag{3.1.1}$$

$$(\nabla^2 + k_2{}^2)n_2 = S_2 \frac{\rho^S}{e} \quad . \tag{3.1.2}$$

The propagation constants of the n_1 and n_2 waves, that is,

k_1 and k_2, are shown graphically in Figures 2.3 to 2.7 for various electron and ion temperatures and various collision frequencies.

Since equations (3.1.1) and (3.1.2) are of the same form, only a common equation such as

$$(\nabla^2 + k^2)n = S \frac{\rho^S}{e} \tag{3.1.3}$$

will be considered. Equation (3.1.3) is a scalar inhomogeneous Helmholtz equation whose solution is

$$n(\vec{r}) = -\frac{S}{4\pi e} \int_{v'} \rho^S(\vec{r}') \frac{e^{-jk|\vec{r} - \vec{r}'|}}{|\vec{r} - \vec{r}'|} dv' \tag{3.1.4}$$

where the primed coordinates refer to the source points and the unprimed coordinates represent the field point. We assume that the antenna dimensions are small compared with a free space electromagnetic wavelength and the observation point is in the far zone of the antenna that the far zone approximations of $|\vec{r} - \vec{r}'| \simeq r$ for the amplitude term and $|\vec{r} - \vec{r}'| \simeq r - z' \cos\theta$ for the phase term can be used.

The radiation patterns of the generalized electro-acoustic wave (n_2 wave) and the generalized ionacoustic wave (n_1 wave) excited by various antennas can be calculated from equation (3.1.4) For the n_2 wave, we use n_2, S_2 and k_2 to replace n, S and k in equation (3.1.4) while for the n_1 wave we use n_1, S_1 and k_1 instead.

3.2 Hertzian Dipole Antenna

3.2.1 Geometry and Statement of the Problem

The geometrical configuration of a Hertzian dipole antenna is shown in Figure 3.1 using a spherical coordinate system (r, θ, ϕ). A Hertzian dipole antenna, with the assumption that the radius of the wire is thin and its length, dl, is very short compared with the wavelength, is immersed in the plasma. The ends of the antenna are large enough that the charge distribution of the antenna can be given approximately as

$$\rho^S = \begin{cases} Q\delta(z' - dl)\delta(x)\delta(y) \\ -Q\delta(z' + dl)\delta(x)\delta(y) \end{cases} \tag{3.2.1}$$

where Q is the charge in coulomb and δ is the Dirac delta function.

The generalized electroacoustic and ionacoustic waves excited by a Hertzian dipole antenna can be obtained from equation (3.1.4) after the substitution of ρ^S from equation (3.2.1). Using the far zone approximations, the integral in equation (3.1.4) becomes

$$\int_{v'} \rho^S(\vec{r}\,') \frac{e^{-jk|\vec{r} - \vec{r}\,'|}}{|\vec{r} - \vec{r}\,'|} dv' = j2Q \frac{e^{-jkr}}{r}[\sin(kdl \cos\theta)] \tag{3.2.2}$$

where k is the propagation constant of a particular wave. For the generalized electroacoustic wave, we use k_2 to replace

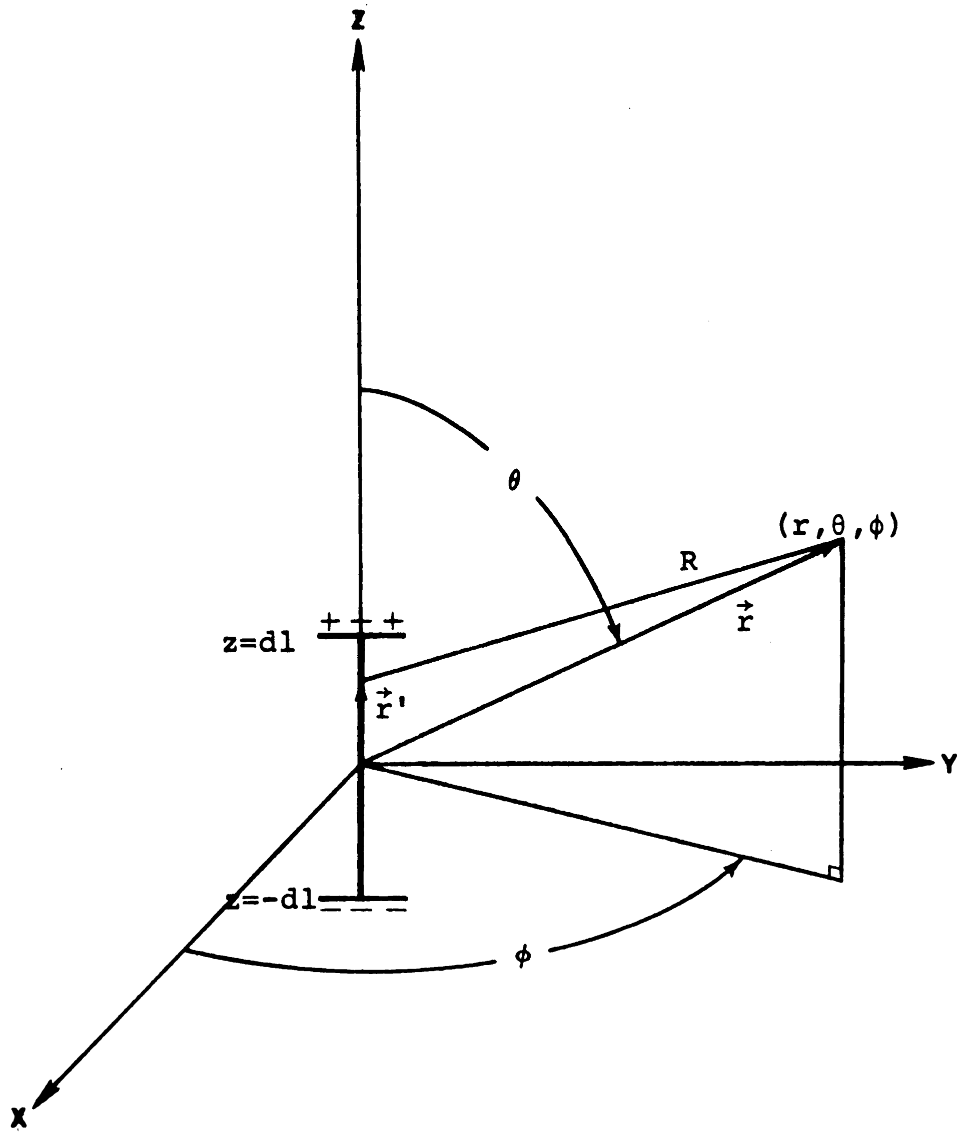

Figure 3.1 Geometry of a Hertzian dipole antenna.

k, while for the generalized ionacoustic wave we use k_1 to replace k. The term in the bracket in equation (3.2.2) will be used to calculate the radiation patterns of these plasma waves excited by the Hertzian dipole antenna.

3.2.2 Radiation Patterns of the Generalized Ionacoustic Wave (n_1 Wave)

The radiation pattern function of the generalized ion-acoustic wave can be obtained from equation (3.2.2) after replacing k by k_1. The pattern function can be expressed as

$$F_1(\theta) = \sin(k_1 dl \cos\theta) \quad . \tag{3.2.3}$$

Since $k_1/(\omega/V_i)$ has been calculated by using the computer for a xenon gas plasma, we can determine the value of k_1 by assuming the values of ω, T_e and T_e/T_i. dl is the antenna half length and is assigned for various values. The phase velocity of the generalized ionacoustic wave, V_{ph1}, at the low frequency range is approximated by $\sqrt{3k(T_e + T_i)/m_i}$ and is called V_A.

The results of some typical cases are plotted in Figures 3.2, 3.3 and 3.4 and their numerical results are given in Tables 1, 2 and 3 of Appendix C.

Figure 3.2 shows the radiation patterns of the generalized ionacoustic wave at various electron temperatures. Since the wave length in the plasma is $\lambda_p = V_{ph1}/f$, as T_e increases, λ_p increases; and consequently, the antenna becomes relatively smaller.

Figure 3.3 shows the radiation patterns of the

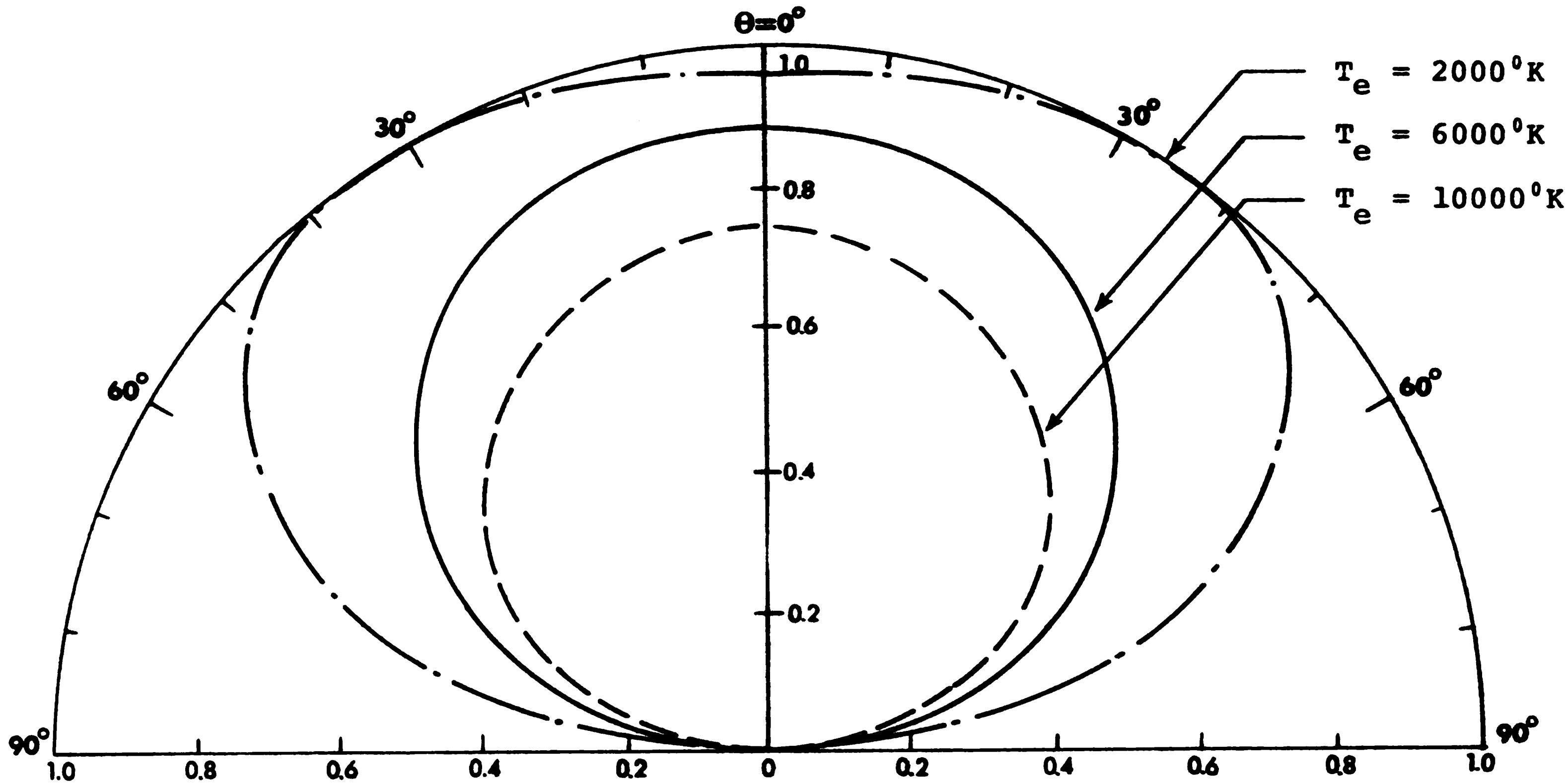

Figure 3.2 Radiation patterns of the generalized ionacoustic wave excited by a Hertzian dipole antenna for various electron temperatures. (f = 30 kHz, T_e/T_i = 10, dl = 1 cm)

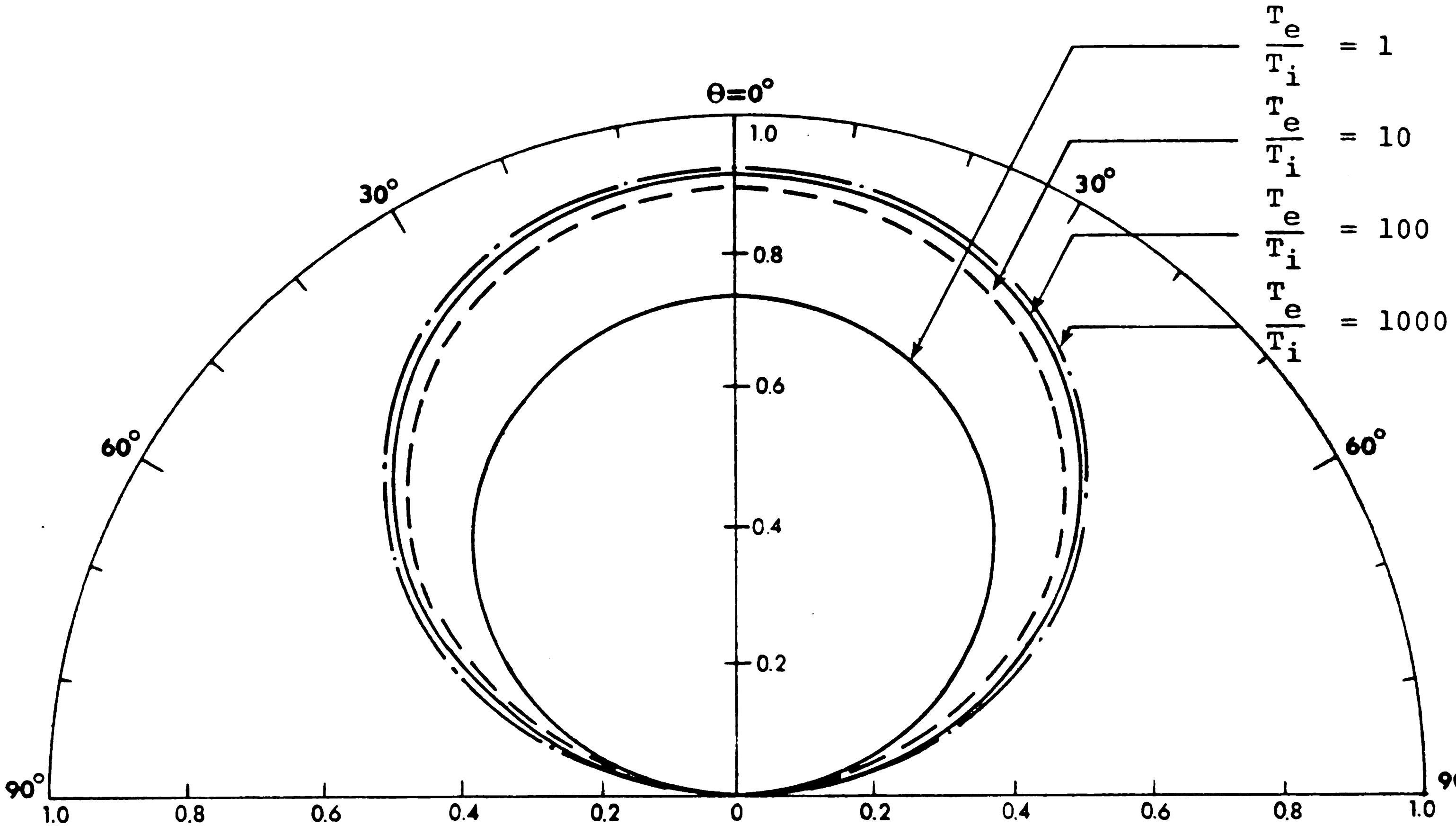

Figure 3.3 Radiation patterns of the generalized ionacoustic wave excited by a Hertzian dipole antenna for various ratios of electron temperature to ion temperature. (f = 30 kHz, T_e = 6000°K, dl = 1 cm)

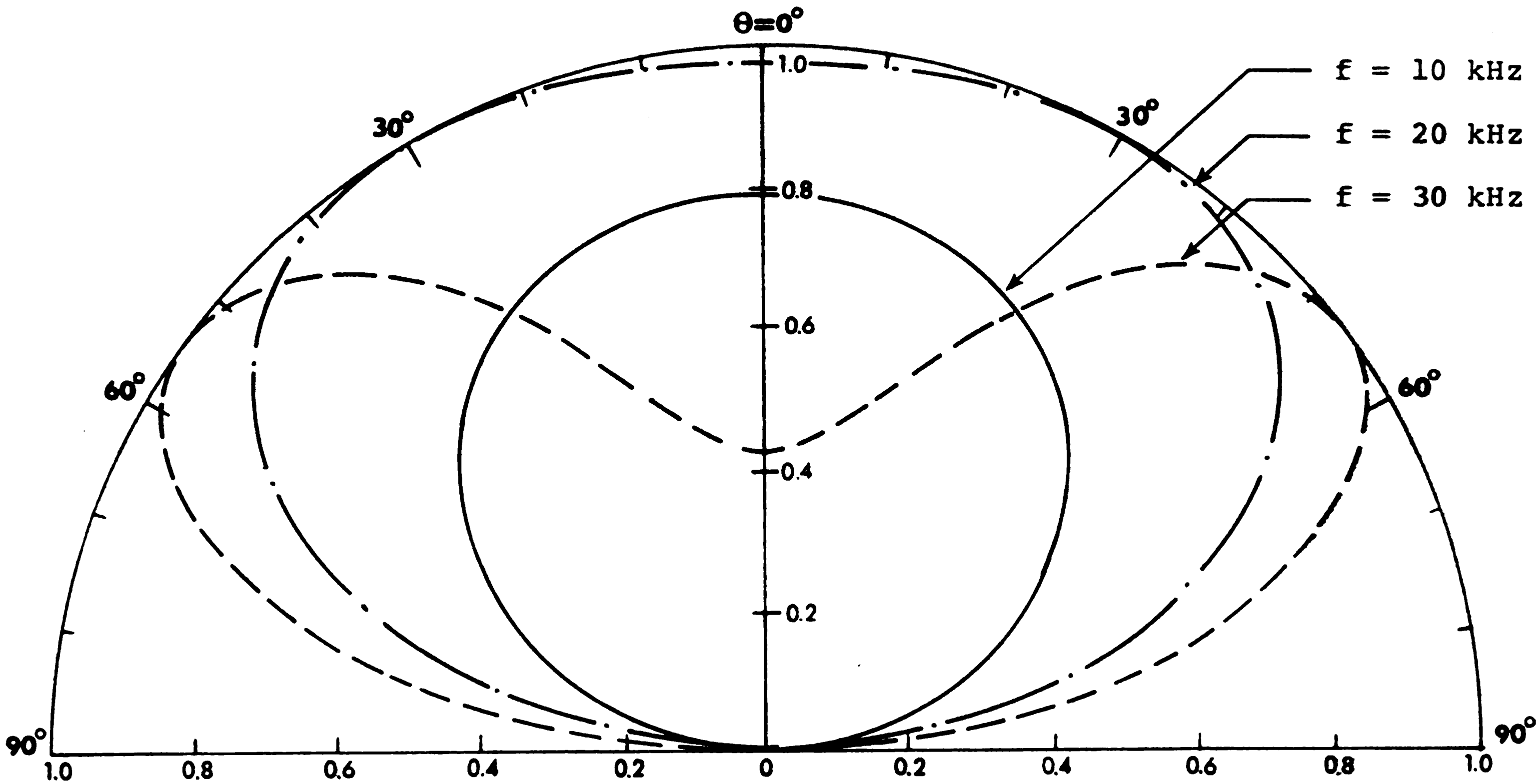

Figure 3.4 Radiation patterns of the generalized ionacoustic wave excited by a Hertzian dipole antenna for various antenna frequencies. (T_e = 6000°K, T_e/T_i = 10, dl = 2.5 cm)

generalized ionacoustic wave at various ratios of electron temperature to ion temperature. It is seen that the change in the ratio T_e/T_i does not affect the radiation patterns significantly.

Figure 3.4 shows the radiation patterns of the generalized ionacoustic wave at various antenna frequencies. It is seen that as the antenna frequency increases, the wavelength of the generalized ionacoustic wave decreases; as a result, the antenna becomes relatively larger.

3.2.3 Radiation Patterns of the Generalized Electroacoustic Wave (n_2 Wave)

The radiation pattern function of the generalized electroacoustic wave can be obtained from equation (3.2.2) after replacing k by k_2. The pattern function can be expressed as

$$F_2(\theta) = \sin(k_2 dl \cos\theta) \quad . \tag{3.2.4}$$

Since $k_2/(\omega/V_e)$ has been calculated by the computer for a xenon gas plasma, we can determine values of k_2 based on assumed values of ω, T_e and T_e/T_i. Some typical cases are chosen and plotted in Figures 3.5 and 3.6 and the corresponding numerical results are given in Tables 4 and 5 of Appendix C.

Figure 3.5 shows the radiation patterns of the excited generalized electroacoustic wave at various electron temperatures. It is seen that as T_e decreases, the phase velocity and the generalized electroacoustic wave length in the plasma

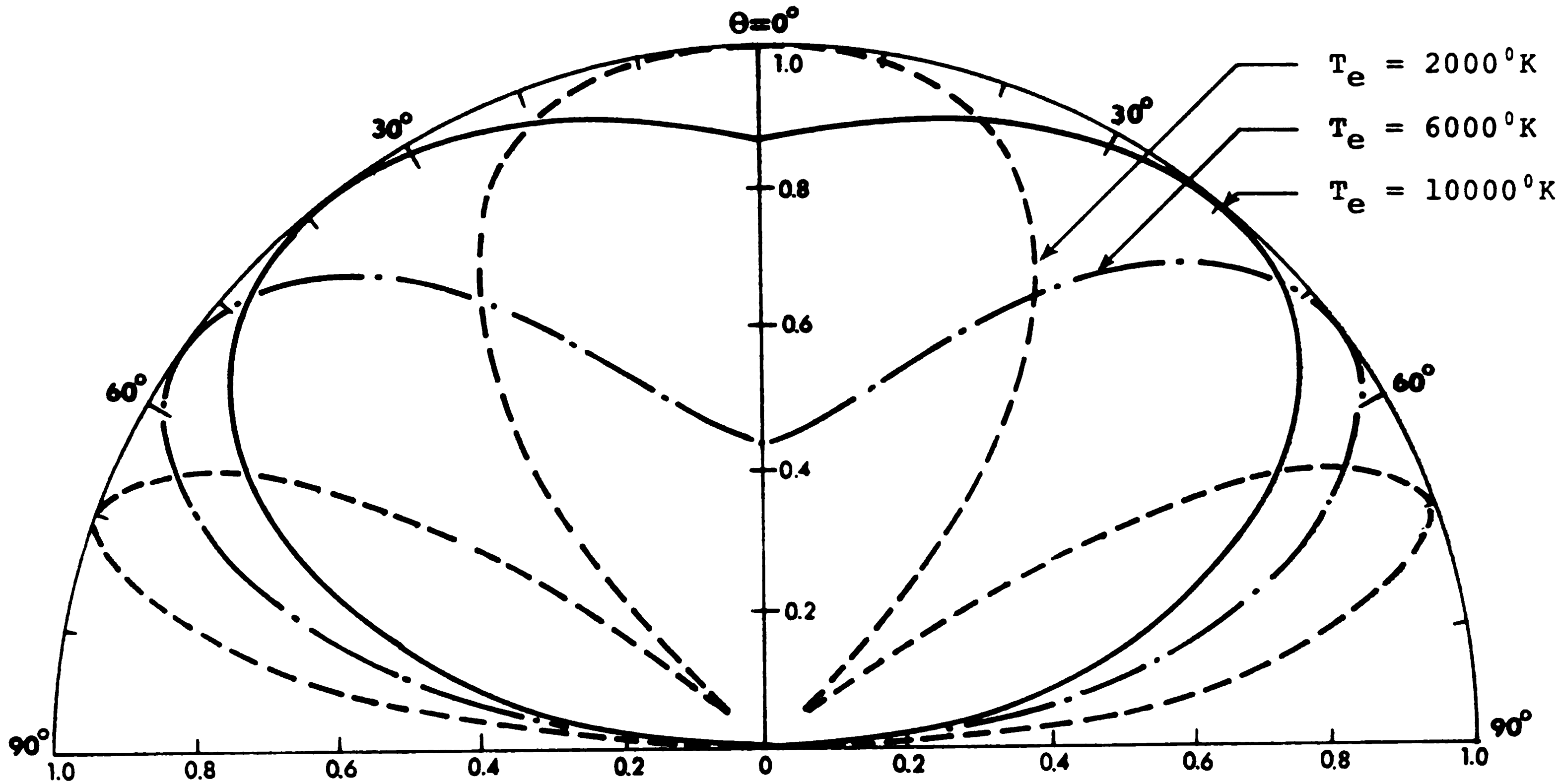

Figure 3.5 Radiation patterns of the generalized electroacoustic wave excited by a Hertzian dipole antenna for various electron temperatures.
(f = 1 GHz, T_e/T_i = 1 to 10^4, ω_e^2/ω^2 = 0.95, dl = 1 mm)

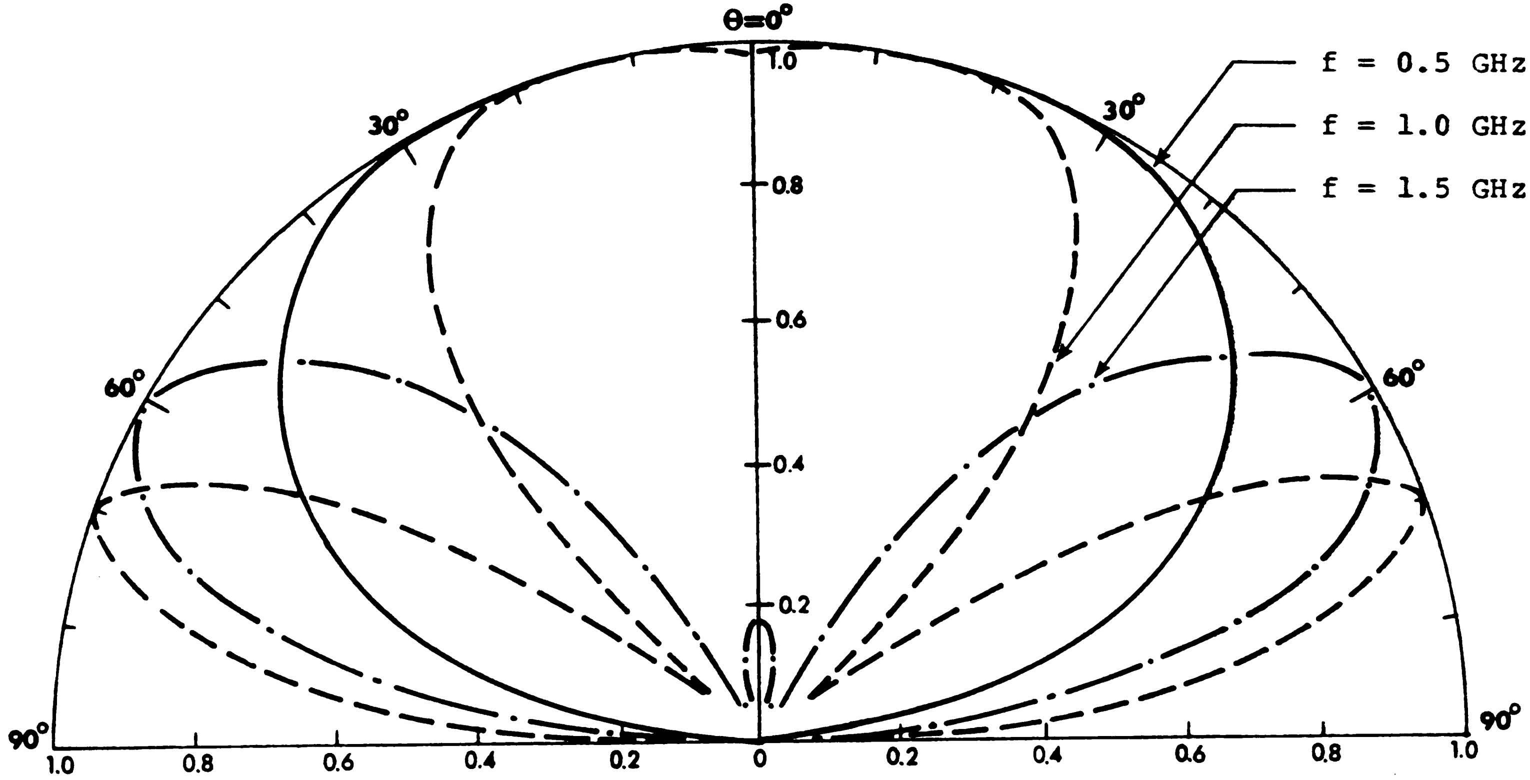

Figure 3.6 Radiation patterns of the generalized electroacoustic wave excited by a Hertzian dipole antenna for various antenna frequencies.
(T_e = 4000°K, T_e/T_i = 1 to 10°, ω_e^2/ω^2 = 0.95, dl = 1 mm)

decreases; and consequently, the antenna becomes relatively larger.

Figure 3.6 shows the radiation patterns of the excited electroacoustic wave at various antenna frequencies.

In both Figures 3.5 and 3.6, we choose the propagation constant, k_2, at the frequency of $\omega_e^2/\omega^2 = 0.95$. The reason for this choice is that the electroacoustic wave suffer less Landau damping when ω is close to ω_e and slightly higher than ω_e.

3.2.4 Radiation Patterns of the Electromagnetic Wave

The magnetic field in the plasma has been determined in Section 6 of Chapter 2 and is given by equation (2.6.10) as

$$\vec{B}(\vec{r}) = \frac{\mu_o}{4\pi} \nabla \times \int_{v'} \vec{J}^S(\vec{r}\,') \frac{e^{-jk_eR}}{R} dv' \qquad (3.2.5)$$

where k_e is the propagation constant of the electromagnetic wave in the plasma and is given as

$$k_e^2 = \omega^2\mu_o\varepsilon_o\left\{1 - \frac{\omega_e^2}{\omega^2 + \gamma_e^2} - \frac{\omega_i^2}{\omega^2 + \gamma_i^2} - j\left[\frac{\omega_e^2\gamma_e}{\omega(\omega^2 + \gamma_e^2)} + \frac{\omega_i^2\gamma_i}{\omega(\omega^2 + \gamma_i^2)}\right]\right\} ; \qquad (3.2.6)$$

$\vec{J}^S(\vec{r}\,')$ is the source current density and is given as

$$\vec{J}^S(\vec{r}\,') = \frac{1}{A}\hat{z} = I_o\hat{z} \qquad \text{for } -dl \le z \le dl \qquad (3.2.7)$$

for a Hertzian dipole antenna whose cross-sectional area is A.

R represents $|\vec{r} - \vec{r}'|$. Substituting equations (3.2.6) and (3.2.7) into equation (3.2.5) and using the far zone approximations, we have

$$\vec{B}(\vec{r}) = \frac{\mu_o I_o}{4\pi} \nabla \times \int_{-dl'}^{dl} \frac{e^{-jk_e(r - z'\cos\theta)}}{r} dz'\hat{z} \quad .$$

(3.2.8)

After evaluating the integral, using $\hat{z} = \hat{r}\cos\theta - \hat{\theta}\sin\theta$, taking the curl of the integral, neglecting $1/r^2$ terms and retaining only the $1/r$ term because of far zone approximation, equation (3.2.8) can be reduced to

$$\vec{B}(\vec{r}) \simeq \hat{\phi}\left(\frac{\mu_o I_o k_e dl}{2\pi}\right)\left(\frac{e^{-jk_e r}}{r}\right)\left[\frac{\sin(k_e dl \cos\theta)}{(k_e dl \cos\theta)}\right]\sin\theta \quad .$$

(3.2.9)

Considering dl as a small number, we have $[\sin(k_e dl \cos\theta)]/(k_e dl \cos\theta) \simeq 1$, and thus,

$$\vec{B}(\vec{r}) \simeq \hat{\phi}\left(\frac{\mu_o I_o k_e dl}{2\pi}\right)\left(\frac{e^{-jk_e r}}{r}\right)\sin\theta \quad . \qquad (3.2.10)$$

The electromagnetic component of $\vec{E}$ field in the plasma can be obtained from equation (2.7.7);

$$\vec{E}_{em} = \frac{1}{P}[(\gamma_e\gamma_i - \omega^2) + j\omega(\gamma_e + \gamma_i)](\nabla \times \vec{B}) \qquad (3.2.11)$$

where $P = \mu_o\varepsilon_o\{[\gamma_i(\omega_e^2 - \omega^2) + \gamma_e(\omega_i^2 - \omega^2)] + j\omega[\omega_e^2 + \omega_i^2 - \omega^2 + \gamma_e\gamma_i]\}$. For collisionless case, i.e.,

$\gamma_i = \gamma_e = 0$, equation (3.2.11) can be reduced to

$$\vec{E}_{em} = \frac{-j\omega}{\mu_o \varepsilon_o (\omega^2 - \omega_e^2 - \omega_i^2)} \nabla \times \vec{B} \qquad (3.2.12)$$

Using equation (3.2.10) in equation (3.2.12), and neglecting $1/r^2$ terms, we have

$$\vec{E}_{em} = \frac{\omega I_o k_e^2 dl}{2\pi\varepsilon_o (\omega^2 - \omega_e^2 - \omega_i^2)} \frac{e^{-jk_e r}}{r} \sin\theta \, \hat{\theta} \quad . \qquad (3.2.13)$$

Equation (3.2.13) is the electromagnetic component of $\vec{E}$ field in the plasma and the corresponding radiation pattern function can be expressed by

$$F_{em}(\theta) = \sin\theta \quad . \qquad (3.2.14)$$

Figure 3.7 is the radiation pattern of the electromagnetic component of the electric field in the plasma. It is seen from equation (3.2.14) that this pattern is independent of plasma parameters.

3.3 Disk Monopole Antenna

3.3.1 Geometry and Statement of the Problem

The geometrical configuration of a disk monopole antenna is shown in Figure 3.8 using a spherical coordinate system (r, θ, ϕ). A metallic disk of radius a is excited by a radio frequency signal source and is immersed in the plasma. It is assumed that the charge is uniformly distributed over

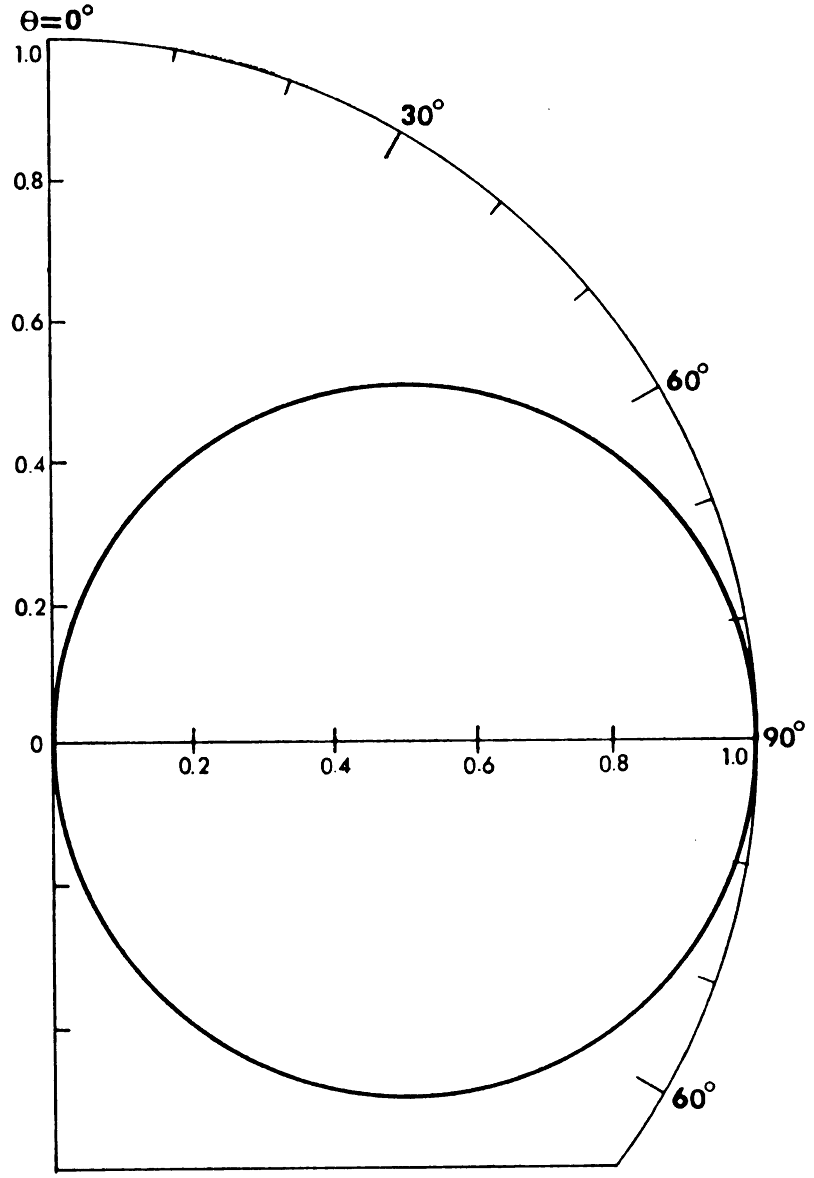

Figure 3.7 Radiation pattern of the electromagnetic wave excited by a Hertzian dipole antenna in a plasma.

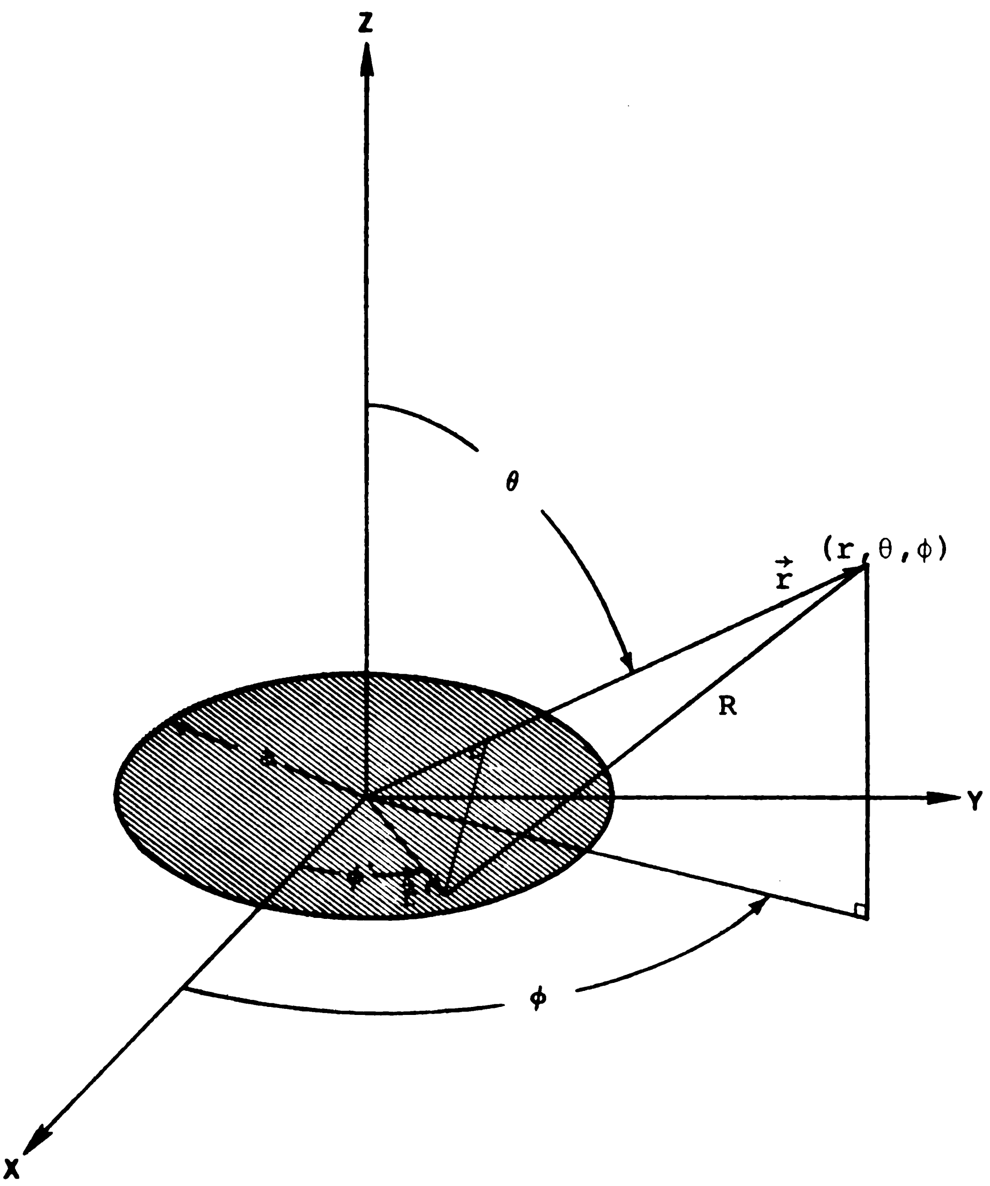

Figure 3.8 Geometry of a disk monopole antenna.

the disk surface. That is,

$$\rho^S_{s'} = \sigma_o \quad . \tag{3.3.1}$$

The generalized electroacoustic and ionacoustic waves excited by this antenna can be calculated by substituting equation (3.3.1) into equation (3.1.4). Using the far zone approximations, the integral in equation (3.1.4) becomes

$$\int_{s'} \sigma_o \frac{e^{-jk[r - r'\sin\theta\cos(\phi - \phi')]}}{r} ds' \quad . \tag{3.3.2}$$

Let ds' = r'dϕ'dr', equation (3.3.2) reduces to

$$\frac{\sigma_o e^{-jkr}}{r} \int_0^a \int_0^{2\pi} e^{jkr'\sin\theta\cos(\phi - \phi')} r'd\phi'dr' \quad . \tag{3.3.3}$$

Since the geometry has cylindrical symmetry, we choose the observation point in the x-z plane (i.e. $\phi = 0$) to simplify the calculation. Equation (3.3.3) then becomes

$$\frac{\sigma_o e^{-jkr}}{r} \int_0^a \int_0^{2\pi} e^{jkr'\sin\theta\cos\phi'} d\phi' r'dr' \quad . \tag{3.3.4}$$

Let us introduce the definite integral for the Bessel function,

$$J_n(\mu) = \frac{1}{2\pi j^n} \int_0^{2\pi} e^{j\mu\cos\phi'} \cos(n\phi')d\phi' \quad . \tag{3.3.5}$$

With n = 0 and μ = kr'sinθ, equation (3.3.4) can be written as

$$\frac{\sigma_o e^{-jkr}}{r} \int_0^a 2\pi J_o(kr'\sin\theta) r'dr' \quad . \tag{3.3.6}$$

Changing the variable from r' to μ, the integral in equation (3.3.6) becomes

$$\frac{2\pi}{(k\ \sin\theta)^2}\int_0^{\mu=ka\ \sin\theta} \mu J_o(\mu)\,d\mu \qquad (3.3.7)$$

where $J_o(\mu)$ is the Bessel function of zero order with argument μ. The recurrent equation of the Bessel function is

$$\frac{d}{d\mu}(\mu^n J_n) = \mu^n J_{n-1}, \text{ with } n = 1 \quad \text{we have}$$

$$\frac{d}{d\mu}(\mu J_1) = \mu J_o \quad \text{or}$$

$$\mu J_1 = \int \mu J_o d\mu.$$

Thus equation (3.3.7) is transformed to

$$\frac{2\pi}{(k\ \sin\theta)^2}\Big[\mu J_1(\mu)\Big]_0^{\mu=ka\ \sin\theta}$$

hence, equation (3.3.6) becomes

$$\frac{2\pi a^2 \sigma_o e^{-jkr}}{r}\left[\frac{J_1(ka\ \sin\theta)}{ka\ \sin\theta}\right]$$

or

$$n(\vec{r}) = \left(\frac{-s}{4\pi e}\right)\left(\frac{2\pi a^2 \sigma_o e^{-jkr}}{r}\right)\left[\frac{J_1(ka\ \sin\theta)}{ka\ \sin\theta}\right] \quad . \qquad (3.3.8)$$

The term in the bracket of equation (3.3.8) will be used to calculate the radiation patterns of the plasma waves excited by a disk monopole antenna.

3.3.2 Radiation Patterns of the Generalized Ionacoustic Wave (n_1 Wave)

The radiation pattern function of the generalized ion-acoustic wave can be obtained from equation (3.3.8) by replacing k by k_1. That is,

$$F_1(\theta) = \frac{J_1(k_1 a \sin\theta)}{k_1 a \sin\theta} \quad . \tag{3.3.9}$$

The numerical values of k_1 for various T_e, T_e/T_i and antenna frequencies are calculated and are given in Tables 6, 7 and 8 of Appendix C.

Figure 3.9 shows the radiation patterns of the generalized ionacoustic wave at various electron temperatures. It is seen that as the electron temperature becomes higher, the pattern becomes broader. This is due to the fact that as T_e increases, the antenna becomes smaller in terms of the ionacoustic wavelength.

Figure 3.10 shows the radiation patterns of the generalized ionacoustic wave for various ratios of electron temperature to ion temperature. The change in the ratio T_e/T_i does not affect significantly on the radiation patterns.

Figures 3.11 to 3.13 are the radiation patterns of the generalized ionacoustic wave at various antenna frequencies.

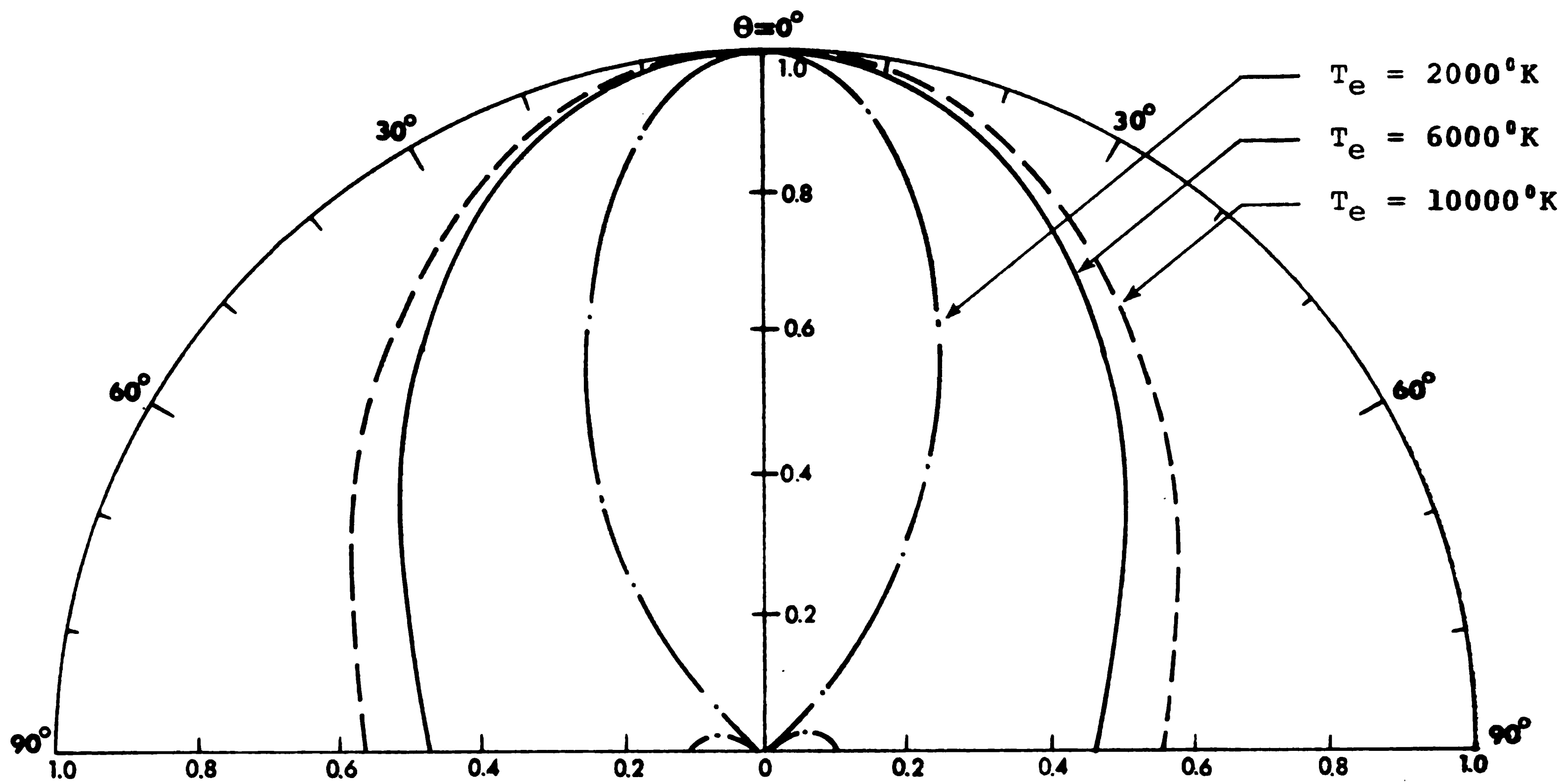

Figure 3.9 Radiation patterns of the generalized ionacoustic wave excited by a disk monopole antenna for various electron temperatures.
(f = 30 kHz, T_e/T_i = 100, a = 2.25 cm)

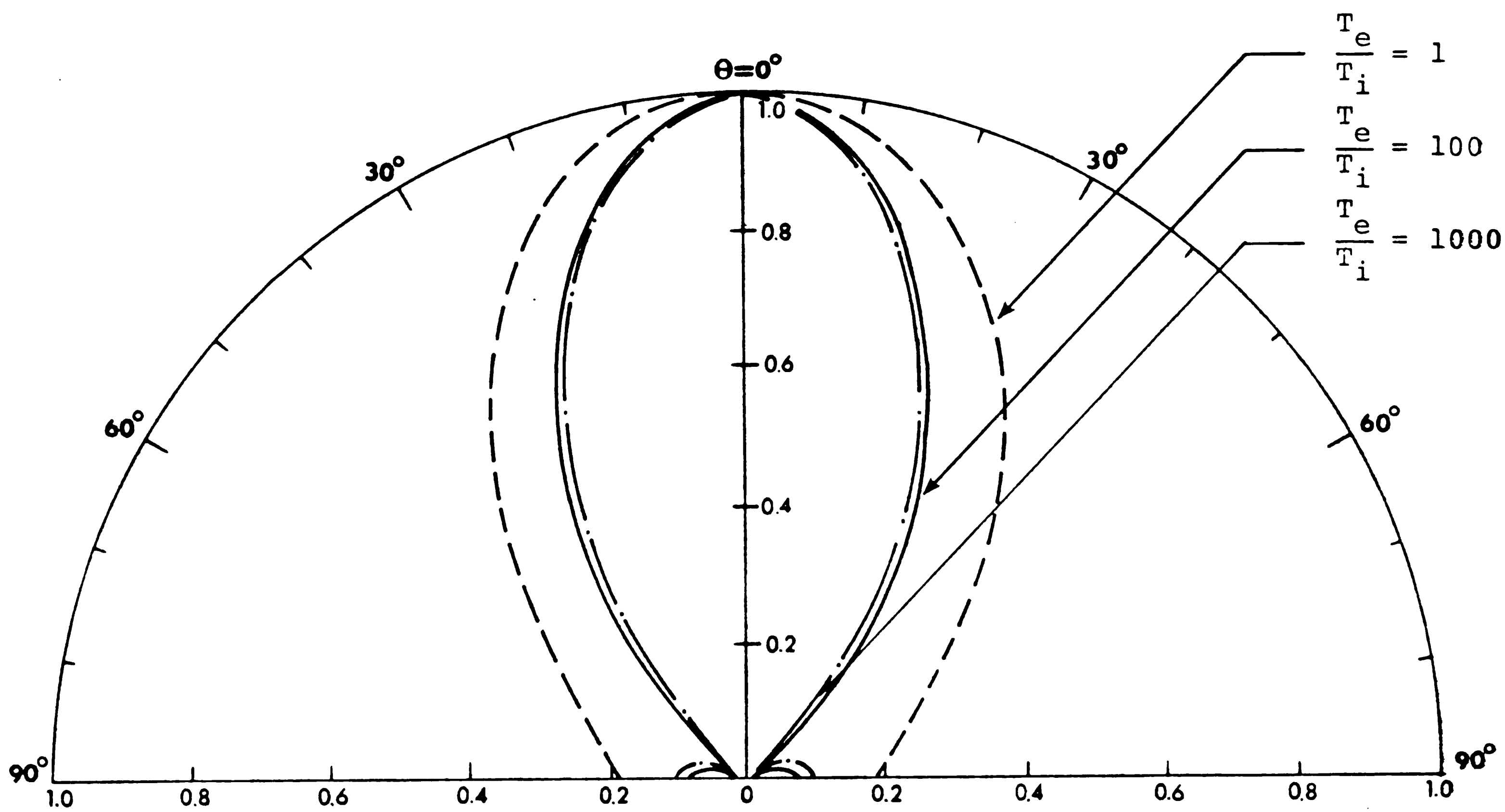

Figure 3.10 Radiation patterns of the generalized ionacoustic wave excited by a disk monopole antenna for various ratios of electron temperature to ion temperature. (f = 30 kHz, T_e = 2000°K, a = 2.25 cm)

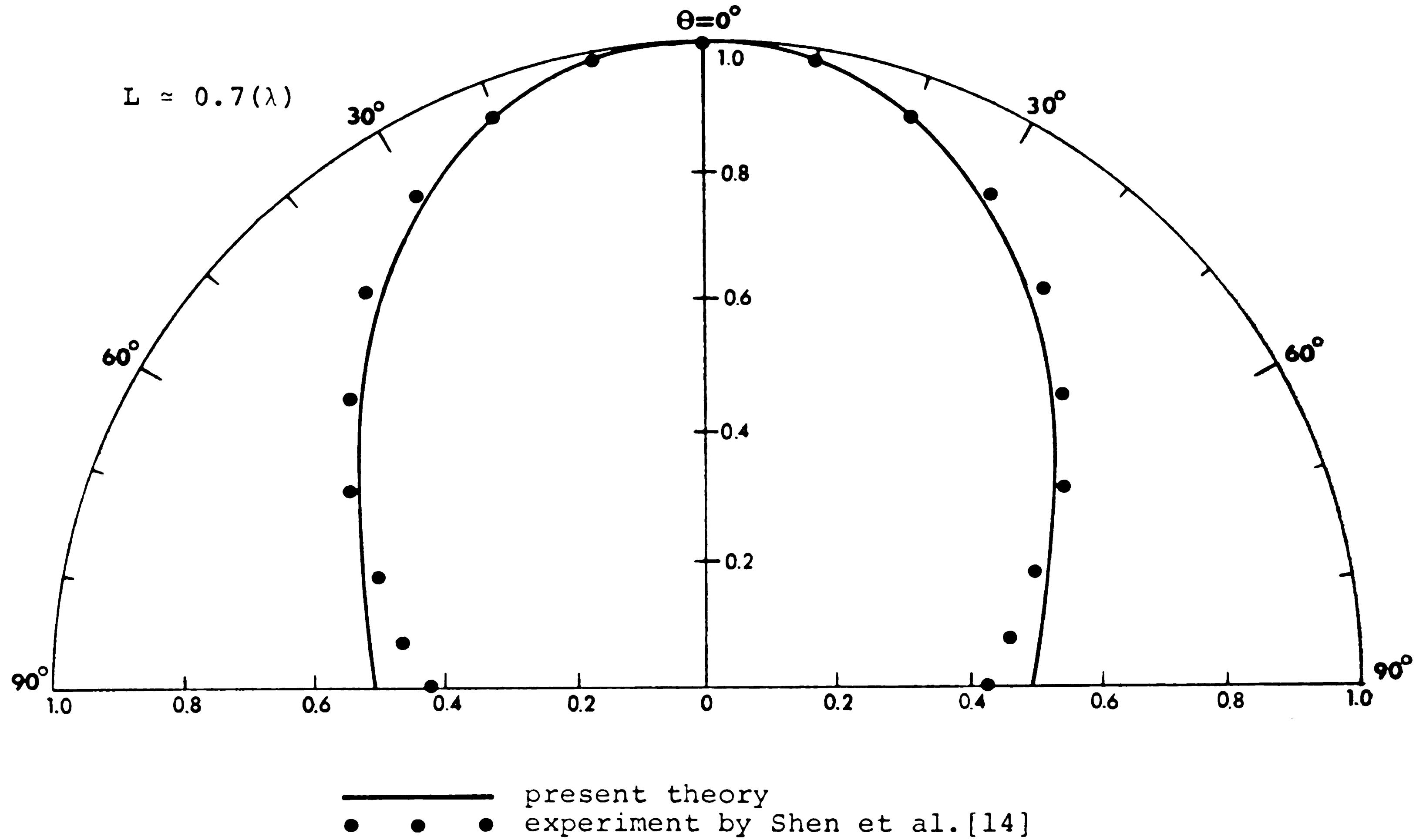

Figure 3.11 Radiation patterns of the generalized ionacoustic wave excited by a disk monopole antenna.
(f = 16.3 kHz, phase velocity V_A = 1.05 x 10^3m/sec, T_e = T_i ≈ 1200°K, a = 2.25 cm)

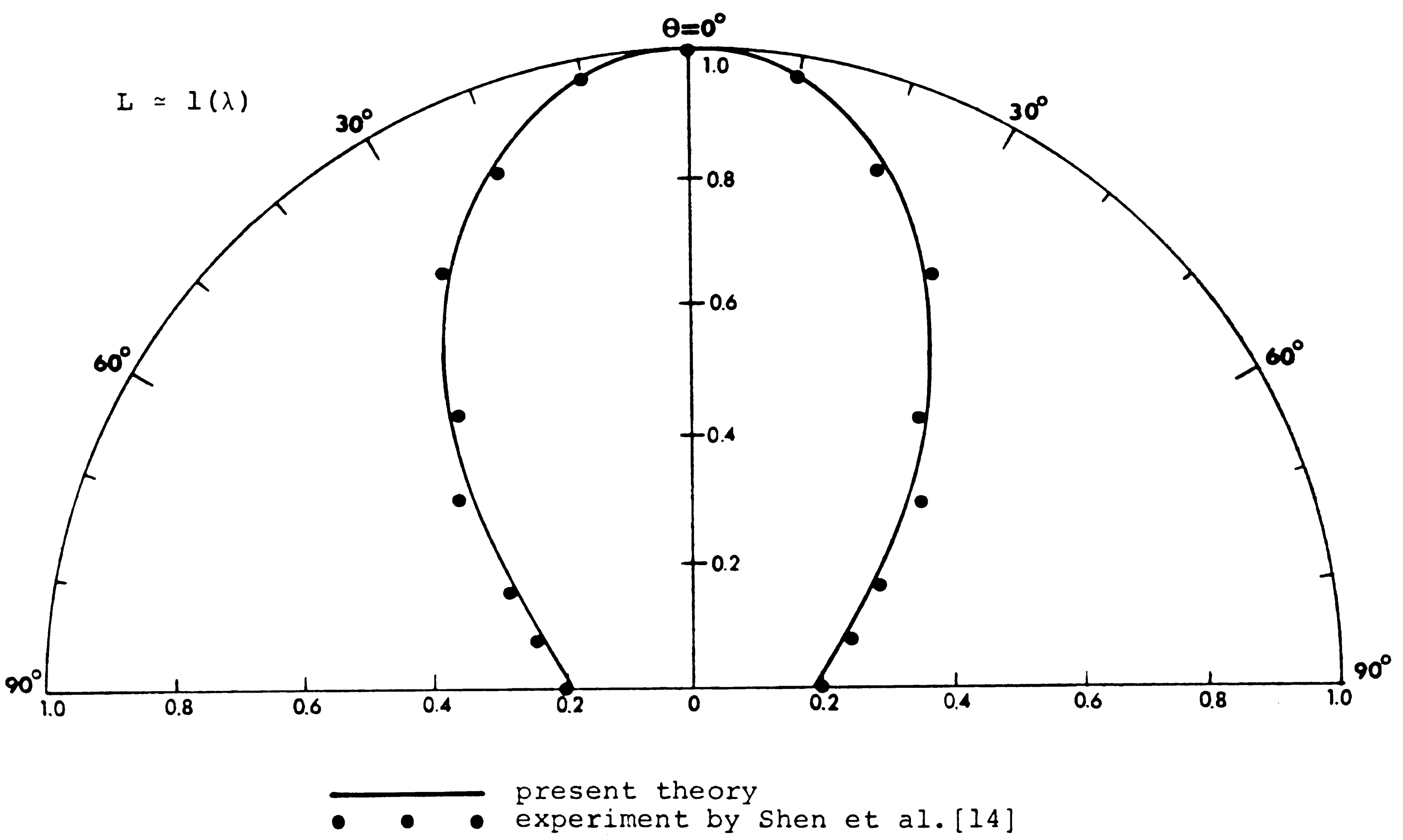

Figure 3.12 Radiation patterns of the generalized ionacoustic wave excited by a disk monopole antenna.
(f = 23.3 kHz, phase velocity $V_A = 1.05 \times 10^3$ m/sec, $T_e = T_i \simeq 1200^0$K, a = 2.25 cm)

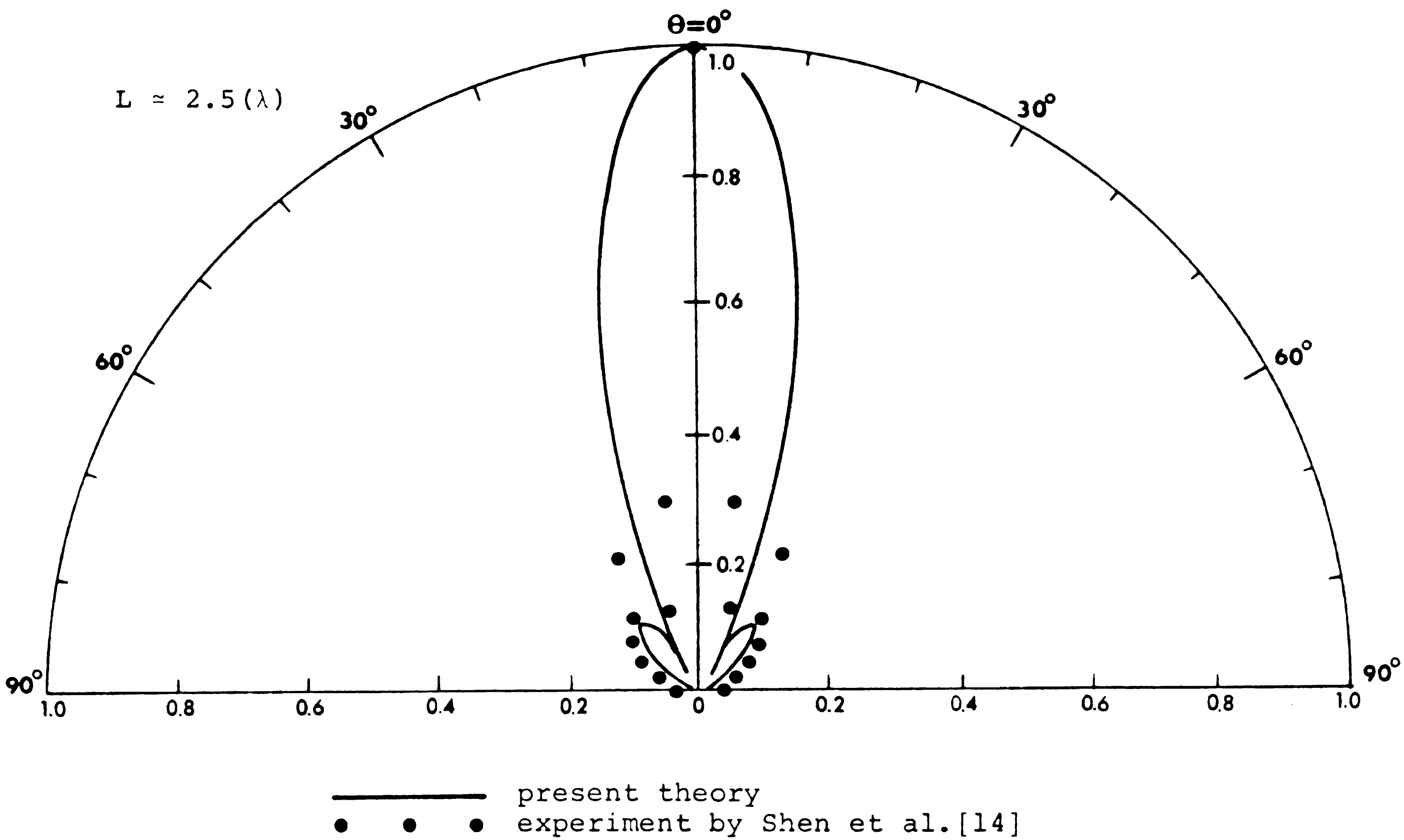

Figure 3.13 Radiation patterns of the generalized ionacoustic wave excited by a disk monopole antenna.
(f = 58.3 kHz, phase velocity $V_A = 1.05 \times 10^3$ m/sec, $T_e = T_i \simeq 1200^0$K, a = 2.25 cm)

We choose the phase velocity of the generalized ionacoustic wave, V_A, as 1.05 x 10^3 meter/sec.; the diameter of the disk antenna, 2a, as 4.5 cm and the normalized antenna length, L, (antenna length with respect to the generalized ionacoustic wavelength, i.e., $L = 2a/(V_A/f)$) as 0.7 (λ), 1 (λ), 2.5 (λ). In these cases, our radiation patterns agree very closely with the experimental result of Shen et al.[14].

3.3.3 Radiation Patterns of the Generalized Electroacoustic Wave (n_2 Wave)

The radiation pattern function of the generalized electroacoustic wave can be obtained from equation (3.3.8) by replacing k by k_2. That is,

$$F_2(\theta) = \frac{J_1(k_2 a \sin\theta)}{k_2 a \sin\theta} \quad . \tag{3.3.10}$$

The numerical values of k_2 are calculated and are given in Table 9 of Appendix C.

Figures 3.14 and 3.15 are the radiation patterns of the generalized electroacoustic wave. We choose (1) $\gamma_e/\omega = 0$ for simplification, (2) $\omega_e^2/\omega^2 = 0.95$ such that Landau damping is small, (3) $T_e/T_i \simeq 1$ to 10^4, (4) the antenna frequency f = 17.5 MHz, and (5) L = 0.6 (λ) and 1.1 (λ) respectively in these two figures. The radiation patterns for T_e between 2000°K and 4000°K agree very closely with the experimental results of Nakamura et al.[12] who used the grid with the plate as an antenna.

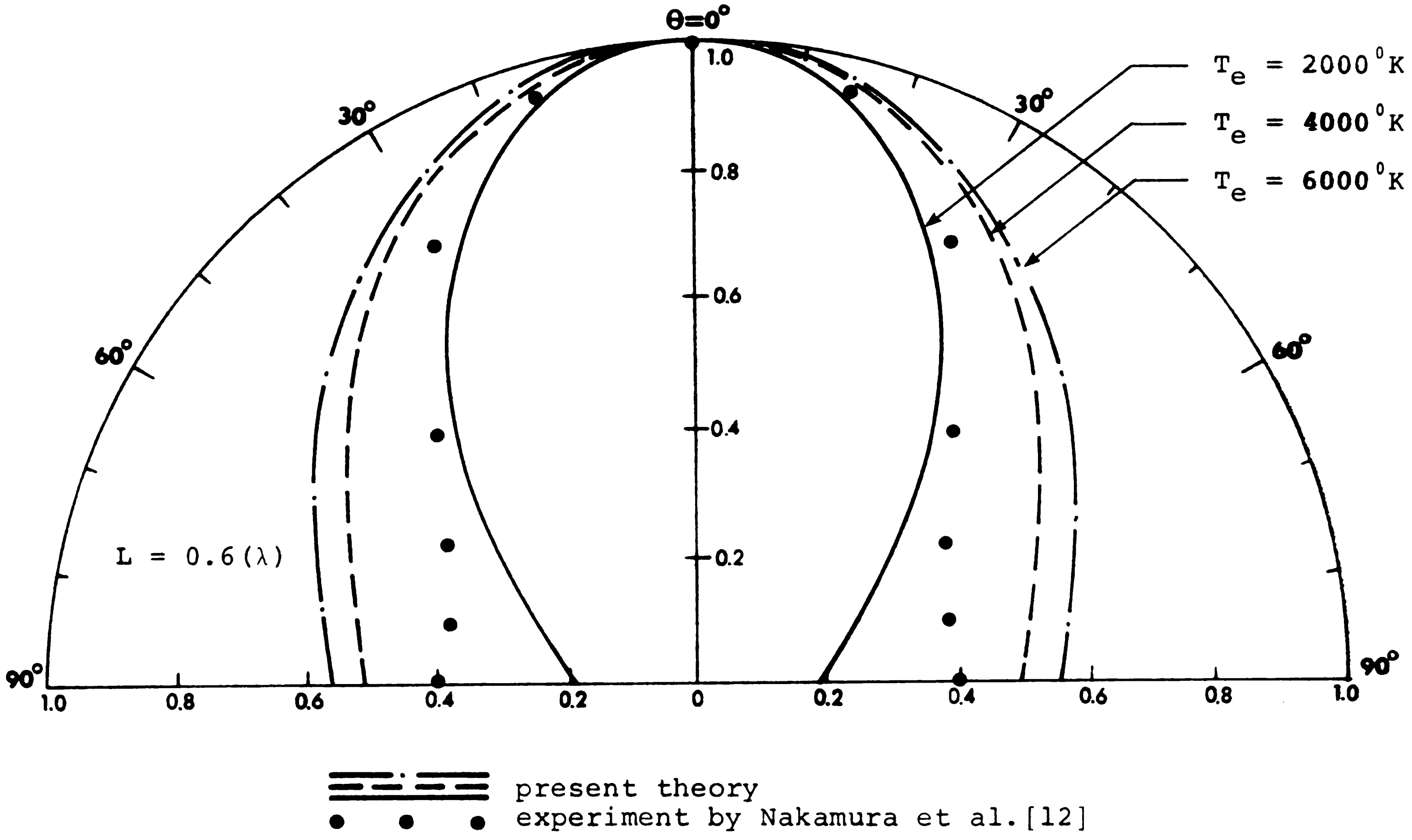

Figure 3.14 Radiation patterns of the generalized electroacoustic wave excited by a disk monopole antenna for various electron temperatures. (f = 17.5 MHz, λ = 13.1 cm, $\omega_e^2/\omega^2 = 0.95$, $\gamma_e/\omega = 0$, T_e/T_i = 1 to 10^4, $2a = 0.6\ \lambda$)

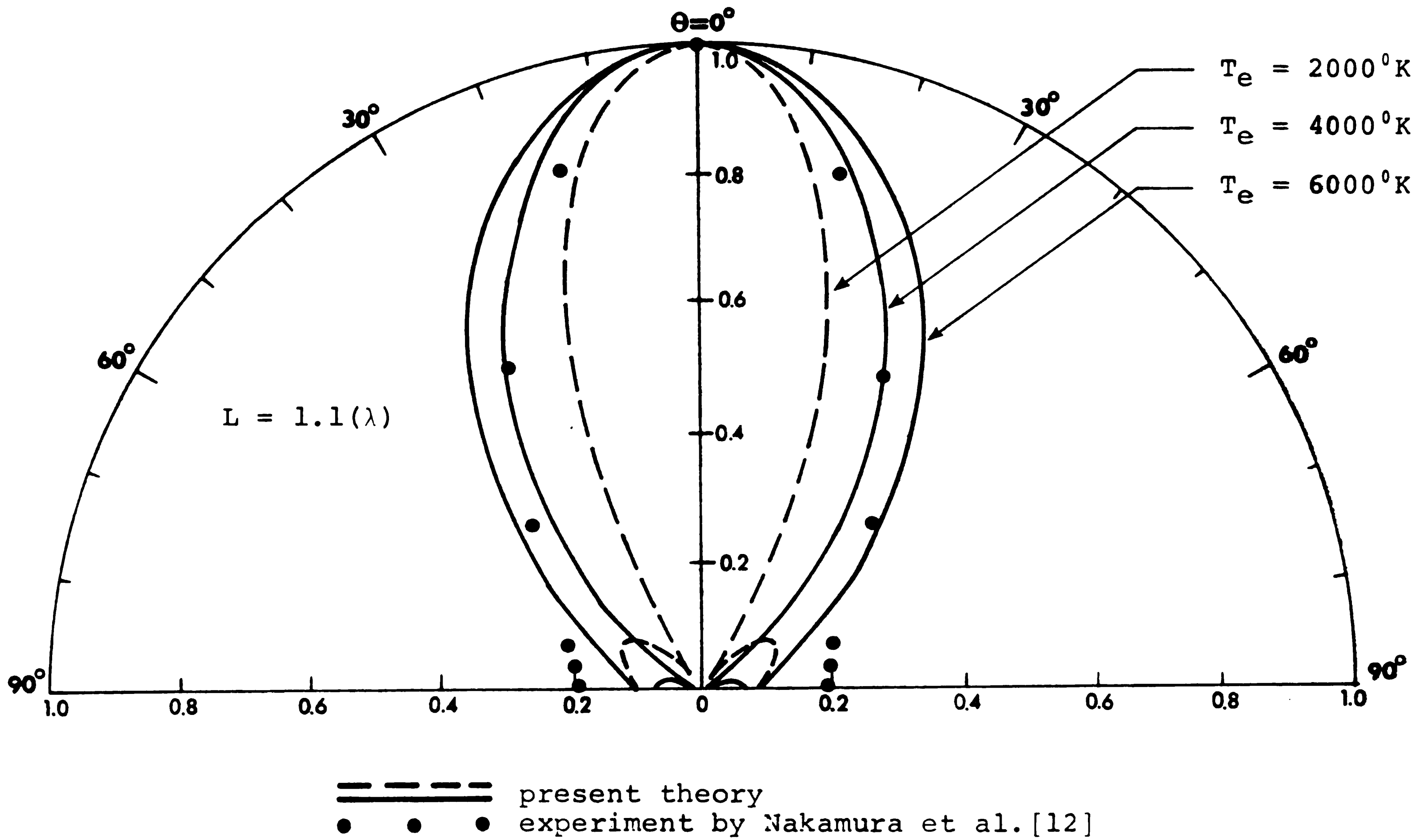

Figure 3.15 Radiation patterns of the generalized electroacoustic wave excited by a disk monopole antenna for various electron temperatures. (f = 17.5 MHz, λ = 13.1 cm, ω_e^2/ω^2 = 0.95, γ_e/ω = 0, $T_e/T_i \simeq 1$ to 10^4, $2a$ = 1.1 λ)

3.4 Disk Dipole Antenna

3.4.1 Geometry and Statement of the Problem

The geometrical configuration of a disk dipole antenna is shown in Figure 3.16 using a spherical coordinate system (r, θ, ϕ). The antenna consists of two half circular metallic disks of radius a is immersed in the plasma. The antenna is excited by a radio frequency signal source and the charge distribution on the antenna can be given as

$$\rho^S = \begin{cases} \sigma_o & \text{for } 0 \leq \phi' \leq \pi \\ -\sigma_o & \text{for } \pi \leq \phi' \leq 2\pi \end{cases} \tag{3.4.1}$$

where σ_o is the surface charge density.

The generalized electroacoustic and ionacoustic waves excited by this antenna can be calculated by substituting equation (3.4.1) into equation (3.1.4). Using the far zone approximations and with $ds' = r'd\phi'dr'$, the integral becomes

$$\frac{\sigma_o e^{-jkr}}{r}\left[\int_{\phi'=0}^{\pi}\int_{r'=0}^{a} e^{jkr'\sin\theta\cos(\phi - \phi')} r'dr'd\phi' - \int_{\phi'=\pi}^{2\pi}\int_{r'=0}^{a} e^{jkr'\sin\theta\cos(\phi - \phi')} r'dr'd\phi'\right] .$$

Assuming that the observation point is in the y-z plane $(\phi = \pi/2)$, we have

$$\frac{\sigma_o e^{-jkr}}{r}\left[\int_0^a r'dr'\int_0^{\pi} e^{jkr'\sin\theta\sin\phi'} d\phi' - \int_0^a r'dr'\int_{\pi}^{2\pi} e^{jkr'\sin\theta\sin\phi'} d\phi'\right] . \tag{3.4.2}$$

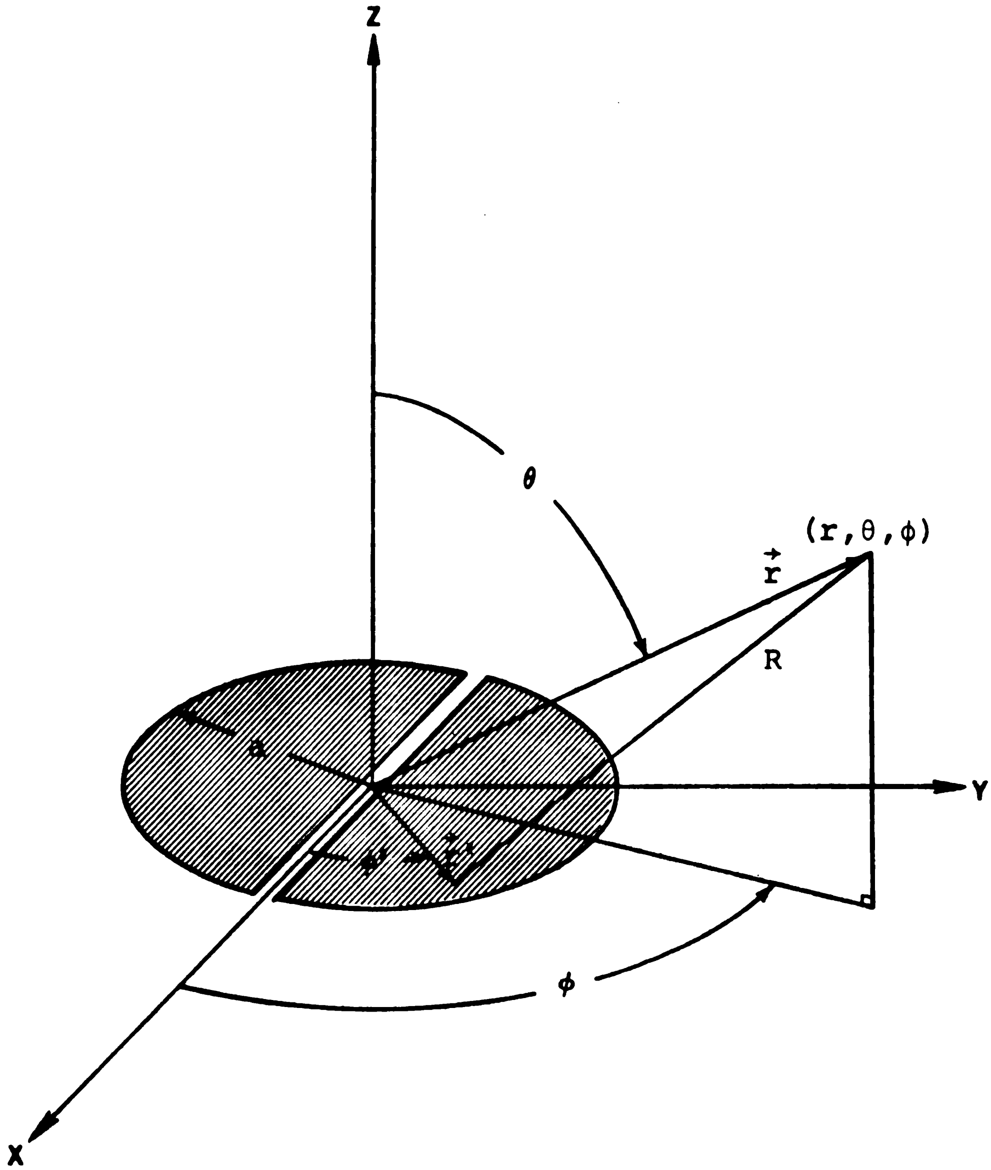

Figure 3.16 Geometry of a disk dipole antenna.

Let $I_1 = \int_{\pi}^{2\pi} e^{jkr'\sin\theta\sin\phi'} d\phi'$ and replace the variable ϕ' with $\beta' = \phi' - \pi$, the integral becomes

$$I_1 = \int_0^{\pi} e^{-jkr'\sin\theta\sin\beta'} d\beta' \quad .$$

Since β' is an independant variable, we can replace β' by ϕ' again and arrive at

$$I_1 = \int_0^{\pi} e^{-jkr'\sin\theta\sin\phi'} d\phi' \quad . \tag{3.4.3}$$

Substituting equation (3.4.3) into equation (3.4.2), we have

$$\frac{\sigma_o e^{-jkr}}{r} \int_0^a r'dr' \int_0^{\pi} \left[e^{jkr'\sin\theta\sin\phi'} - e^{-jkr'\sin\theta\sin\phi'}\right] d\phi'$$

$$= \frac{j2\sigma_o e^{-jkr}}{r} \int_0^a r'dr' \int_0^{\pi} \sin(kr'\sin\theta\sin\phi')d\phi' \quad . \tag{3.4.4}$$

Let $I_2 = \int_0^{\pi} \sin(kr'\sin\theta\sin\phi')d\phi'$. After replacing $kr'\sin\theta$ by Z and ϕ' by $(\psi + \pi/2)$ such that $\sin\phi' = \cos\psi$, the integral becomes

$$I_2 = \int_{-\pi/2}^{\pi/2} \sin(Z\cos\psi)d\psi$$

$$= 2\int_0^{\pi/2} \sin(Z\cos\psi)d\psi,$$

because the integrand is an even function.

The Struve function is defined by the equation

$$H_\nu(Z) = \frac{2\left(\frac{1}{2}Z\right)^\nu}{\sqrt{\pi}\,\Gamma(\nu + \frac{1}{2})} \int_0^{\pi/2} \sin(Z\cos\phi)\sin^{2\nu}\phi\, d\phi \quad .$$

For $\nu = 0$, we have

$$H_o(Z) = \frac{2}{\pi} \int_0^{\pi/2} \sin(Z\cos\phi)d\phi \quad .$$

Thus, I_2 can be expressed by the Struve function as

$$I_2 = \pi H_o(Z) \qquad \text{or}$$

$$= \pi H_o(kr'\sin\theta) \quad . \tag{3.4.5}$$

Substituting equation (3.4.5) into equation (3.4.4), we have

$$\frac{j2\sigma_o e^{-jkr}}{r} \int_0^a \pi H_o(kr'\sin\theta)r'dr' \quad . \tag{3.4.6}$$

Let $I_3 = \int_0^a H_o(kr'\sin\theta)r'dr'$ and replace the variable $kr'\sin\theta$ by Z again, we have

$$I_3 = \int_0^{ka\ \sin\theta} \frac{H_o(Z)ZdZ}{(k\ \sin\theta)^2}$$

$$= \frac{1}{(k\ \sin\theta)^2} \int_0^{ka\ \sin\theta} H_o(Z)ZdZ \quad . \tag{3.4.7}$$

The recurrent equation of the Struve function is

$$\frac{d}{dZ}(Z^\nu H_\nu) = Z^\nu H_{\nu-1}, \text{ or}$$

$$\frac{d}{dZ}(ZH_1) = ZH_o \qquad \text{for } \nu = 1, \text{ or}$$

$$ZH_1 = \int ZH_o dZ \quad . \tag{3.4.8}$$

Substituting equation (3.4.8) into equation (3.4.7), we obtain

$$I_3 = \frac{a^2 H_1(ka \sin\theta)}{ka \sin\theta} \quad .$$

Then equation (3.4.6) or the integral of equation (3.1.4) becomes

$$\frac{j2\pi a^2 \sigma_o e^{-jkr}}{r} \left[\frac{H_1(ka \sin\theta)}{ka \sin\theta}\right] \quad . \tag{3.4.9}$$

The term in the bracket will be used to calculate the radiation patterns of the plasma waves excited by a disk dipole antenna.

3.4.2 Radiation Patterns of the Generalized Ionacoustic Wave (n_1 Wave)

The radiation pattern function of the generalized ionacoustic wave can be obtained from equation (3.4.9) by replacing k by k_1. That is,

$$F_1(\theta) = \frac{H_1(k_1 a \sin\theta)}{k_1 a \sin\theta} \quad . \tag{3.4.10}$$

The results of some typical cases are plotted in Figures 3.17 to 3.21 and their numerical results are given in Tables 10, 11 and 12 of Appendix C.

Figure 3.17 shows the radiation patterns of the generalized ionacoustic wave at various electron temperatures.

Figure 3.18 shows the radiation patterns of the

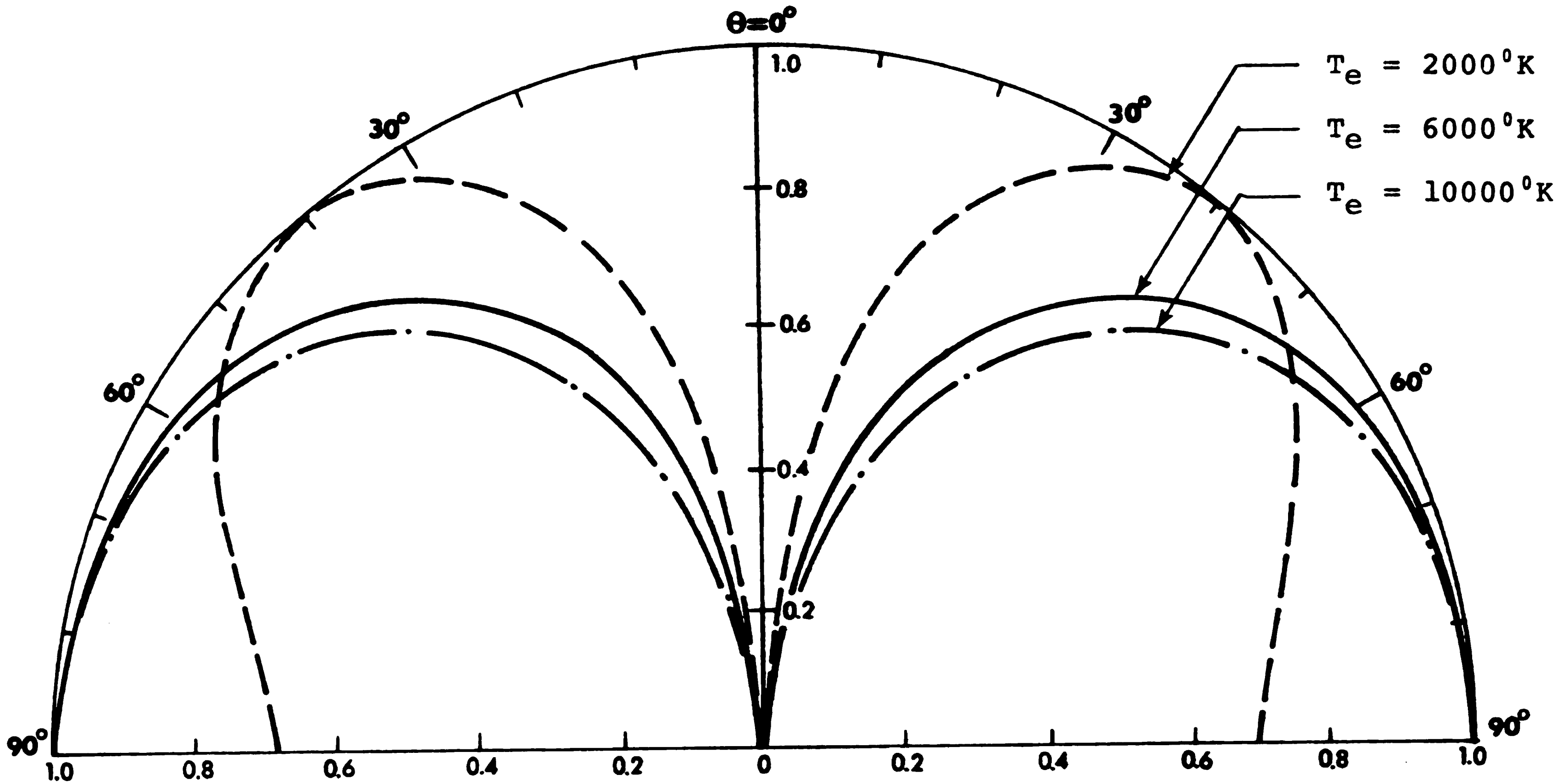

Figure 3.17 Radiation patterns of the generalized ionacoustic wave excited by a disk dipole antenna for various electron temperatures. (f = 30 kHz, T_e/T_i = 10, a = 2.25 cm)

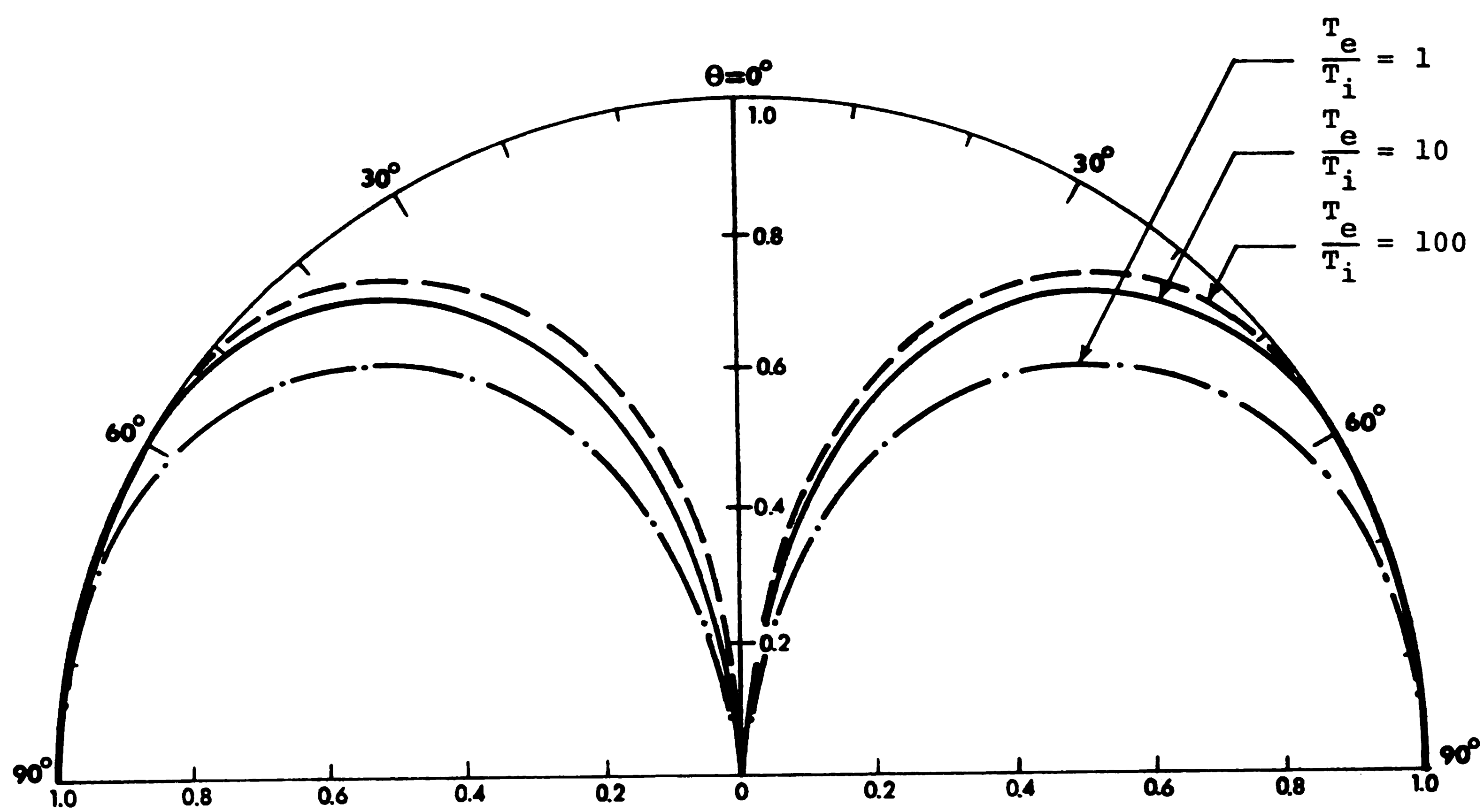

Figure 3.18 Radiation patterns of the generalized ionacoustic wave excited by a disk dipole antenna for various ratios of electron temperature to ion temperature. ($f = 30$ kHz, $T_e = 4000^0$K, $a = 2.25$ cm)

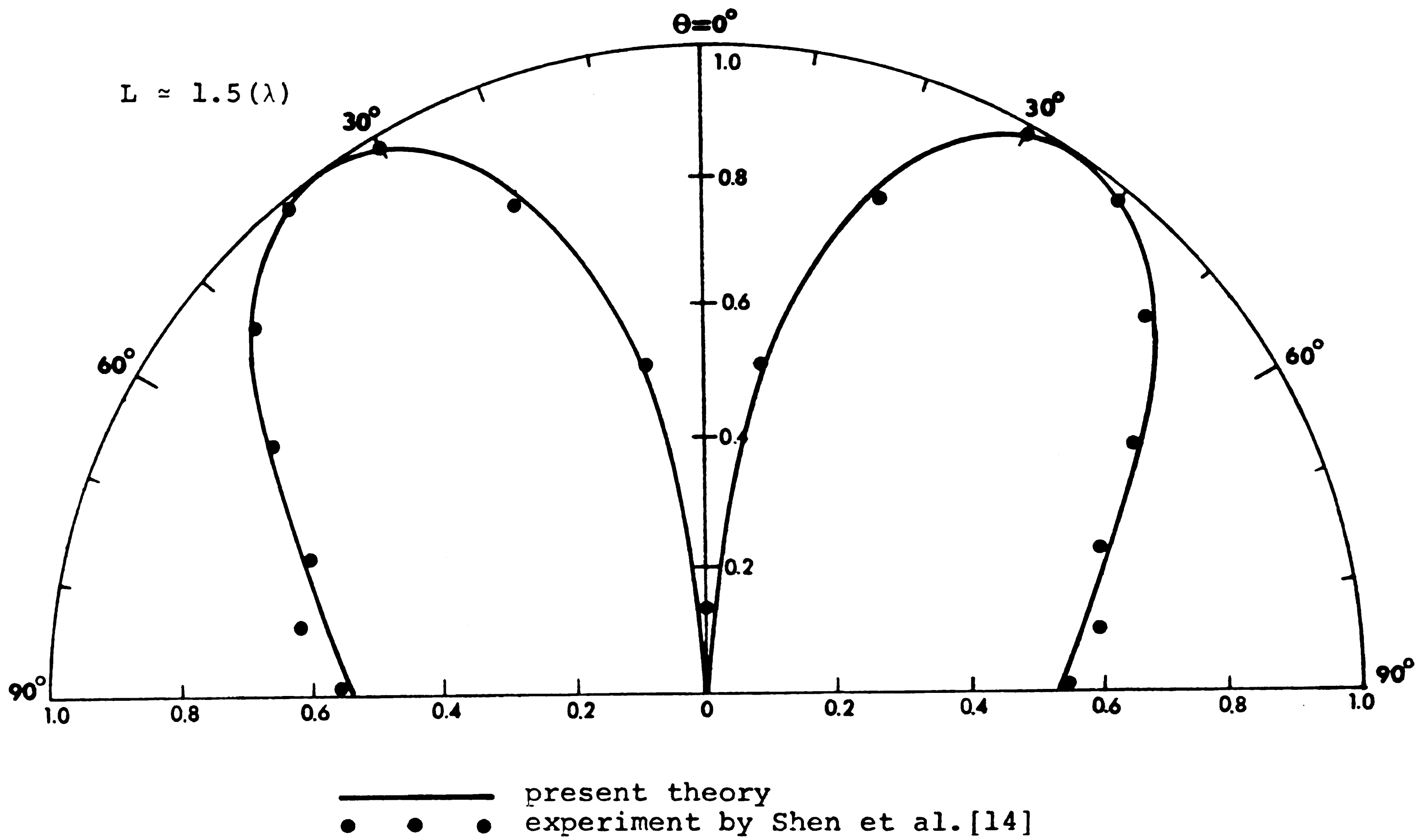

Figure 3.19 Radiation patterns of the generalized ionacoustic wave excited by a disk dipole antenna.
(f = 35 kHz, phase velocity $V_A = 1.05 \times 10^3$ m/sec, $T_e = T_i \simeq 1200^0$K, a = 2.25 cm)

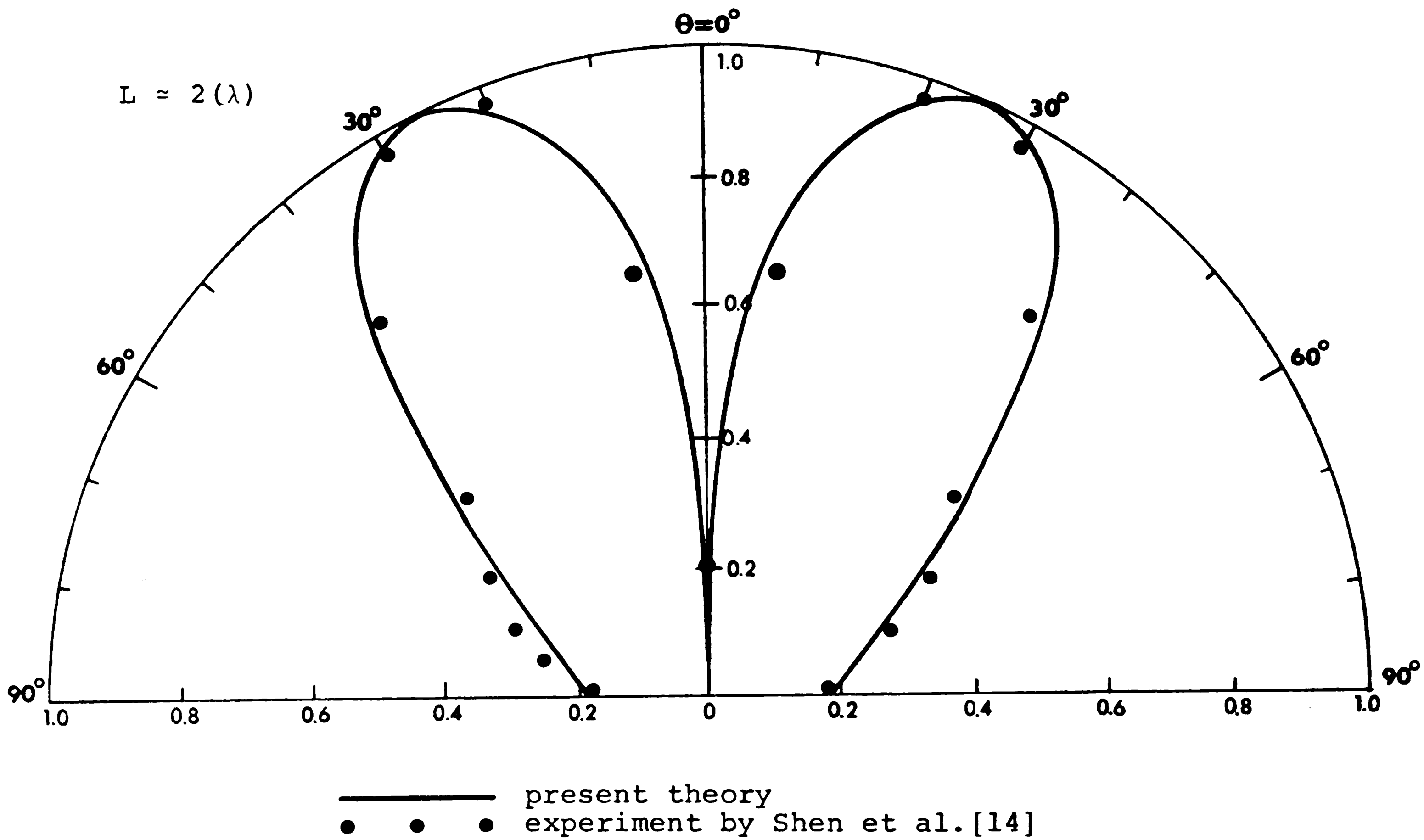

Figure 3.20 Radiation patterns of the generalized ionacoustic wave excited by a disk dipole antenna.
(f = 46.6 kHz, phase velocity $V_A = 1.05 \times 10^3$ m/sec, $T_e \simeq T_i \simeq 1200^\circ K$, a = 2.25 cm)

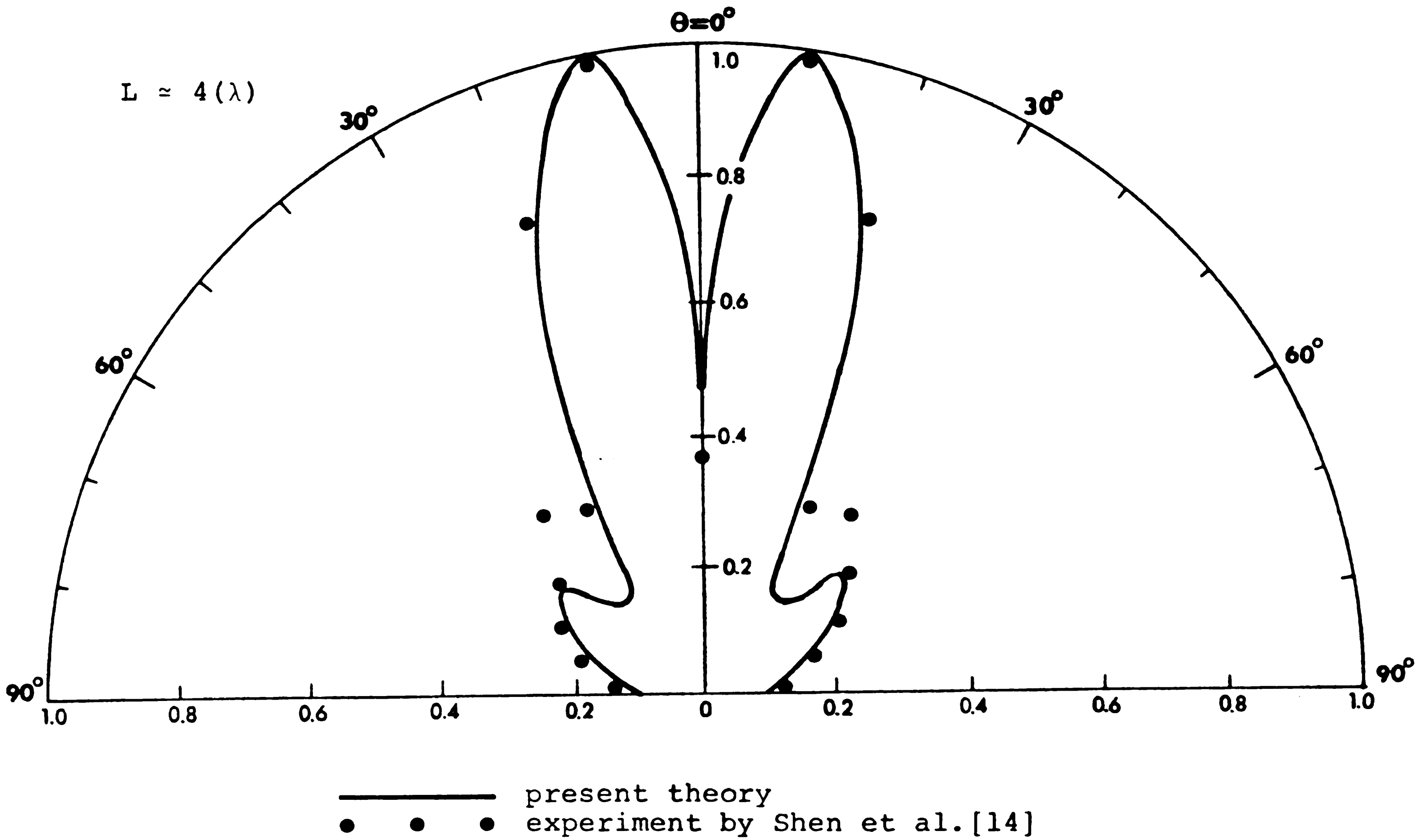

Figure 3.21 Radiation patterns of the generalized ionacoustic wave excited by a disk dipole antenna.
(f = 93.3 kHz, phase velocity $V_A = 1.05 \times 10^3$ m/sec, $T_e = T_i \approx 1200^0$K, a = 2.25 cm)

generalized ionacoustic wave at various ratios of T_e/T_i.

Figures 3.19 to 3.21 show the radiation patterns of the generalized ionacoustic wave at various antenna frequencies. We choose the phase velocity of the generalized ionacoustic wave, V_A, to be 1.05×10^3 meter/sec., the diameter of the disk antenna, 2a, to be 4.5 cm, and the normalized antenna length, L, as 1.5 (λ), 2 (λ), 4 (λ). In these cases, our radiation patterns again agree very closely with the experimental results of Shen et al.[14].

3.4.3 Radiation Patterns of the Generalized Electroacoustic Wave (n_2 Wave)

The radiation pattern function of the generalized electroacoustic wave can be obtained from equation (3.4.9) by replacing k by k_2. That is,

$$F_2(\theta) = \frac{H_1(k_2 a \sin\theta)}{k_2 a \sin\theta} \quad . \tag{3.4.11}$$

The results of two typical cases are plotted in Figures 3.22 and 3.23 and their numerical results are given in Tables 13 and 14 of Appendix C.

Figure 3.22 shows the radiation patterns of the generalized electroacoustic wave at various electron temperatures. Figure 3.23 shows the radiation patterns of the generalized electroacoustic wave at various antenna frequencies.

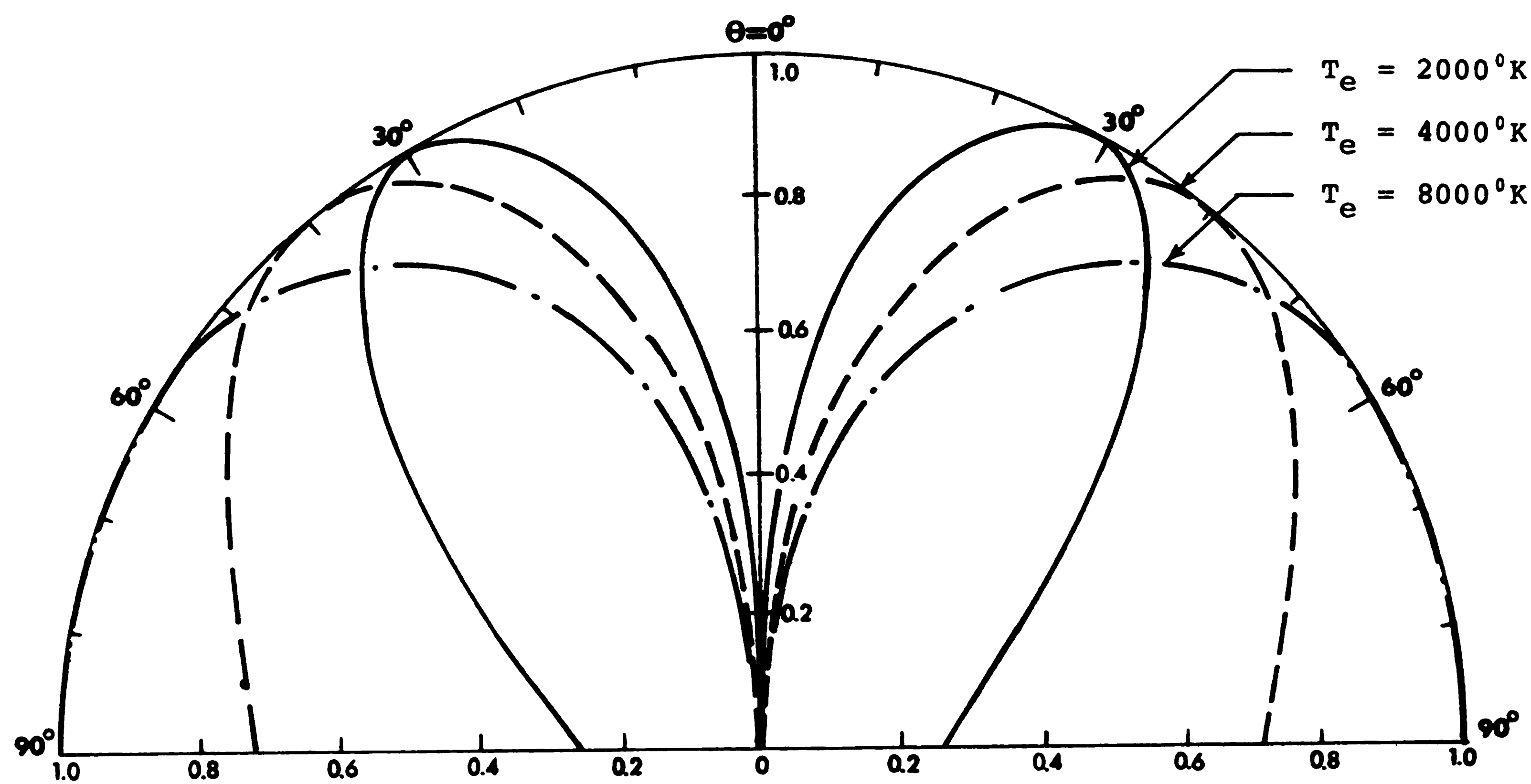

Figure 3.22 Radiation patterns of the generalized electroacoustic wave excited by a disk dipole antenna for various electron temperatures. (f = 17.5 MHz, $\omega_e^2/\omega^2 = 0.95$, $\gamma_e/\omega = 0$, $T_e/T_i \simeq 1$ to 10^4, a = 7.2 cm)

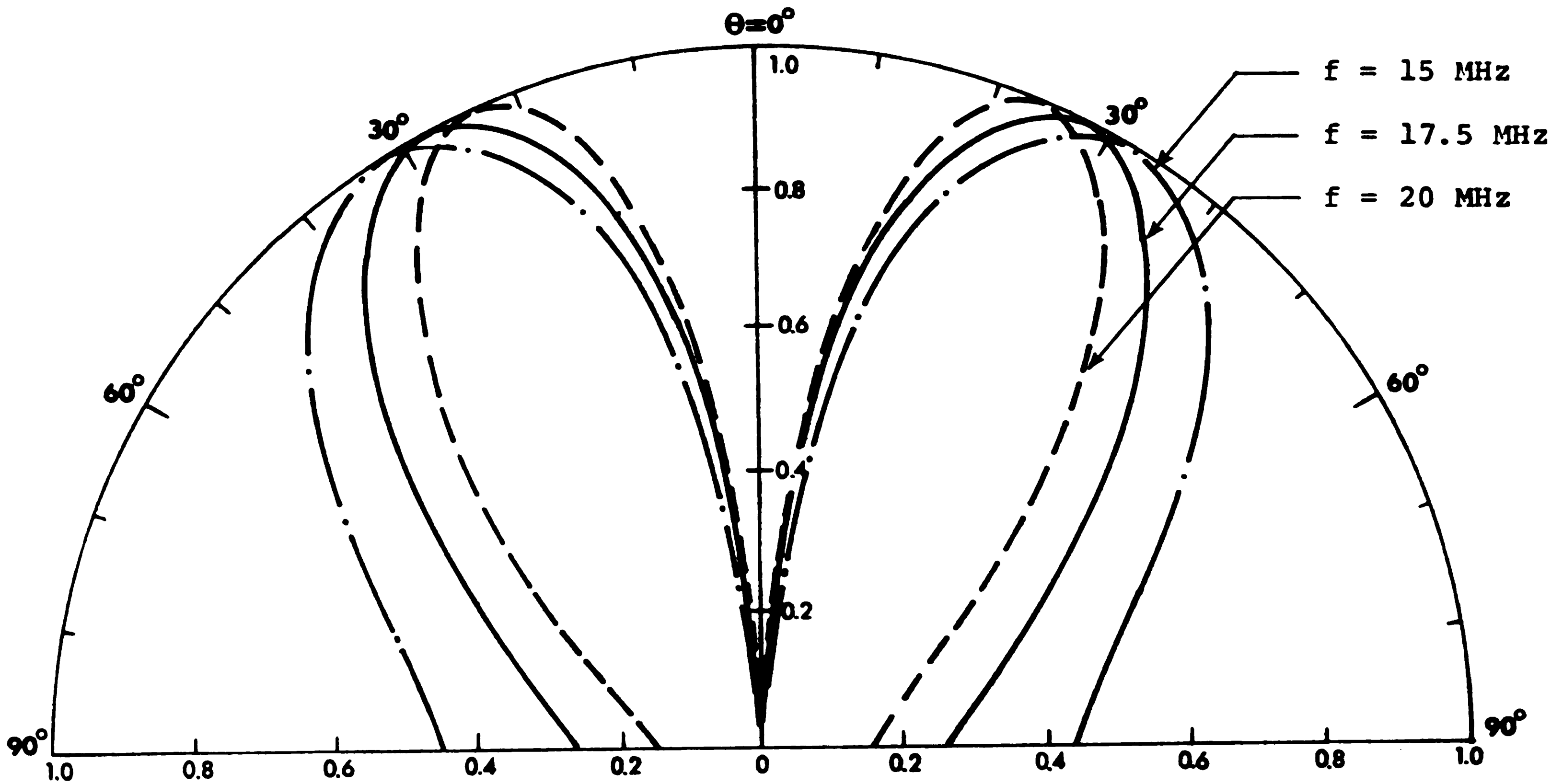

Figure 3.23 Radiation patterns of the generalized electroacoustic wave excited by a disk dipole antenna for various antenna frequencies.
(T_e = 2000°K, ω_e^2/ω^2 = 0.95, γ_e/ω = 0, $T_e/T_i \simeq$ 1 to 10^4, a = 7.2 cm)

3.5 Cylindrical Antenna

3.5.1 Geometry and Statement of the Problem

The geometrical configuration of a cylindrical antenna is shown in Figure 3.24 using a spherical coordinate system (r, θ, ϕ). A cylindrical antenna with a thin radius is immersed in the plasma. For this antenna, charge and current distributions can be given approximately as

$$\rho^S = \begin{cases} \rho_o \cos[k(h - z')] & \text{for } 0 \le z' \le h \\ -\rho_o \cos[k(h + z')] & \text{for } -h \le z' \le 0 \end{cases} \tag{3.5.1}$$

$$\vec{I}^S = \begin{cases} I_m \sin[k(h - z')]\hat{z} & \text{for } 0 \le z' \le h \\ I_m \sin[k(h + z')]\hat{z} & \text{for } -h \le z' \le 0 \end{cases} \tag{3.5.2}$$

The propagation constant, k, of the antenna charge or current is still not well known. Some theoretical studies performed by Seshadri [30] and Wunsch [31] predict an electroacoustic component in the antenna current while experimental studies conducted by Chen et al. [32,33] and Ishizone et al. [34] found the antenna current to be predominantly electromagnetic in nature. This justifies the approximation of $k = k_e$ where k_e is the propagation constant of the electromagnetic wave in the plasma. In our numerical calculation, k is assumed to be k_e which is given by equation (2.6.8).

The generalized electroacoustic and ionacoustic waves excited by a cylindrical antenna can be obtained by substituting equation (3.5.1) into equation (3.1.4). Using the far zone approximations, the integral becomes

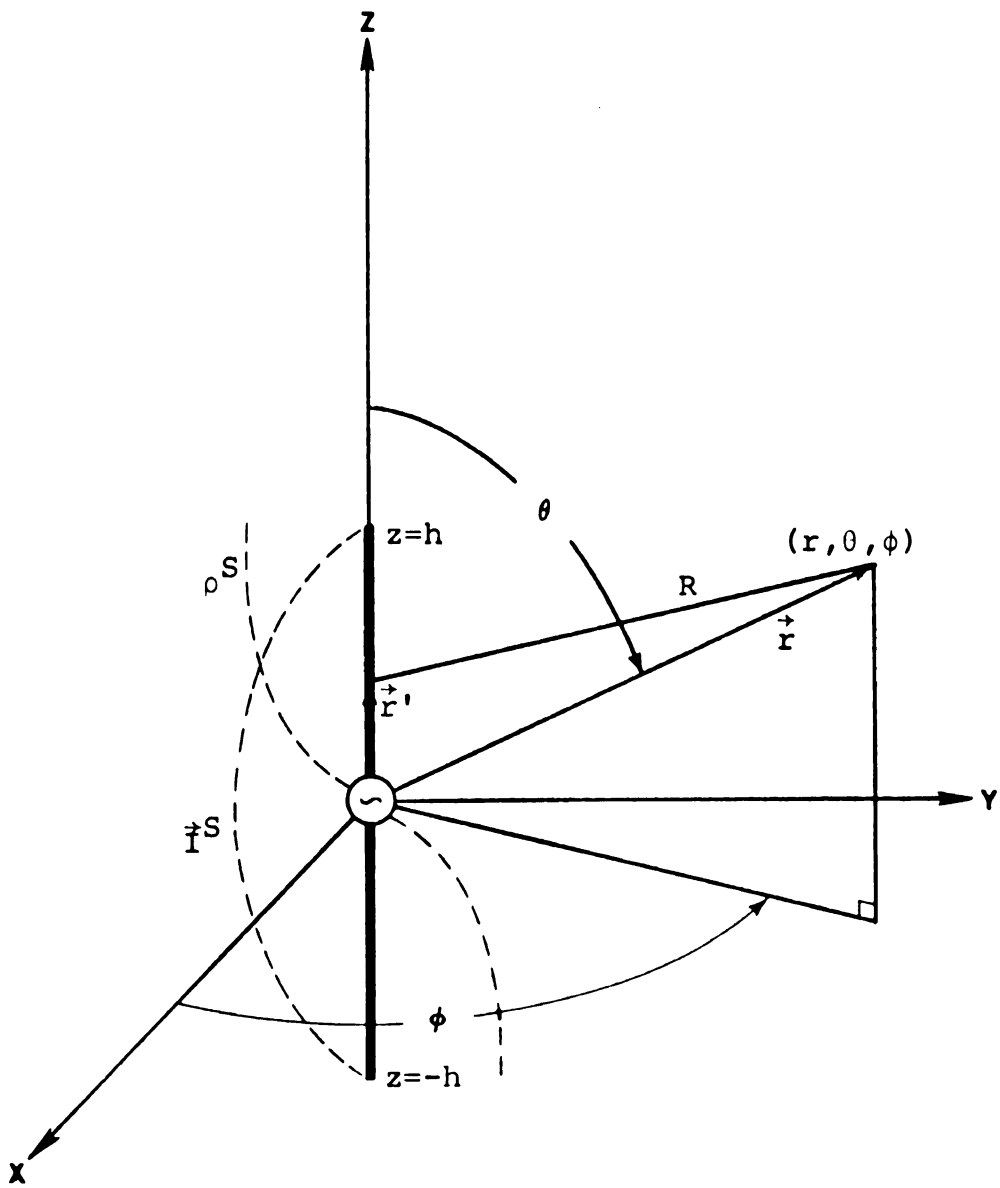

Figure 3.24 Geometry of a cylindrical antenna.

$$\int_{v'} \rho^S(\vec{r})\frac{e^{-jkR}}{R}\,dv' = \frac{2\rho_o k}{j} \frac{\cos(kh\cos\theta) - \cos(k_e h)}{k^2\cos^2\theta - k_e^2}\cos\theta\,\frac{e^{-jkr}}{r} .$$

Thus,

$$n(\vec{r}) = \frac{jS\rho_o}{2\pi e k}\left[\frac{\cos(kh\cos\theta) - \cos(k_e h)}{\cos^2\theta - (k_e/k)^2}\right]\cos\theta\,\frac{e^{-jkr}}{r} \tag{3.5.3}$$

where k is the propagation constant of the particular wave.

3.5.2 <u>Radiation Patterns of the Generalized Ionacoustic Wave (n_1 Wave)</u>

The radiation pattern function of the generalized ion-acoustic wave can be obtained from equation (3.5.3) by replacing k by k_1. That is,

$$F_1(\theta) = \frac{\cos(k_1 h\cos\theta) - \cos(k_e h)}{\cos^2\theta - (k_e/k_1)^2}\cos\theta \quad . \tag{3.5.4}$$

In order to excite the ionacoustic wave which does not suffer excessive Landau damping, we need to operate the antenna at low frequency region where $\omega_e >> \omega$. In this region the electromagnetic wave is cut off and it implies that k_e is a pure imaginary number. In the present consideration, we have $k_e h << 1$ and $k_e/k_1 \simeq 0$. Consequently, equation (3.5.4) is reduced to

$$F_1(\theta) = \frac{\cos(k_1 h\cos\theta) - 1}{\cos\theta} \quad . \tag{3.5.5}$$

The results of some typical cases are plotted in Figures 3.25 to 3.29 and their numerical results are given in Tables 15, 16 and 17 of Appendix C.

Figures 3.25 and 3.26 show the radiation patterns of the generalized ionacoustic waves at various electron temperatures.

Figures 3.27 and 3.28 show the radiation patterns of the generalized ionacoustic waves for the cases of various ratios of electron temperature to ion temperature.

Figure 3.29 shows the radiation patterns of the generalized ionacoustic wave at various antenna frequencies.

3.5.3 Radiation Patterns of the Generalized Electroacoustic Wave (n_2 Wave)

The radiation pattern function of the generalized electroacoustic wave can be obtained from equation (3.5.3) by replacing k by k_2. That is,

$$F_2(\theta) = \frac{\cos(k_2 h \cos\theta) - \cos(k_e h)}{\cos^2\theta - (k_e/k_2)^2} \cos\theta \quad . \qquad (3.5.6)$$

To excite an electroacoustic wave without suffering substantial Landau damping, the antenna frequency, ω, is chosen to be slightly higher than the plasma frequency, ω_e. The results of some typical cases are plotted in Figures 3.30 to 3.34 and their numerical results are given in Tables 18, 19 and 20 of Appendix C.

Figure 3.30 shows the radiation patterns of the

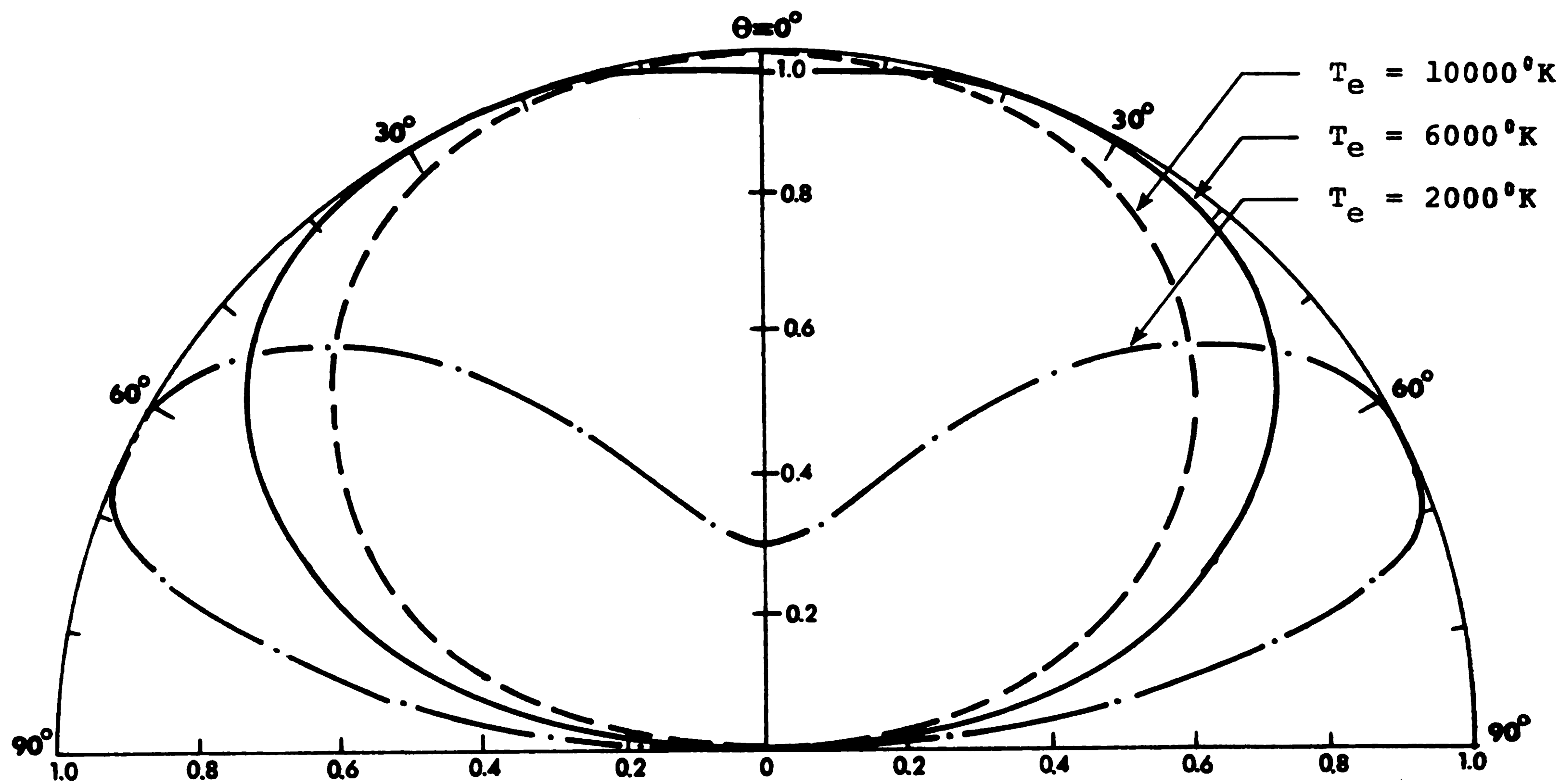

Figure 3.25 Radiation patterns of the generalized ionacoustic wave excited by a cylindrical antenna for various electron temperatures. (f = 30 kHz, T_e/T_i = 10, h = 2.5 cm)

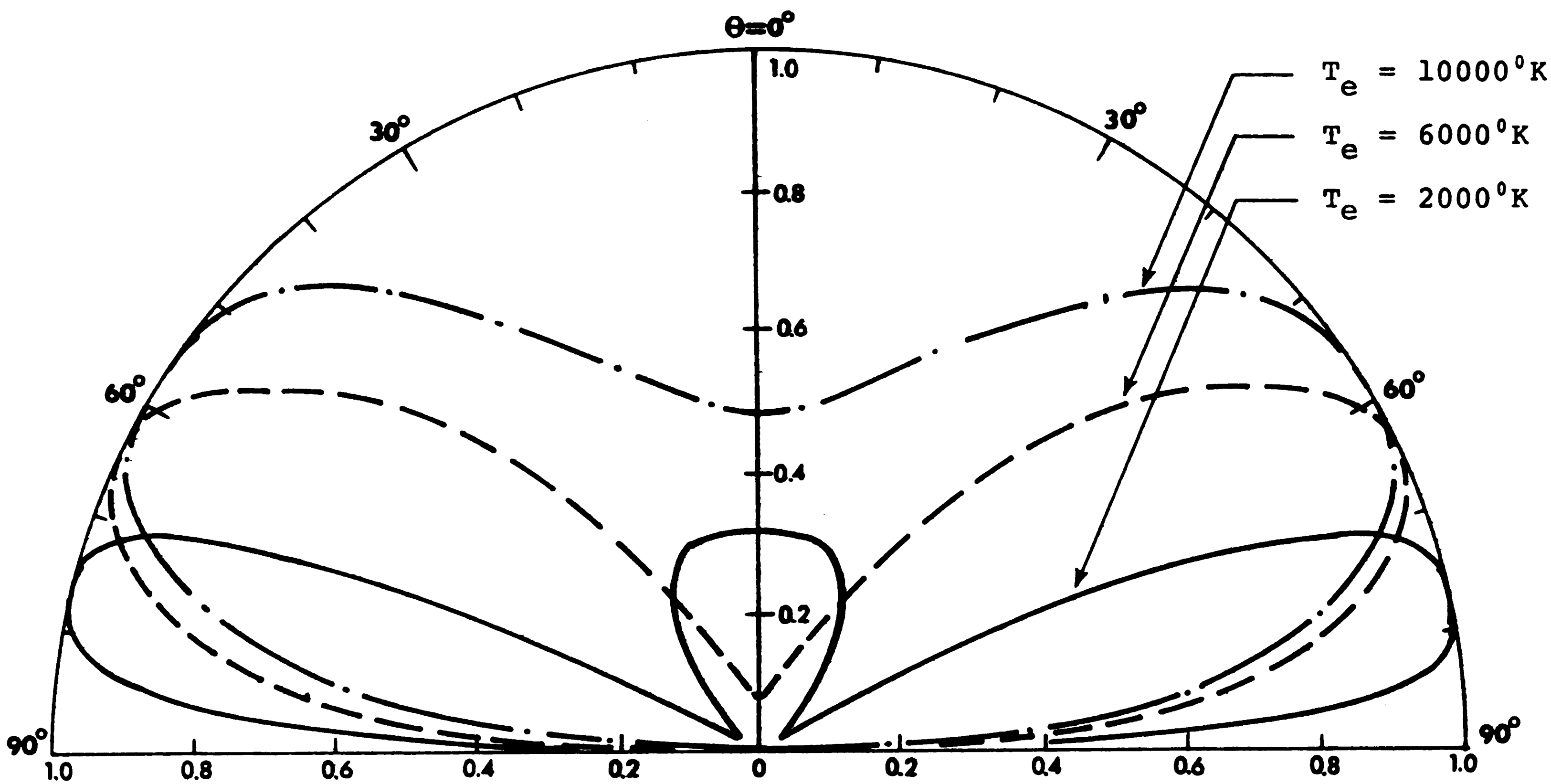

Figure 3.26 Radiation patterns of the generalized ionacoustic wave excited by a cylindrical antenna for various electron temperatures.
(f = 30 kHz, T_e/T_i = 10, h = 5 cm)

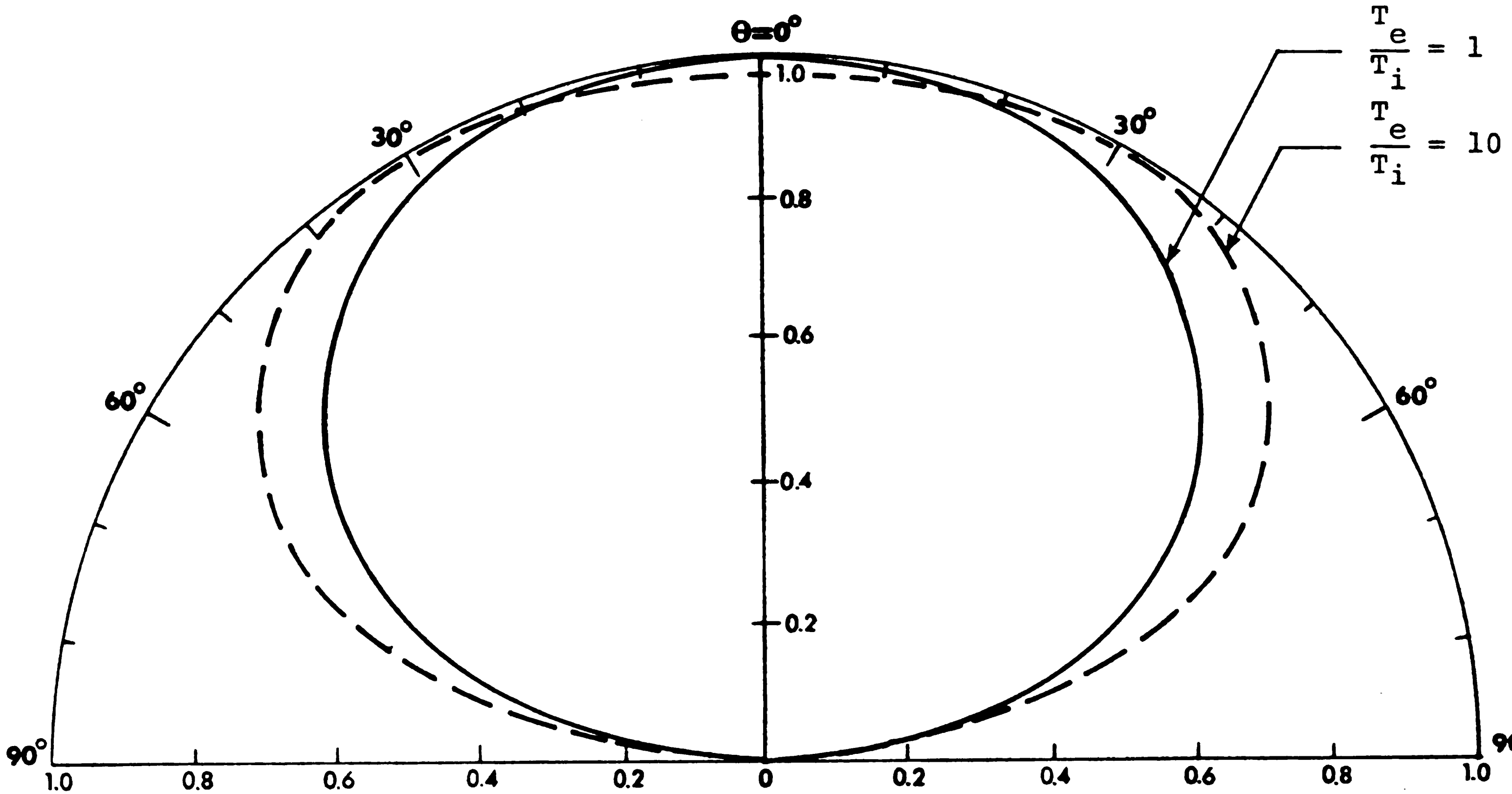

Figure 3.27 Radiation patterns of the generalized ionacoustic wave excited by a cylindrical antenna for various ratios of electron temperature to ion temperature. (f = 30 kHz, T_e = 6000°K, h = 2.5 cm)

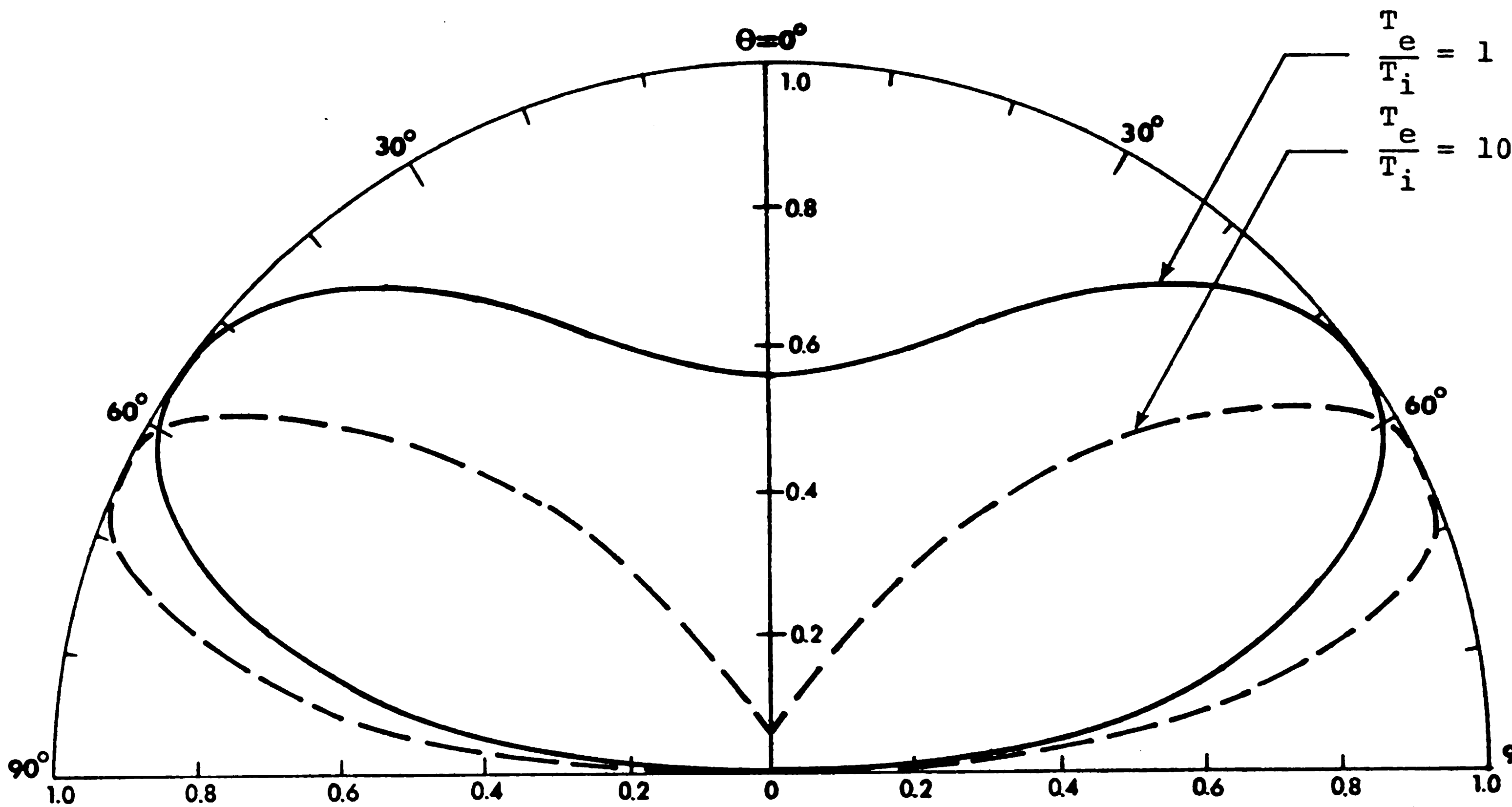

Figure 3.28 Radiation patterns of the generalized ionacoustic wave excited by a cylindrical antenna for various ratios of electron temperature to ion temperature. (f = 30 kHz, T_e = 6000°K, h = 5 cm)

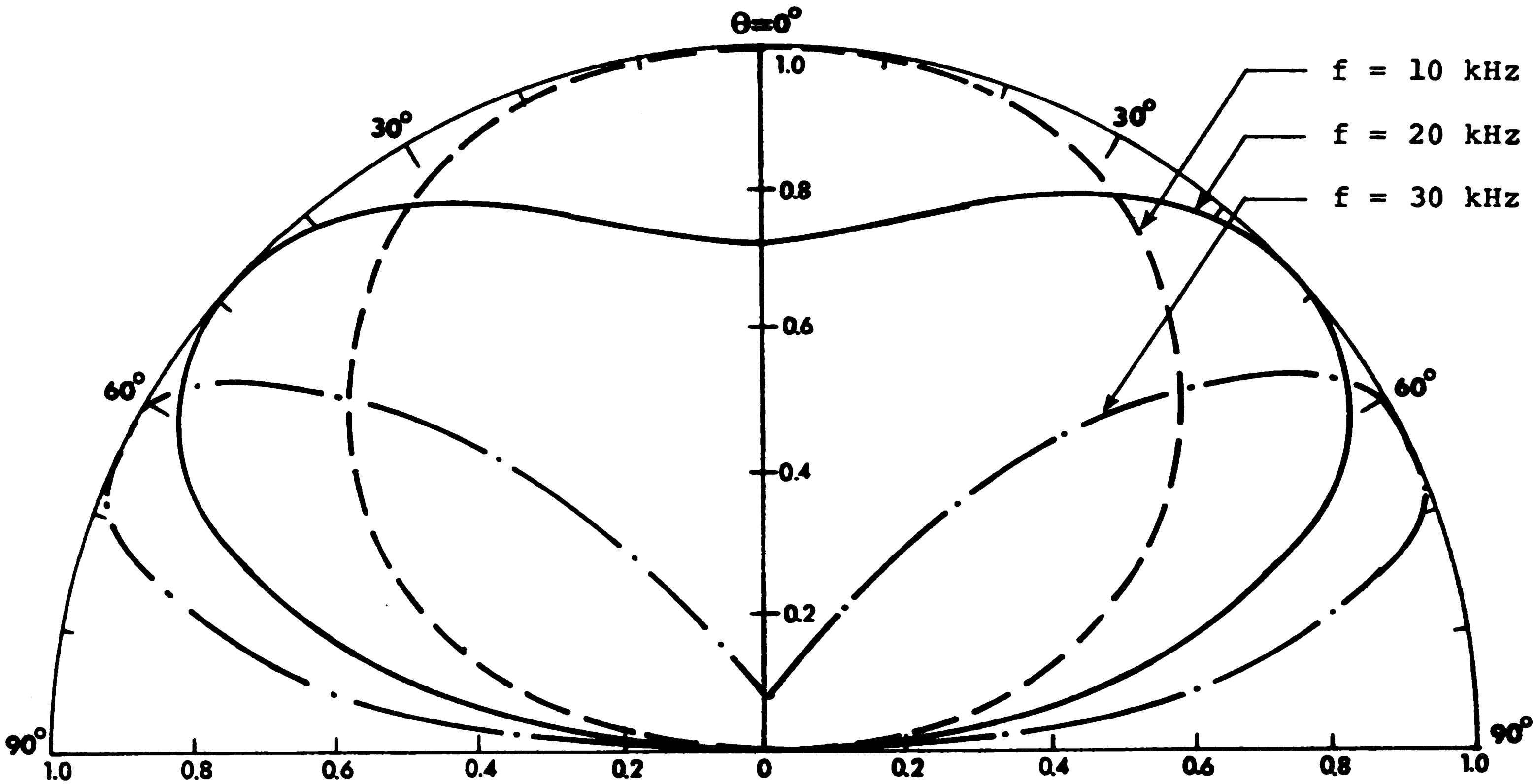

Figure 3.29 Radiation patterns of the generalized ionacoustic wave excited by a cylindrical antenna for various antenna frequencies. (T_e = 6000°K, T_e/T_i = 10, h = 5 cm)

generalized electroacoustic wave at various electron temperatures in comparison with an experimental pattern measured by Ishizone et al.[13].

Figure 3.31 shows the radiation patterns of the generalized electroacoustic wave at various antenna frequencies.

Figures 3.32 to 3.34 show the radiation patterns of the generalized electroacoustic waves predicted by the present theory in comparison with the experimental patterns measured by Ishizone et al.[13].

3.5.4 Radiation Patterns of the Electromagnetic Wave

To determine $\vec{B}(\vec{r})$, the integral

$$\int_{v'} \vec{J}^S(\vec{r}\,')\frac{e^{-jk_eR}}{R}\,dv'$$

in equation (2.6.10) is to be evaluated. For a cylindrical antenna, we assume

$$\vec{J}^S(\vec{r}\,') = \frac{I}{A}\hat{z} = \frac{\vec{I}^S}{A}$$

where A is the cross-sectional area of the antenna and

$$\vec{I}^S = \begin{cases} I_m \sin[k_e(h - z')]\hat{z} & \text{for } z' > 0 \\ I_m \sin[k_e(h + z')]\hat{z} & \text{for } z' < 0 \end{cases} \quad . \qquad (3.5.7)$$

k_e is the propagation constant of the electromagnetic wave in the plasma and is given by equation (3.2.6). For the collisionless case, equation (3.2.6) is reduced to

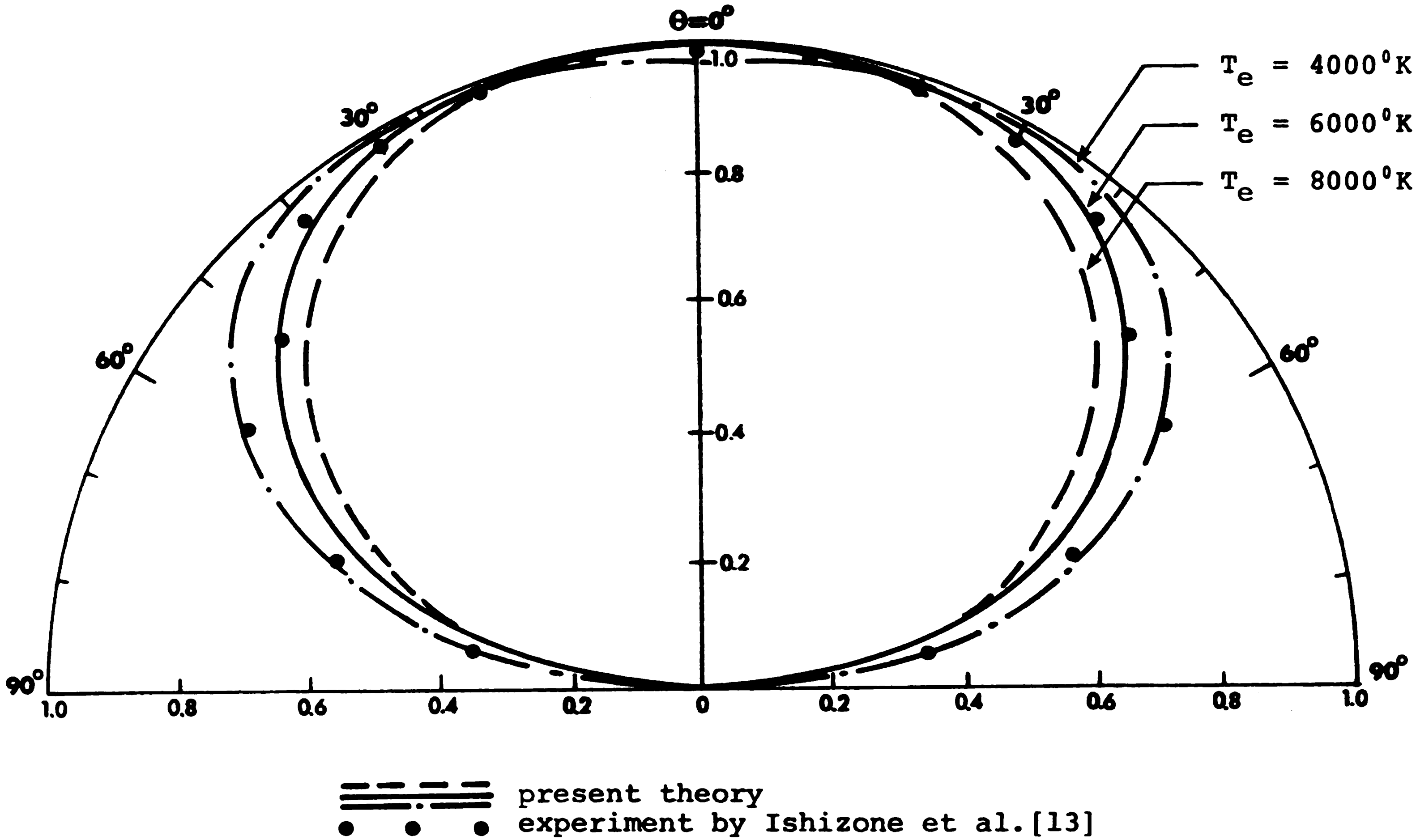

Figure 3.30 Radiation patterns of the generalized electroacoustic wave excited by a cylindrical antenna for various electron temperatures.
(f = 5.5 MHz, f_p = 4.5 MHz, $\gamma_e/\omega = 0$, $T_e/T_i \simeq 1$ to 10^4, $2h/\lambda = 0.7$, h = 6 cm)

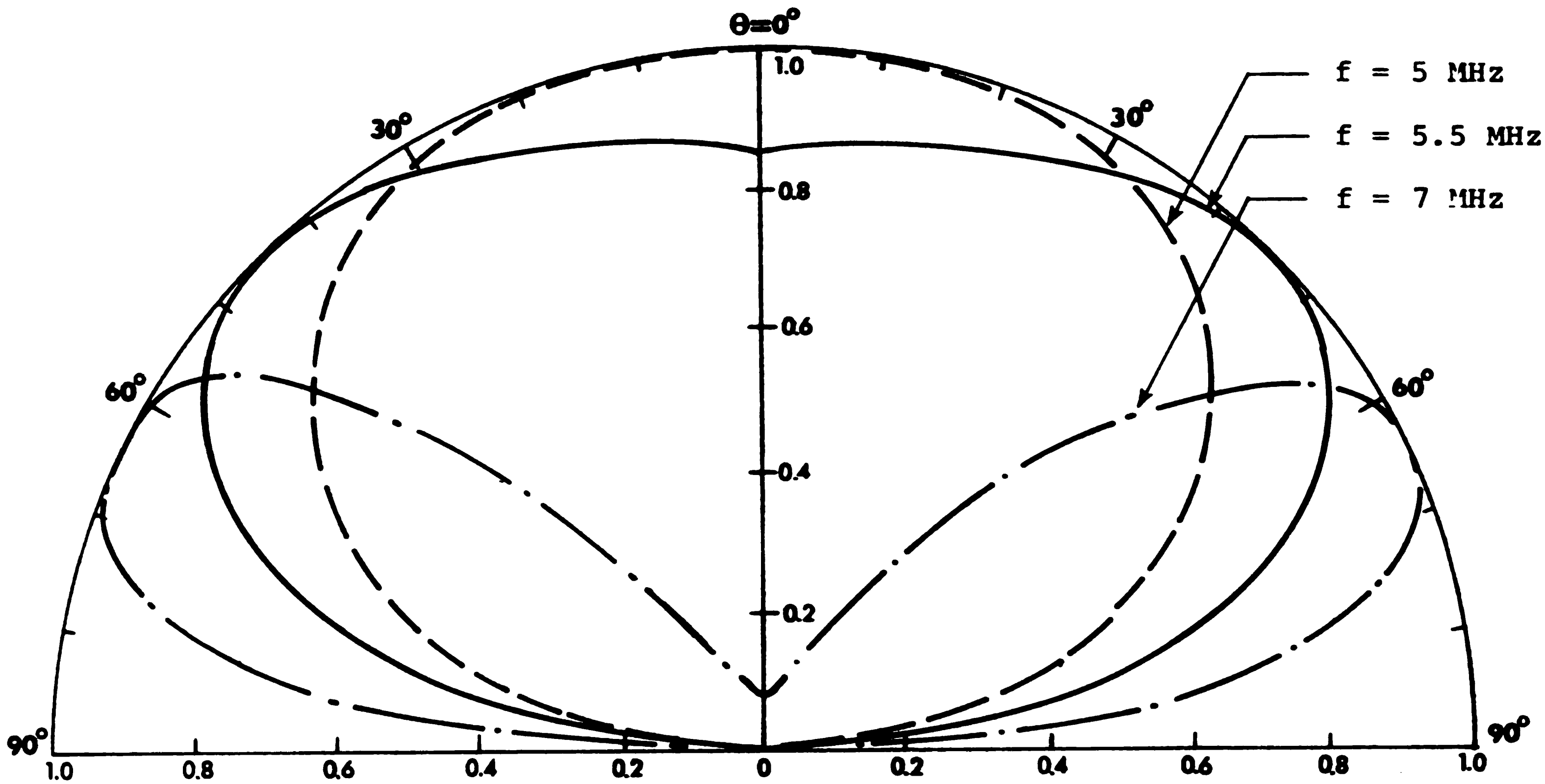

Figure 3.31 Radiation patterns of the generalized electroacoustic wave excited by a cylindrical antenna for various antenna frequencies. (f_p = 4.5 MHz, T_e = 6000°K, γ_e/ω = 0, $T_e/T_i \simeq$ 1 to 10^4, h = 8.5 cm)

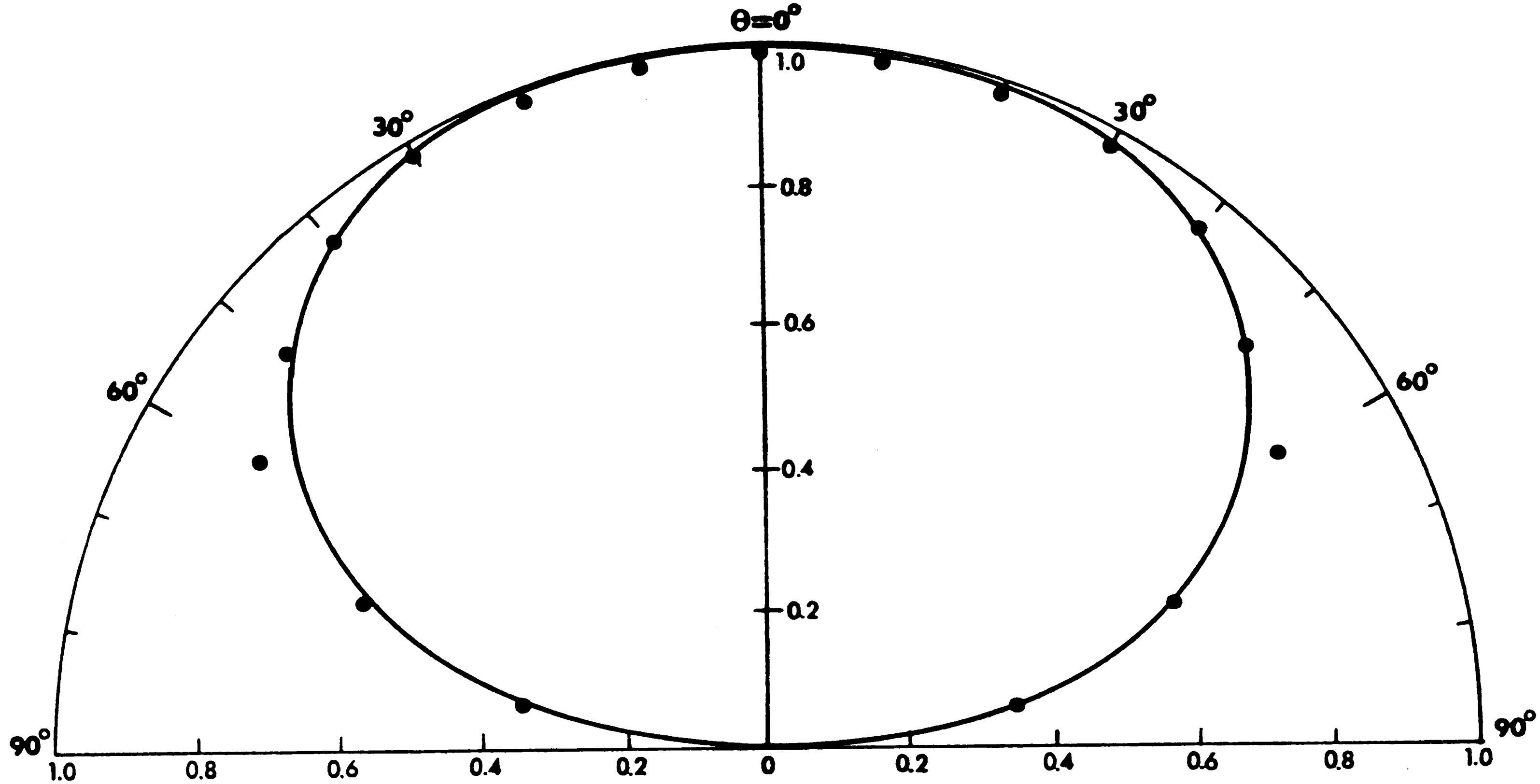

——— present theory
● ● ● experiment by Ishizone et al.[13]

Figure 3.32 Radiation pattern of the generalized electroacoustic wave excited by a cylindrical antenna.
(T_e = 5150^{0}K, f_p = 4.5 MHz, f = 5.5 MHz, h = 6 cm)

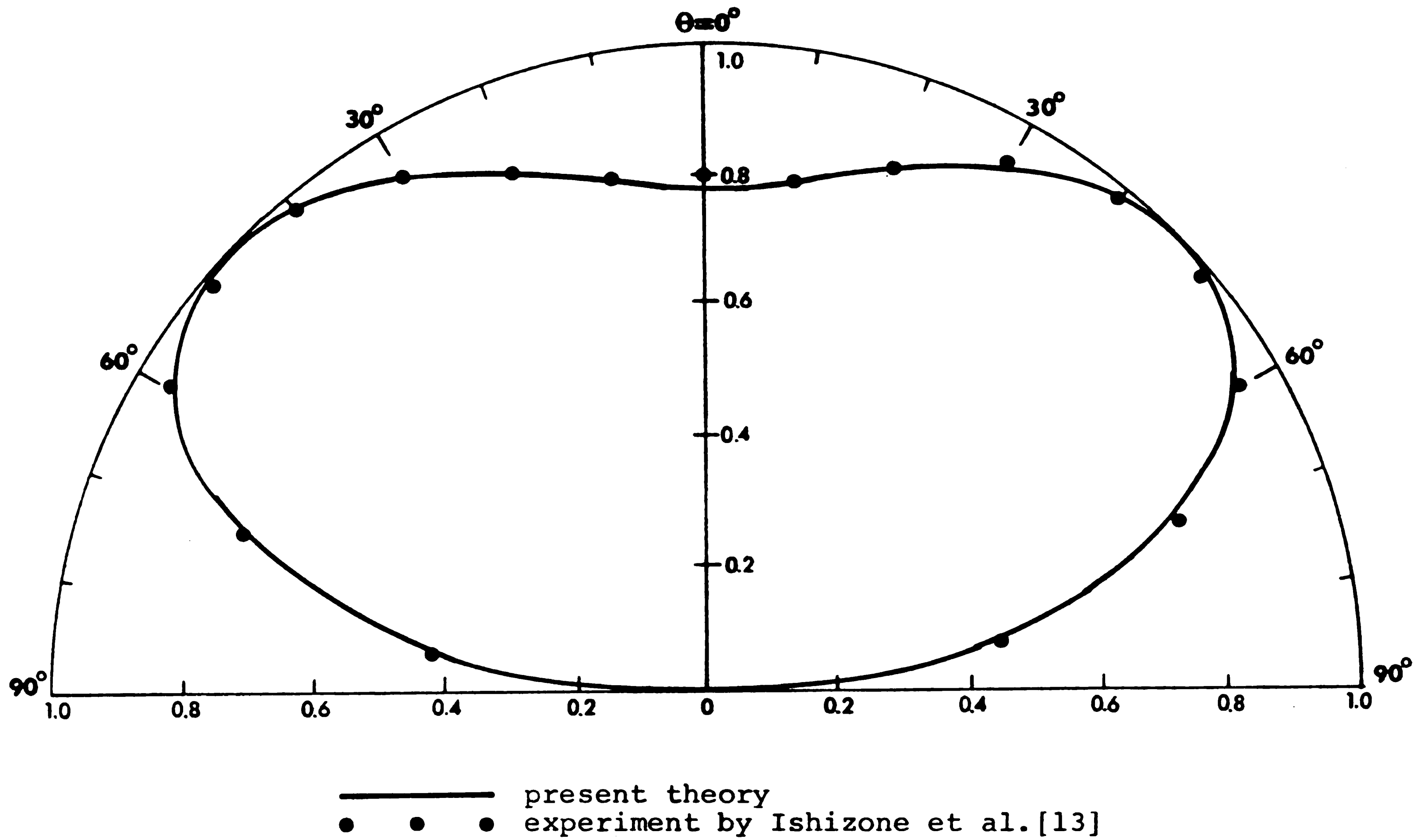

Figure 3.33 Radiation pattern of the generalized electroacoustic wave excited by a cylindrical antenna.
(T_e = 5150°K, f_p = 4.5 MHz, f = 5.5 MHz, h = 8.5 cm)

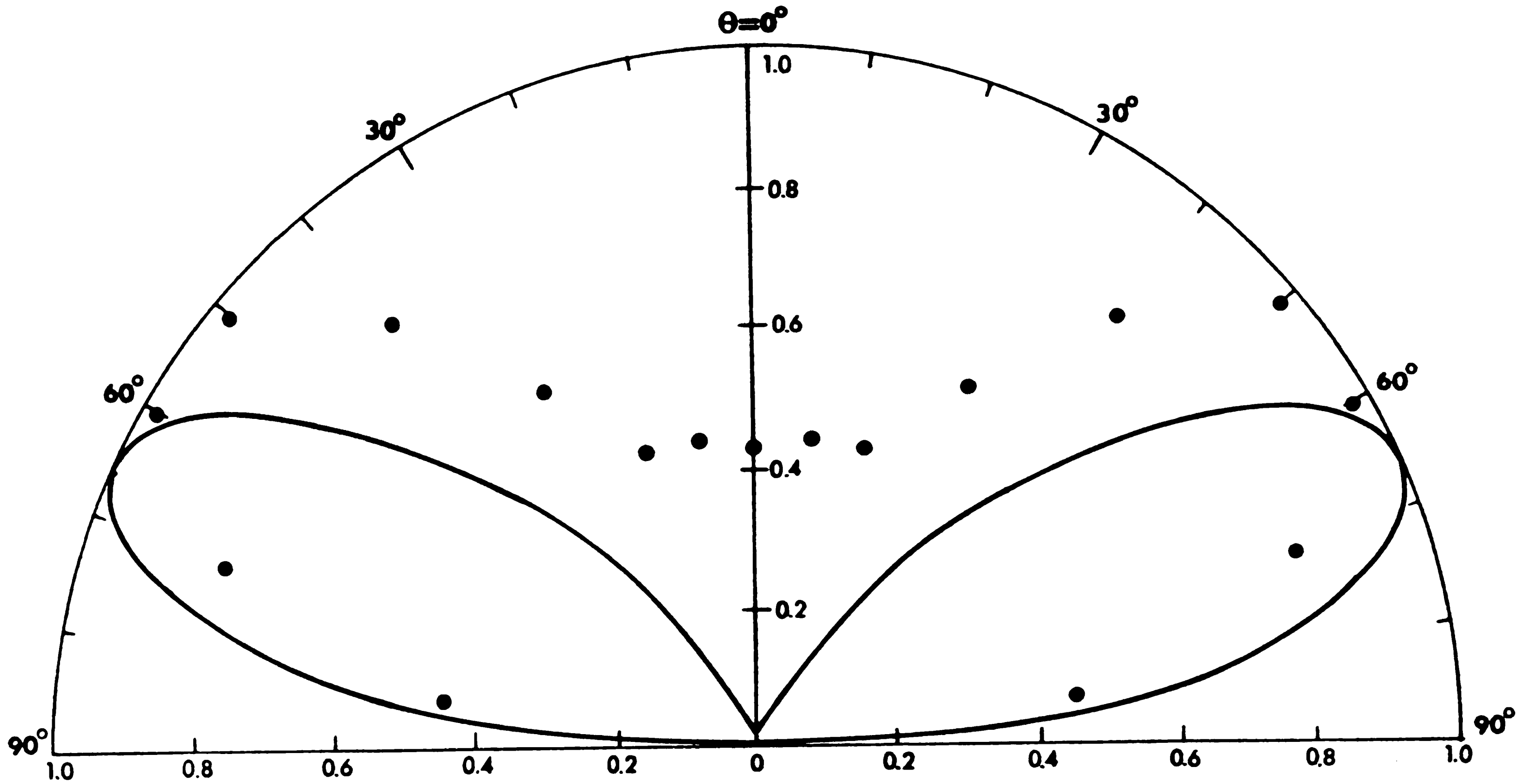

— present theory
● ● ● experiment by Ishizone et al.[13]

Figure 3.34 Radiation pattern of the generalized electroacoustic wave excited by a cylindrical antenna.
(T_e = 5150°K, f_p = 4.5 MHz, f = 7 MHz, h = 8.5 cm)

$$k_e^{\ 2} = \omega^2 \mu_o \varepsilon_o \left(1 - \frac{\omega_e^{\ 2}}{\omega^2}\right) \quad . \tag{3.5.8}$$

After using the far zone approximations and neglecting $1/r^2$ terms, $\vec{B}(\vec{r})$ is determined to be

$$\vec{B}(\vec{r}) \simeq \hat{\phi} \, \frac{-jI_m\mu_o}{2\pi A} \, \frac{\cos(k_e h \cos\theta) - \cos(k_e h)}{\cos^2\theta - 1} \, \sin\theta \, \frac{e^{-jk_e r}}{r} \quad . \tag{3.5.9}$$

It is evident in equation (2.7.7) that $\vec{E}$ field contains ionacoustic, electroacoustic as well as electromagnetic components. To calculate the radiation patterns of the electromagnetic wave, only the electromagnetic component is considered. This component can be obtained as

$$\vec{E}_{em} = \frac{-j\omega}{\mu_o \varepsilon_o (\omega^2 - \omega_e^{\ 2} - \omega_i^{\ 2})} \, \nabla \times \vec{B} \quad . \tag{3.5.10}$$

Substituting equation (3.5.9) into equation (3.5.10) and neglecting $1/r^2$ terms, we have

$$\vec{E}_{em} = \hat{\theta} \, \frac{-j\omega I_m k_e}{2\pi A \varepsilon_o (\omega^2 - \omega_e^{\ 2} - \omega_i^{\ 2})} \, \frac{\cos(k_e h \cos\theta) - \cos(k_e h)}{\cos^2\theta - 1} \, \sin\theta \, \frac{e^{-jk_e r}}{r} \quad . \tag{3.5.11}$$

The corresponding radiation pattern function can be expressed by

$$F_{em}(\theta) = \frac{\cos(k_e h \cos\theta) - \cos(k_e h)}{\cos^2\theta - 1} \sin\theta \quad . \qquad (3.5.12)$$

Figure 3.35 shows the radiation patterns of the electromagnetic component of the electric field in the plasma. In this example, the plasma frequency is assumed to be 4.5 MHz and the antenna frequency is assumed to be 5, 5.5 and 7 MHz. The numerical results are given in Table 21 of Appendix C. Over this range of antenna frequency, the radiation patterns of the excited electromagnetic wave largely remains circular as shown in Figure 3.35.

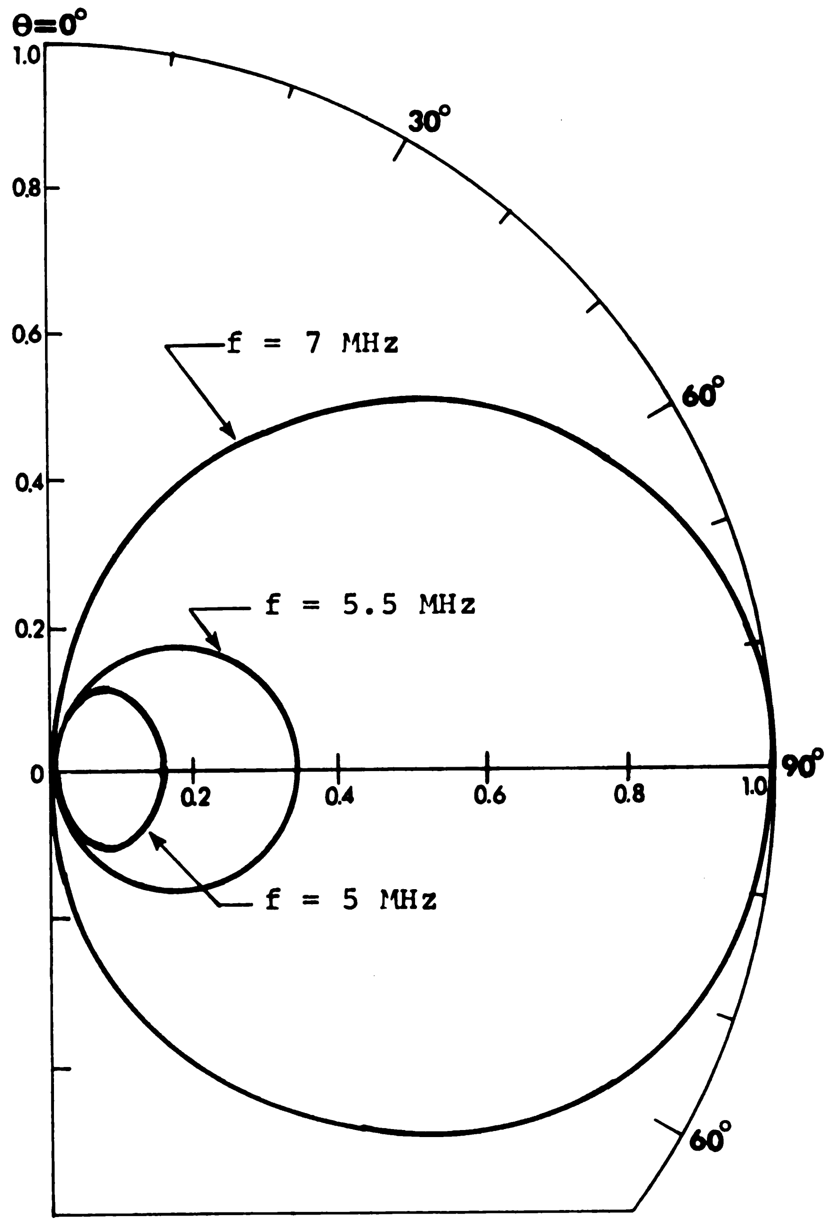

Figure 3.35 Radiation patterns of the electromagnetic wave excited by a cylindrical antenna in a plasma for various antenna frequencies.
(f_p = 4.5 MHz, h = 8.5 cm)

CHAPTER 4

EXCITATION OF AN ELECTROACOUSTIC WAVE IN THE PLASMA SHEATH SURROUNDING A CYLINDRICAL ANTENNA

4.1 Introduction

The excitation of an electroacoustic wave by an antenna in an infinite, homogeneous, isotropic, compressible and lossy plasma was studied in Chapter 2. In practice, when an antenna is in contact with a compressible plasma, a plasma sheath is created on the antenna surface. In this chapter, we like to study the excitation of the electroacoustic wave by an actual antenna surrounded by a plasma sheath and imbedded in a compressible plasma. Main objectives of this chapter are (1) to study the effect of the plasma sheath on the excitation of the electroacoustic wave and (2) to seek the evidence of the excitation of the electroacoustic wave by an actual antenna.

4.2 Experimental Setup

The schematic diagram of the experimental setup is shown in Figure 4.1. A mercury arc discharge was employed to produce the large volume and high density plasma in a large plasma tube which is made of an open end pyrex bell

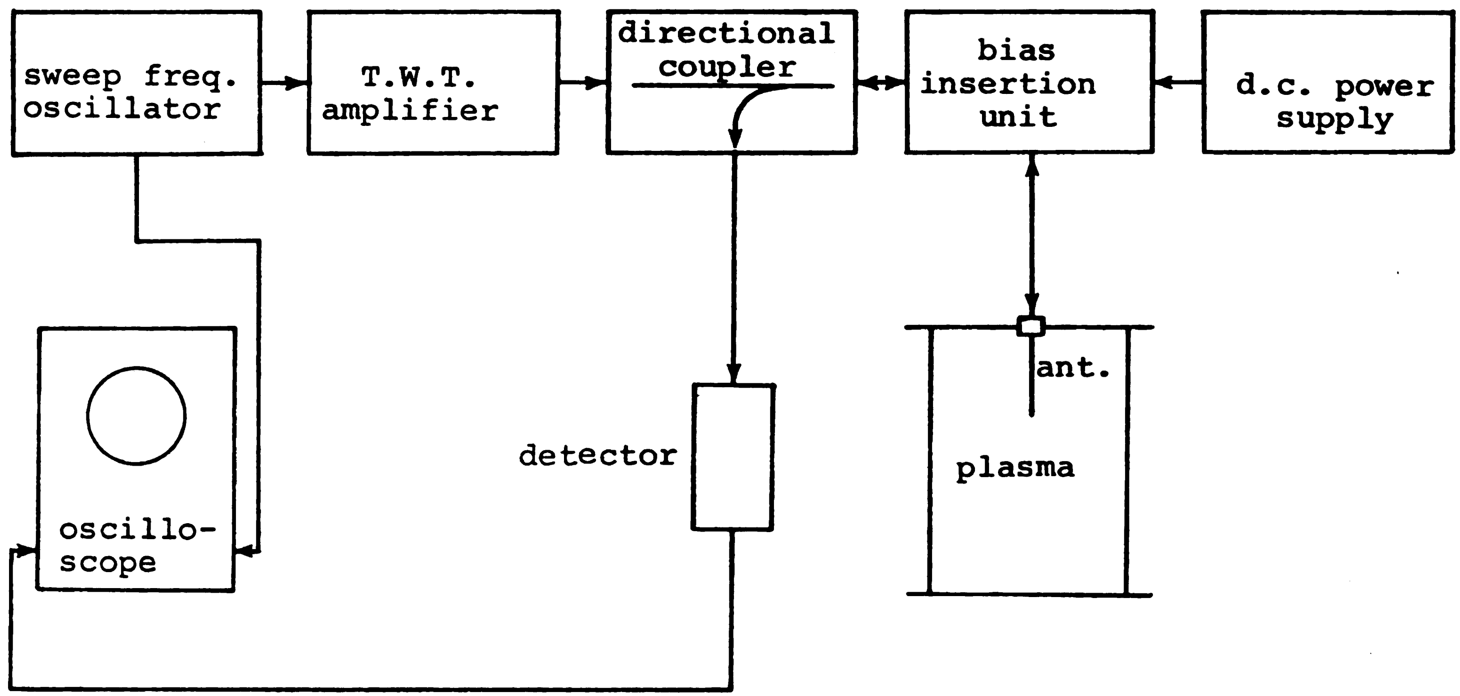

Figure 4.1 Experimental setup for the excitation of the electroacoustic wave in the plasma sheath surrounding a cylindrical antenna.

jar with the dimensions of 14-inch diameter and 18-inch length. The upper end of the tube is the anode with a cylindrical monopole antenna feeding through its center. The lower end of the tube is the cathode which consists of a mercury pool. A floating metallic ring is placed at the middle of the mercury pool to fix the moving hot spots of the mercury arc. An ignition circuit is installed in the mercury pool for the purpose of starting the plasma. Between the anode and the cathode, a d.c. power supply circuit is connected. Under the normal operation, the discharge current can run from zero to 50 amperes. The pumping system consists of two mechanical pumps and a mercury diffusion pump. The tube is continuously pumped during the experiment, and the pressure of the plasma is kept around 1 micron (10^{-3} mm Hg). The structure of the large plasma tube is shown in Figure 4.2. The output of a sweep frequency oscillator covering the frequency band of 0.4 to 1.4 GHz is amplified by a travelling wave tube amplifier and then connected through a directional coupler. It then passes through a bias insertion unit before reaching the antenna. Through this bias insertion unit, the d.c. bias voltage of the antenna can be varied from negative 40 volts to positive 25 volts. When the antenna excites an electro-acoustic wave in the plasma sheath, this effect appears in the reflected wave from the antenna. The reflected wave containing this electroacoustic resonance information is taken out through the directional coupler, and then connected to the

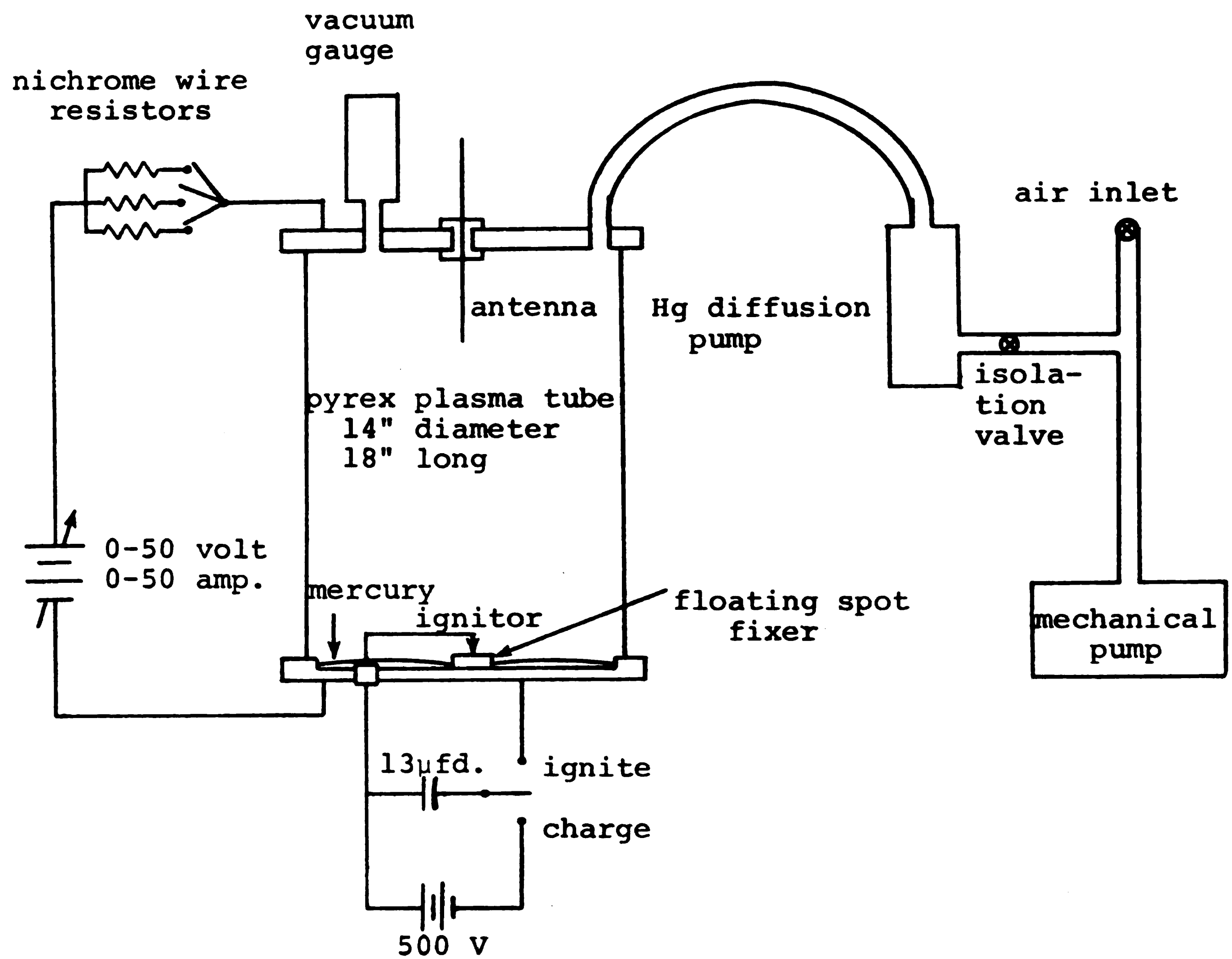

Figure 4.2 The plasma tube and accessories.

vertical input of the oscilloscope after detection. The horizontal input of the oscilloscope is fed by the sweep voltage of the sweep frequency oscillator. The curve displayed on the oscilloscope is the reflected wave versus the sweeping antenna frequency.

The scheme of the experiment is to observe the change in the curve of reflected wave versus sweeping frequency (RW-SF curve) as the antenna d.c. bias voltage is varied. As the bias voltage is varied, the size of the plasma sheath surrounding the antenna is changed. The observed change in the RW-SF curve as the bias voltage is varied supports the conjecture that this change is due to the excited electroacoustic wave, because the excited electromagnetic wave should not be affected by the change of the plasma sheath which is at least a magnitude of order smaller than the electromagnetic wavelength.

4.3 Experimental Results

When the sweep frequency signal covering the frequency range of 0.4 to 1.4 GHz was fed to the cylindrical antenna which is immersed in a large volume of compressible plasma, the reflected wave versus sweeping frequency displayed a curve such as shown in Figure 4.3 on the oscilloscope. Dips and peaks in the curve were probably due to the reflection of the electromagnetic wave from the antenna tip and the resonances excited by the electroacoustic wave in the plasma sheath. It

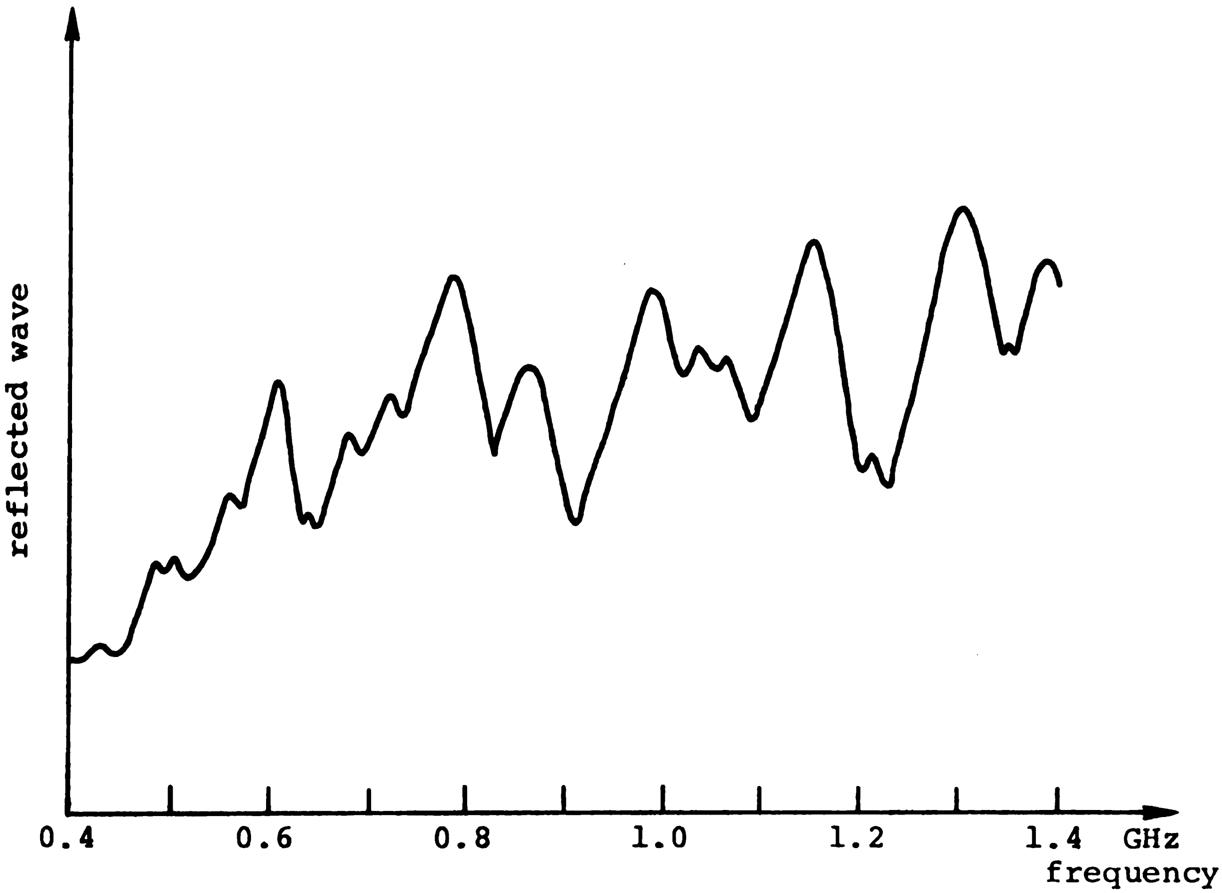

Figure 4.3 A typical reflected wave versus sweeping frequency curve.

is well known that at discrete numbers of frequencies, the excited electroacoustic wave can set up resonances in the plasma sheath. Whenever an electroacoustic resonance is set up, a dip in the RW-SF curve is expected.

The antenna bias voltage was then varied to observe the change in the RW-SF curve.

The antenna was first biased positively with respect to the plasma. As the bias voltage was varied from zero volt to positive 25 volts, the RW-SF curve was not changed at all. When the bias voltage reached beyond positive 25 volts, the antenna started to draw a heavy d.c. current from the plasma evidenced by a red glowing at the antenna tip. It was concluded that the variation of the antenna bias voltage, which was positive relative to the plasma, did not change the RW-SF curve.

The next step was to bias the antenna negatively with respect to the plasma. When the antenna bias voltage was varied from zero volt to negative 40 volts, a significant change in the RW-SF curve was observed. As the negative antenna bias voltage was substantially varied, the alternation of the RW-SF curve stopped at a particular frequency for a particular plasma density (discharge current). As the plasma density was increased, this particular frequency moved up indicating that a longer frequency range of the RW-SF curve was changed. This phenomenon is demonstrated in Figure 4.4. Figure 4.4(a) shows the RW-SF curve for the plasma current of

10 amperes, subject to the variation of antenna bias voltage from zero volt to negative 40 volts. It is clearly seen in this oscillogram that the lower frequency part (0.5 to 0.68 GHz) is substantially changed. Figure 4.4(b) shows the RW-SF curve for the case of 15 amperes plasma current. The frequency band of 0.5 to 0.78 GHz is affected. Figure 4.4(c) shows the RW-SF curve for the case of 20 amperes plasma current. The frequency band of 0.5 to 0.92 GHz is affected.

Three oscillograms in Figure 4.5 show the similar phenomena. In these oscillograms, the range of sweeping frequency is from 0.4 to 1.4 GHz which is wider than the case of Figure 4.4.

To understand the physics behind the observed phenomena, the correlation, between the plasma density and the highest frequency beyond which the antenna bias voltage ceased to affect the RW-SF curve, was investigated. It was found that this highest frequency was very close to the ambient plasma frequency. This finding implied that as the antenna bias voltage was varied, the affected part of the RW-SF curve was in the frequency band lower than the ambient plasma frequency. This phenomenon also implied that every possible electroacoustic resonance was excited in the plasma sheath for the antenna frequency lower than the ambient plasma frequency.

Figure 4.6 summarizes the affected frequency bands of the RW-SF curves due to the variation of negative antenna

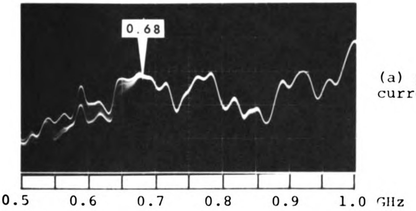

(a) plasma current: 10 amp.

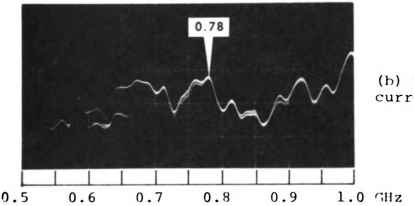

(b) plasma current: 15 amp.

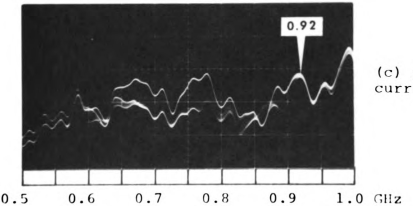

(c) plasma current: 20 amp.

Figure 4.4 Oscillograms of the reflected wave versus sweeping frequency curves for various plasma currents. Frequency range from 0.5 to 1.0 GHz.

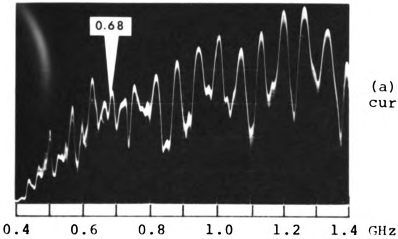

(a) plasma current: 10 amp.

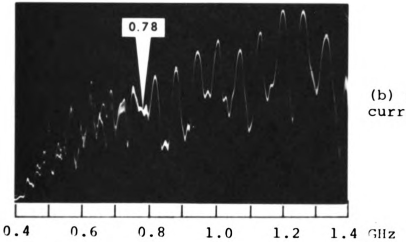

(b) plasma current: 15 amp.

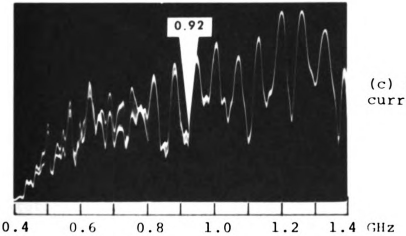

(c) plasma current: 20 amp.

Figure 4.5 Oscillograms of the reflected wave versus sweeping frequency curves for various plasma currents. Frequency range from 0.4 to 1.4 GHz.

bias voltage for various plasma densities (plasma currents). The ambient plasma frequency in each case is indicated in the figure showing it to be close to the upper bound of the affected frequency band. It is noted that the ambient plasma frequency was measured by the conventional Langmuir probe method. The ambient plasma frequencies in the central part of the plasma tube, corresponding to various plasma currents, are shown in Table 4.1.

Table 4.1 Ambient plasma frequency versus plasma current.

Plasma current	Ambient plasma frequency
5	0.46
10	0.57
15	0.68
20	0.87
25	1.00
30	1.12
35	1.30
40	1.47
45	1.47

4.4 Interpretation of the Experimental Results

The excitation of an electroacoustic wave in a compressible plasma, and the resonance of the electroacoustic wave in a plasma sheath leading to the so-called Tonks-Dattner's

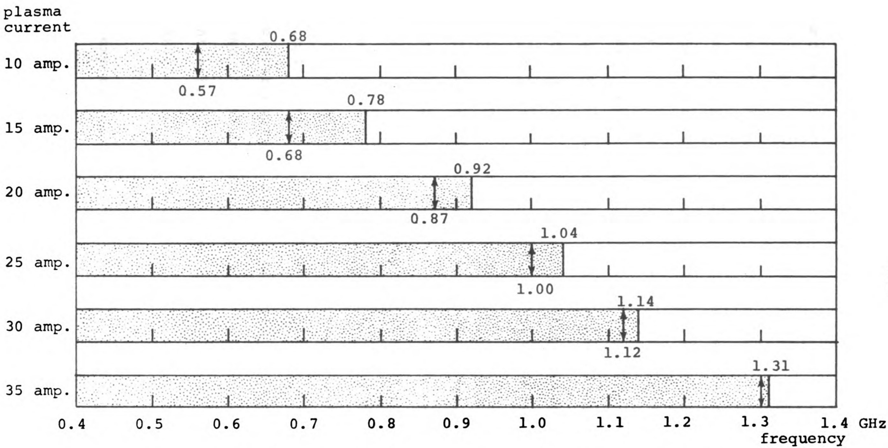

Figure 4.6 Affected frequency bands of the RW-SF curves for the cases of various plasma currents. (▒ is the affected frequency band. ↕ is the ambient plasma frequency measured by Langmuir probe method.)

resonance or the thermal resonance have been studied by numerous workers.

Recently, Baldwin [28] and Parbhakar and Gregory [29], through their theoretical and experimental studies, proposed a new physical mechanism for the electroacoustic resonance in the plasma sheath of a cylindrical plasma column. This new physical mechanism is the following: When an electromagnetic wave is incident upon a bounded non-uniform plasma, the electromagnetic field will excite an electroacoustic wave at the critical density point on the density profile where the local plasma density is equal to the frequency of the incident wave. The electromagnetic energy is coupled to the electroacoustic wave at this critical density point. The excited electroacoustic wave then propagates in both directions; one attenuates into the overdense plasma and the other propagates, and sets up a standing wave in the underdense plasma region or the plasma sheath. In this physical mechanism, it is implied that in order to excite an electroacoustic wave, an electromagnetic wave is required to interact with the plasma at the critical density point. If no critical density point exists in the plasma, an electroacoustic wave may not be excited.

This new physical mechanism will be used to interpret our experimental results.

4.4.1 The Case When the Cylindrical Antenna is Biased Positively:

When the antenna is biased positively with respect to the plasma, the electron density in the vicinity of the antenna is increased and it may create a density profile surrounding the antenna as shown in Figure 4.7.

In our experiment, the antenna frequency was continuously swept over a band and, at the same time, the antenna bias voltage was varied. At a particular instant, the antenna frequency is assumed to be ω_1. If ω_1 is higher than the ambient plasma frequency, an electroacoustic wave is excited at the critical density point where $\omega_p = \omega_1$ somewhere on the density profile in the antenna vicinity.

The excited electroacoustic wave which propagates outwardly in a large volume of underdense ambient plasma is essentially a travelling wave because of the large plasma volume. It appears that the amount of energy used to excite the electroacoustic wave remains rather constant even for various antenna frequencies and various density profile which is changed by the variation of antenna bias voltage.

The excited electroacoustic wave which propagates inwardly toward the antenna becomes evanescent because an overdense plasma surrounds the antenna. Thus, no standing electroacoustic wave can be set up in this situation and no electroacoustic resonance can be observed through the reflected wave of the antenna.

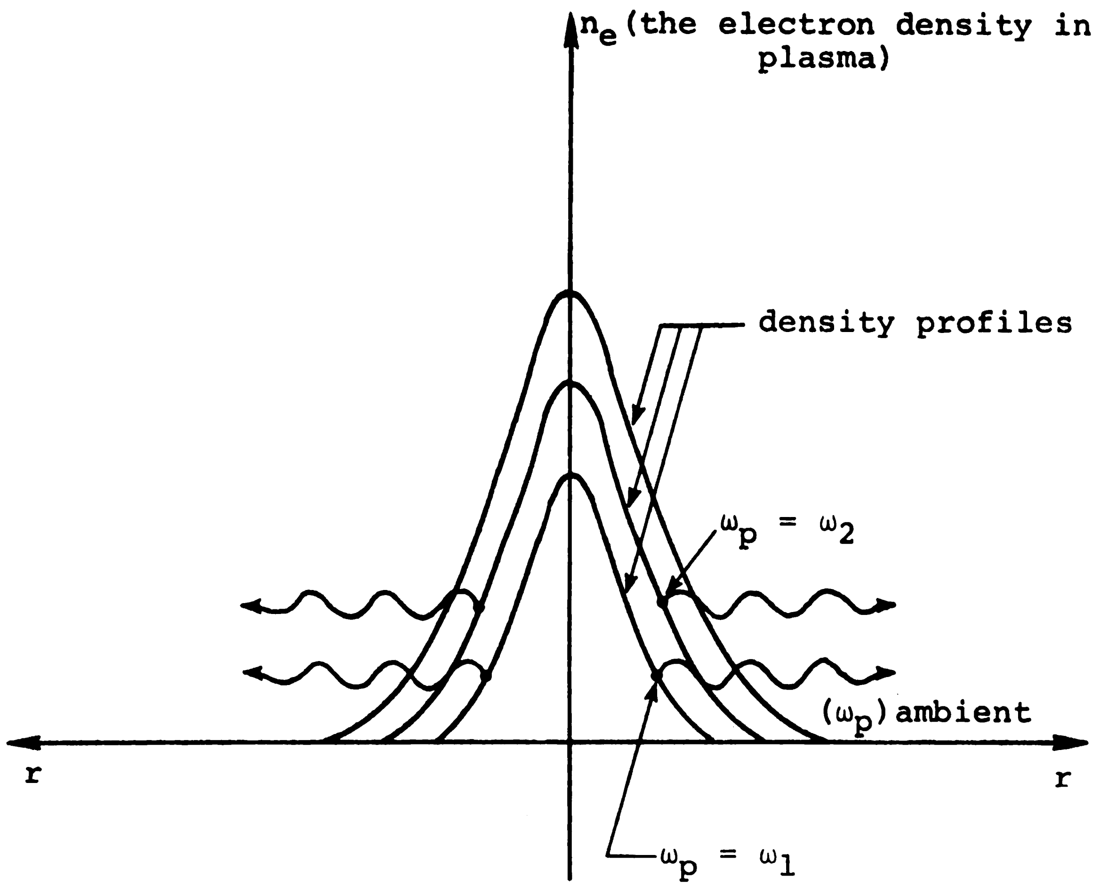

Figure 4.7 Plasma density profiles surrounding the antenna for various positive bias voltages.

If the antenna frequency band is lower than the ambient plasma frequency, neither electroacoustic wave can be excited nor propagates in the plasma because every point in the plasma volume is overdense with respect to this frequency band.

Therefore, one would not expect to observe any significant effect on the RW-SF curve as the antenna bias voltage is varied positively.

4.4.2 The Case When the Cylindrical Antenna is Biased Negatively:

When the antenna is biased negatively with respect to the plasma, electrons in the antenna vicinity are repelled. This will create an electron-deficient region surrounding the antenna, or a conventional plasma sheath with a density profile as shown in Figure 4.8.

For this situation, the local plasma frequency in the plasma sheath region is lower than the ambient plasma frequency. When the antenna frequency is lower than the ambient plasma frequency, an electroacoustic wave can be excited at a critical density point on the density profile of the plasma sheath. This excited electroacoustic wave attenuates outwardly; but can propagate inwardly because the plasma sheath region is underdense with respect to this frequency. The inward electroacoustic wave is essentially trapped in the finite plasma sheath region, so that it will set up a standing pattern. Furthermore, when the width of the plasma sheath is roughly in the order of an integral multiple of the half

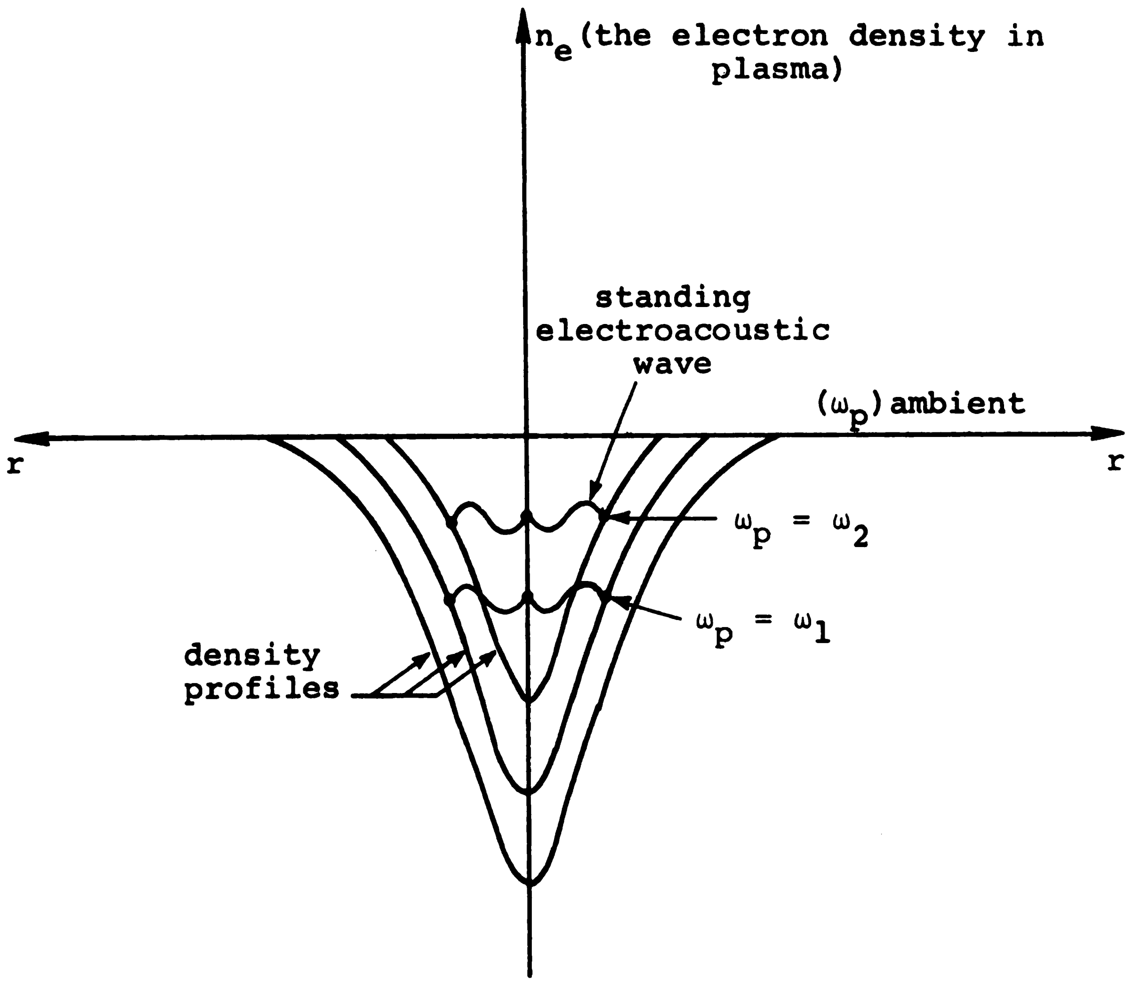

Figure 4.8 Plasma density profiles surrounding the antenna for various negative bias voltages.

electroacoustic wavelength, the electroacoustic wave will reach a resonance condition. Whenever the electroacoustic resonance is reached at a particular antenna frequency and at a particular antenna bias voltage, more power is transfered from the antenna to the plasma resulting a dip in the reflected wave from the antenna. Thus, as the antenna bias voltage is varied, while the antenna frequency is being swept, the electroacoustic resonance is reached at some discrete frequencies. Since these discrete frequencies are dependent on the density profile of the plasma sheath, which are controlled by the antenna bias voltage, the low frequency part of the RW-SF curve will be altered when the antenna bias voltage is varied.

When the antenna frequency is higher than the ambient plasma frequency, no critical density point can be found at any point of the plasma volume. Thus, according to Baldwin's [28] theory, no electroacoustic wave can be excited in the plasma. If no electroacoustic wave is excited for the frequency band higher than the ambient plasma frequency, no significant change on the RW-SF curve can be observed when the antenna bias voltage is varied.

Therefore, when the negative antenna bias voltage is varied, only the part of the RW-SF curve where the antenna frequency is lower than the ambient plasma frequency is affected.

4.5 Potential Application

The result of study described in this chapter may lead to a convenient technique for plasma diagnostics; especially for the measurement of the local plasma density.

A feasible scheme can be the following: A small movable monopole can be built to probe the density of a plasma volume. The exciting frequency of the monopole is swept over an appropriate frequency range. The bias voltage of the monopole is made variable from zero volt to a certain negative volt. The reflected wave versus sweeping frequency curve is displayed on the scope. As the bias voltage is varied (usually manually), the lower frequency part of the RW-SF curve will be altered. The highest frequency of this altered frequency band is the local plasma frequency at the location of this monopole probe.

The advantage of this diagnostic technique is the direct reading of the local plasma frequency and the quickness of obtaining results. Unlike the conventional Langmuir probe method, this method does not require any graphical or computational intermediate steps. The disadvantage of this method is the requirement of a sweep frequency generator and a variable bias voltage setup. The commercially available sweep frequency generators usually have limited sweeping frequency bands so that the measurable range of the plasma density may also be limited.

4.6 Analysis of the Coupling between the Electromagnetic Mode and Electroacoustic Mode in the Plasma Sheath

In this section, we aim to show that the electric field set up by the charge on the antenna will excite an electroacoustic wave in the plasma sheath surrounding the antenna. The excitation of an electroacoustic wave is possible because the gradient of the electron density in the plasma sheath surrounding the antenna and the electric field on the antenna surface are both in the same direction--the radial direction. Thus, a strong coupling between the electroacoustic mode and the electromagnetic mode can exist. The theory presented in this section is to confirm the experimental observation that an antenna can excite an electroacoustic wave in the plasma sheath surrounding the antenna.

Since we are concerned only with the electroacoustic wave in this section, the motion of positive ions is ignored in the analysis. Consider the geometry of Figure 4.9 where a cylindrical antenna is located along the z-axis. The electron density profile in the plasma sheath surrounding the antenna is also shown in this figure. Starting from the basic equations which govern the system,
Maxwell's equations in the plasma sheath are

$$\nabla \times \vec{E} = - j\omega\mu_o\vec{H} \tag{4.6.1}$$

$$\nabla \times \vec{H} = - en_o\vec{U}_e + j\omega\varepsilon_o\vec{E} \quad . \tag{4.6.2}$$

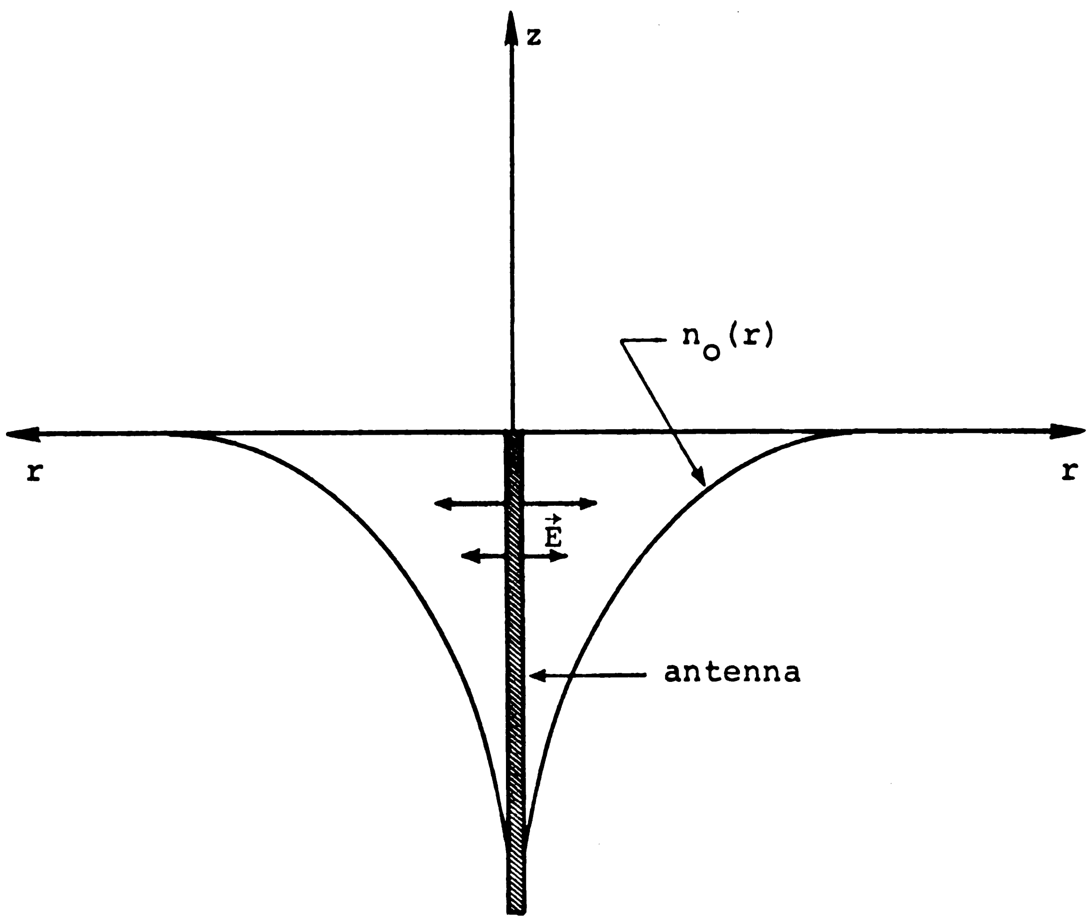

Figure 4.9 Geometry of a cylindrical antenna surrounded by a plasma sheath.

The equation of mass conservation of electrons is

$$\frac{\partial N_e}{\partial t} + \nabla \cdot (N_e \vec{U}_e) = 0 \qquad (4.6.3)$$

where

$$N_e = n_o(\vec{r}) + n_e(\vec{r},t) \ . \qquad (4.6.4)$$

Thus, equation (4.6.3) becomes

$$j\omega n_e + \nabla \cdot (n_o \vec{U}_e) = 0 \qquad (4.6.5)$$

when $n_e << n_o$.

The equation of momentum conservation of electrons is

$$\frac{\partial \vec{U}_e}{\partial t} + \gamma_e \vec{U}_e = - \frac{e}{m_e} \vec{\xi} - \frac{V_e}{n_o} \nabla N_e \qquad (4.6.6)$$

where

$$\vec{\xi} = \vec{E}_{dc} + \vec{E} \ . \qquad (4.6.7)$$

For the d.c. component of equation (4.6.6),

$$0 = - \frac{e}{m_e} \vec{E}_{dc} - \frac{V_e}{n_o} \nabla n_o \ . \qquad (4.6.8)$$

Equation (4.6.8) shows that the plasma density profile $n_o(\vec{r})$ is maintained by the d.c. component of the electric field. For the a.c. component of equation (4.6.6)

$$(j\omega + \gamma_e)\vec{U}_e = - \frac{e}{m_e} \vec{E} - \frac{V_e}{n_o} \nabla n_e \ . \qquad (4.6.9)$$

Taking the divergence of equation (4.6.2) and using equation (4.6.5), we have

$$0 = j\omega e n_e + j\omega\varepsilon_o \nabla \cdot \vec{E} \qquad (4.6.10)$$

or

$$\nabla \cdot \vec{E} = -\frac{e n_e}{\varepsilon_o} \ . \qquad (4.6.11)$$

Taking the curl of equation (4.6.1) and using equation (4.6.2), we have

$$\nabla \times \nabla \times \vec{E} = \omega^2 \mu_o \varepsilon_o \vec{E} + j\omega\mu_o e n_o \vec{U}_e \ . \qquad (4.6.12)$$

Using equation (4.6.9), equation (4.6.12) reduces to

$$\begin{aligned} \nabla \times \nabla \times \vec{E} &= \omega^2 \mu_o \varepsilon_o \left[1 - \frac{\omega_e^2}{\omega^2 + \gamma_e^2} - j\,\frac{\gamma_e \omega_e^2}{\omega(\omega^2 + \gamma_e^2)}\right]\vec{E} \\ &\quad + \left(\frac{\omega^2 + j\omega\gamma_e}{\omega^2 + \gamma_e^2}\right)\mu_o \varepsilon_o V_e^2 \nabla(\nabla \cdot \vec{E}) \\ &= \beta_{em}^2 \vec{E} + \alpha \nabla(\nabla \cdot \vec{E}) \end{aligned} \qquad (4.6.13)$$

where

$$\beta_{em}^2 = \omega^2 \mu_o \varepsilon_o \left[1 - \frac{\omega_e^2}{\omega^2 + \gamma_e^2} - j\,\frac{\gamma_e \omega_e^2}{\omega(\omega^2 + \gamma_e^2)}\right] \qquad (4.6.14)$$

= propagation constant of the electromagnetic wave in the plasma sheath.

$$\alpha = \left(\frac{\omega^2 + j\omega\gamma_e}{\omega^2 + \gamma_e^2}\right)\frac{V_e^2}{c^2} \tag{4.6.15}$$

and $c^2 = \dfrac{1}{\mu_o \varepsilon_o}$.

Let us assume that $\vec{E} = \vec{E}_e + \vec{E}_p$ where $\vec{E}_e$ corresponds to the electric field of the electromagnetic wave such that $\nabla \cdot \vec{E}_e = 0$ and $\vec{E}_p$ corresponds to the electric field of the longitudinal electroacoustic wave such that $\nabla \times \vec{E}_p = 0$.

Equation (4.6.13) then reduces to

$$(\nabla^2 + \beta_{em}^{\ 2})\vec{E}_e + (\alpha\nabla^2 + \beta_{em}^{\ 2})\vec{E}_p = 0 \quad . \tag{4.6.16}$$

Taking the curl of equation (4.6.16), we have

$$(\nabla^2 + \beta_{em}^{\ 2})(\nabla \times \vec{E}_e) = -(\nabla\beta_{em}^{\ 2}) \times (\vec{E}_e + \vec{E}_p) \quad . \tag{4.6.17}$$

Taking the divergence of equation (4.6.16), we have

$$(\nabla^2 + \frac{\beta_{em}^{\ 2}}{\alpha})(\nabla \cdot \vec{E}_p) = -(\frac{1}{\alpha}\nabla\beta_{em}^{\ 2}) \cdot (\vec{E}_e + \vec{E}_p) \quad .$$

Using $\nabla \cdot \vec{E}_p = -\dfrac{en_e}{\varepsilon_o}$ from equation (4.6.11), we got

$$(\nabla^2 + \frac{\beta_{em}^{\ 2}}{\alpha})n_e = \frac{\varepsilon_o}{e}(\frac{1}{\alpha}\nabla\beta_{em}^{\ 2}) \cdot (\vec{E}_e + \vec{E}_p) \quad . \tag{4.6.18}$$

Equation (4.6.18) is the inhomogeneous wave equation for the electroacoustic wave. In this equation, $\beta_{em}^{\ 2}$ is in the r direction. $\vec{E}_e$ is also in the r direction on the antenna surface because the electric field on the conductor surface is perpendicular to the surface. Therefore, there is a strong coupling between the electromagnetic mode and the plasma mode. In other words, the radial component of $\vec{E}_e$ field on the antenna surface can excite an electroacoustic wave, through the gradient of the density profile, in the plasma sheath.

CHAPTER 5

EXCITATION OF ELECTROACOUSTIC RESONANCES IN VARIOUS PLASMA GEOMETRIES AND STUDY OF THE REFLECTION BEHAVIOR OF ELECTROACOUSTIC WAVES ON VARIOUS SURFACES

5.1 Introduction

Electroacoustic resonances are excited in (1) a cylindrical plasma column, (2) a rectangular plasma column and (3) a single-slope density profile plasma column. The nature of the electroacoustic resonances in different plasma geometries is studied.

The techniques of exciting electroacoustic resonances are applied to study the reflection behavior of electroacoustic wave on (1) dielectric surface and (2) metallic surface.

5.2 Experimental Setup

For the experiments in this chapter, two types of mercury-vapor plasma tubes have been constructed. One type was the cylindrical glass tube with a length of about 30 cm, outside diameter of 8 mm, inside diameter of 6 mm, and mercury pressure of about 1 micron. The structure of this tube is shown in Figure 5.1. The other type was the rectangular glass tube with a length of about 30 cm, outside cross sectional dimensions of 12 mm by 8 mm with a wall thickness of 1 mm, and the mercury pressure of about 1 micron. This rectangular tube was divided into 3 sections; an uniform density section, a single-slope density profile (single-profile) section with a metallic reflector and a single-profile section with a glass reflector. A single-profile can be created in this tube by squeezing the plasma current flow at a gap close to the wall by means of a built-in glass plate. The structure of this tube is shown in Figure 5.2.

The single-profile plasma column was constructed primarily for the purpose of studying the reflection behavior of an electroacoustic wave on various surfaces. It was hoped that the electromagnetic field of the electroacoustic probe can excite an electroacoustic wave in the region between the reflector and a point on the plasma density profile and not in the plasma sheath at the glass wall next to the electro-acoustic probe. Assuming that an electroacoustic wave can be excited in the region mentioned above by the electromagnetic field of the electroacoustic probe, a standing electroacoustic wave will be set up between the critical density point and the reflector if a sufficient amount of electroacoustic wave is reflected from the reflector surface. This standing electroacoustic wave will appear as resonances in the reflected electromagnetic wave which is picked up by the electroacoustic probe when the plasma current is varied. If the reflector surface absorbs the incident electroacoustic wave, no standing electroacoustic wave will be set up and no resonances will be observed. From the patterns of resonances observed with different reflectors, the reflection behavior of the electroacoustic wave on various reflector surfaces can be studied.

The schematic diagram of the experimental setup is shown in Figure 5.3. The incident c. w. electromagnetic wave which excites an electroacoustic wave in the plasma column is fed to the electroacoustic probe which is essentially an open-ended coaxial line with a protruding center conductor with a disk tip. The reflected electromagnetic wave from the plasma column is picked up by the same electroacoustic probe. This reflected electromagnetic wave is passed through a directional coupler and a detector before reaching the vertical input terminal of the oscilloscope. The horizontal input of the oscilloscope synchronizes with 60 Hz sweeping of the plasma discharge current. The display of the reflected electromagnetic wave on the oscilloscope contains all the information on the electroacoustic and dipole resonances and is called the reflection curve in the later sections of this chapter.

5.3 Electroacoustic Resonances and Dipole Resonance in a Cylindrical Plasma Column

In this experiment, a cylindrical plasma tube was used in the setup as shown in Figure 5.3. The electromagnetic source was set at 2.4 GHz and the tube discharge current was

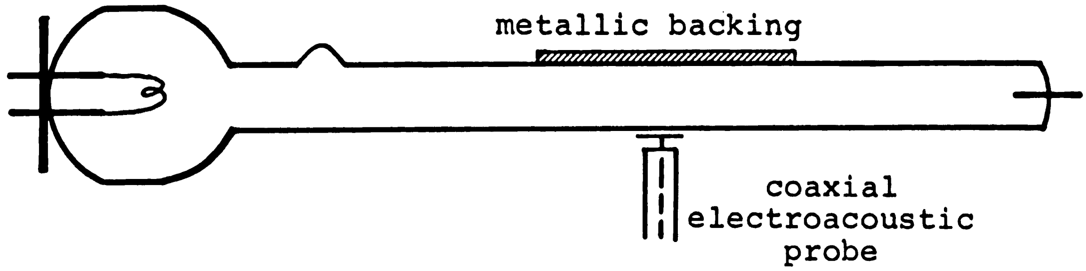

Figure 5.1 Structure of the cylindrical plasma tube.

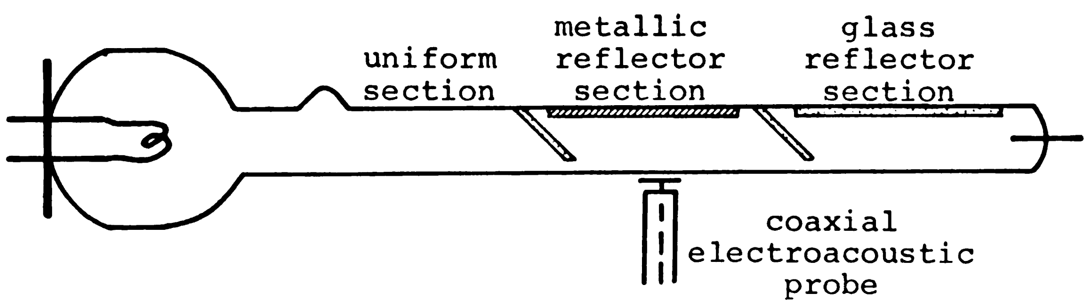

Figure 5.2 Structure of the rectangular plasma tube.

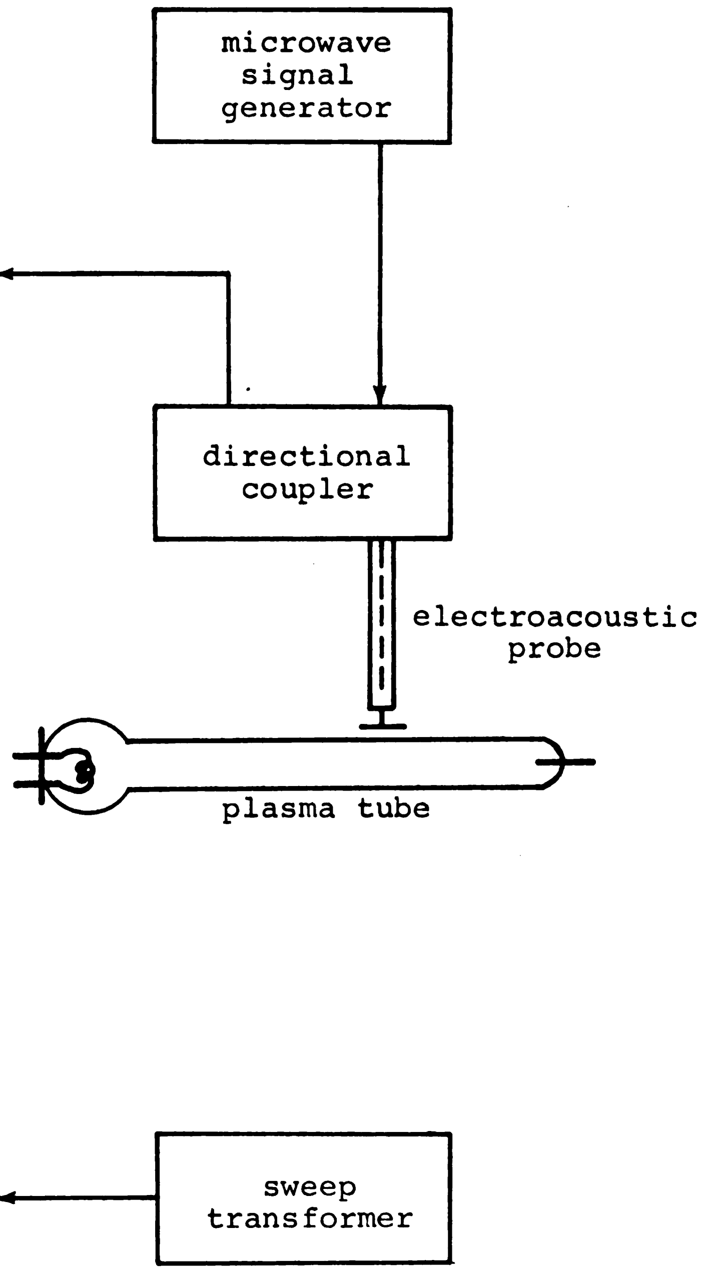

Figure 5.3 Experimental setup for the excitation and observation of electroacoustic resonances in different plasma geometries.

swept 60 Hz in the experiment. The reflected electromagnetic wave picked up by the electroacoustic probe went through the directional coupler (or a matched coaxial hybrid), detector and then was displayed on the oscilloscope. Resonance peaks were observed at various discharge currents. When a metallic backing was placed on the back side of the tube as shown in Figure 5.4, one of the resonance peaks was affected. Three sets of oscillograms were taken in this experiment and they are shown in Figures 5.6, 5.7 and 5.8.

Figure 5.6 shows the resonance curves in the lower discharge current region. The operating frequency was set at 2.4 GHz and the plasma current was swept around 95 mA. No effect on this part of the resonance curve was observed with a metallic backing to the tube. It is evident that these peaks are electroacoustic resonances which are excited in the plasma sheath directly near the probe. A metallic backing in the back side of the tube has little effect on this locally excited electroacoustic standing wave. This phenomenon is shown in Figure 5.5.

Figures 5.7 and 5.8 show the resonance curves in the higher discharge current region observed in two different plasma tubes of same dimensions. When the tube was placed with a metallic backing on the back side, some effect was observed on the first highest peak of the resonance curve. This first highest peak is recognized as the dipole resonance which is physically different from the remaining electroacoustic

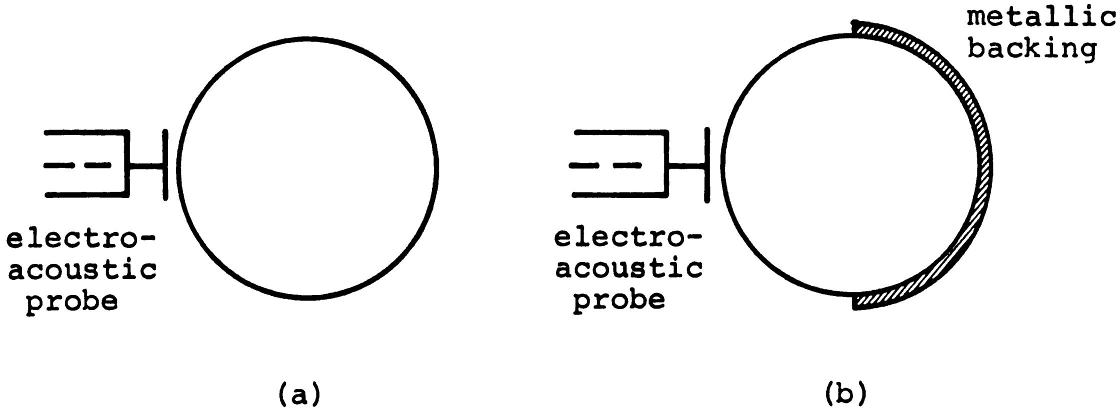

Figure 5.4 Cross-sectional view of the cylindrical plasma tube. (a) without metallic backing (b) with metallic backing

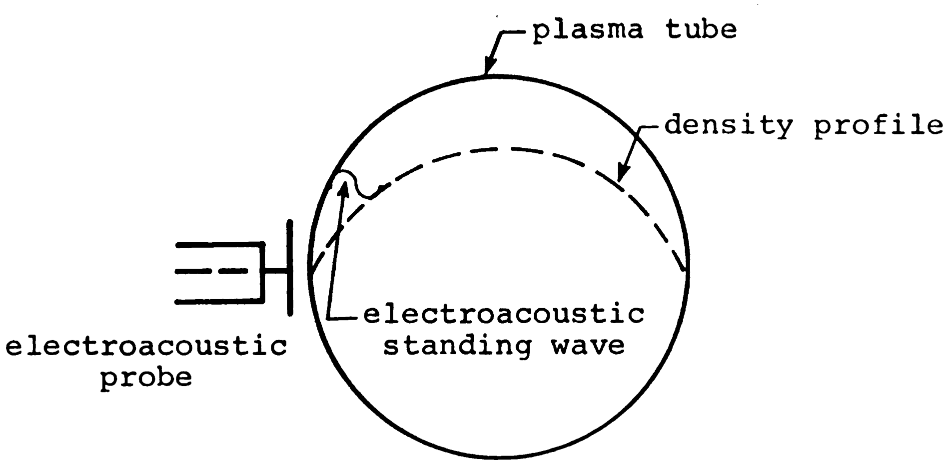

Figure 5.5 Electroacoustic resonance in a cylindrical plasma column.

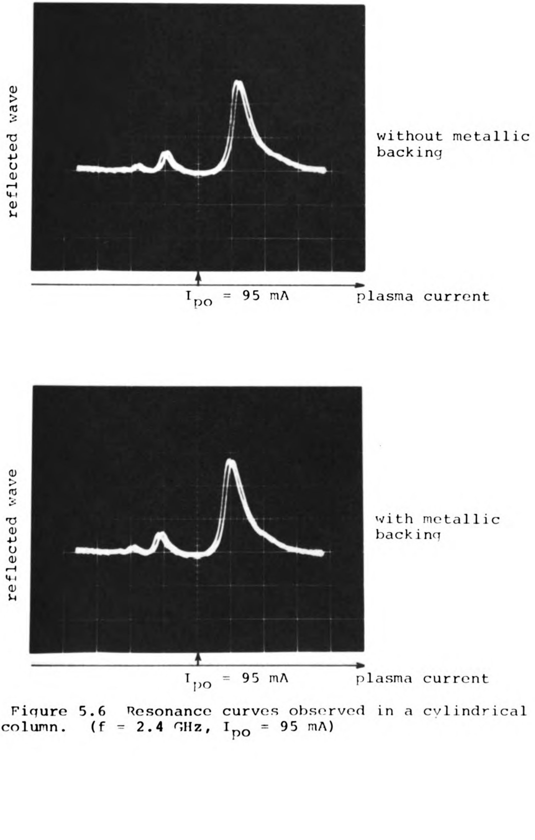

Figure 5.6 Resonance curves observed in a cylindrical plasma column. (f = 2.4 GHz, I_{po} = 95 mA)

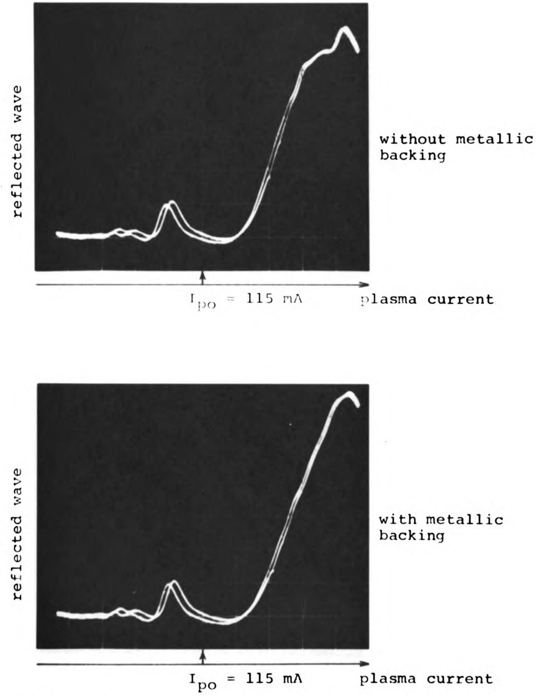

Figure 5.7 Resonance curves observed in a cylindrical plasma column. (f = 2.4 GHz, I_{po} = 115 mA)

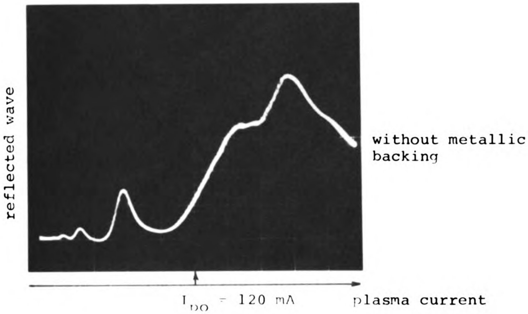

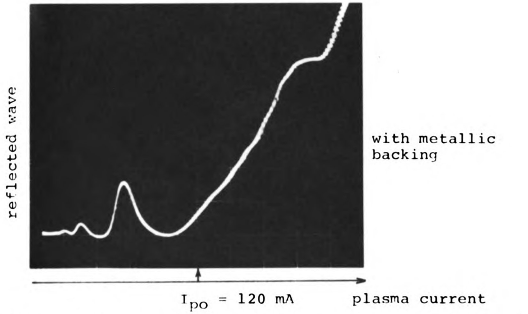

Figure 5.8 Resonance curves observed in a cylindrical plasma column. (f = 2.45 GHz, I_{po} = 120 mA)

resonances. Since a dipole resonance is an electromagnetic resonance and is excited over the whole column, a metallic backing will alter drastically the boundary condition and lead to a change in the dipole resonance peak.

5.4 Electroacoustic Resonances and Dipole Resonance in a Rectangular Plasma Column

In this experiment, a rectangular plasma tube was used in the setup as shown in Figure 5.3. The electro-acoustic probe was placed at the uniform plasma section. The resonance curves were observed in both the low and the high discharge current regions and a complete series of electroacoustic and dipole resonances can be reconstructed in four oscillograms in Figure 5.9. To our best knowledge, the electroacoustic and dipole resonances have not been studied in this rectangular geometry. In Figure 5.9, it is observed that the resonance curve consists mainly of four distinct peaks; the highest peak occurs at the high discharge current end and the rest with descending order of magnitude toward the low discharge current end. This curve looks similar to the resonance curve observed in the cylindrical plasma tube.

Figures 5.10 and 5.11 show the effect of a metallic backing on the resonance peaks. When the metallic backing was placed on the tube, the second highest peak was affected; but not the first highest peak as in the case of the cylindrical

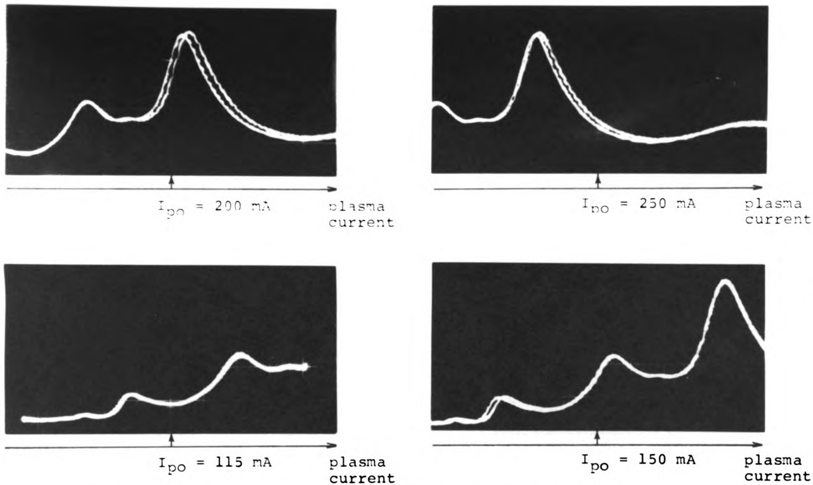

Figure 5.9 Resonance curves observed in the uniform section of a rectangular plasma tube. (f = 2.4 GHz, I_{po} = 115 mA, 150 mA, 200 mA, 250 mA)

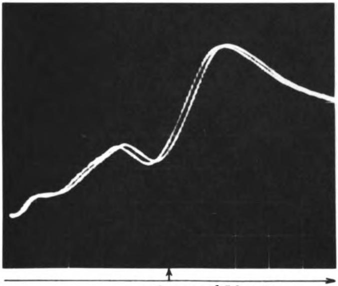

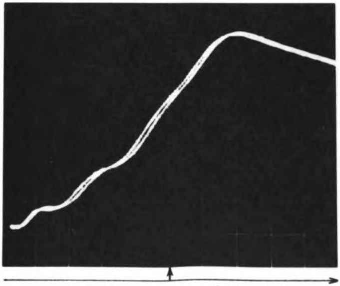

Figure 5.10 Resonance curves observed in the uniform region of a rectangular plasma tube. (f = 2 GHz, I_{po} = 150 mA)

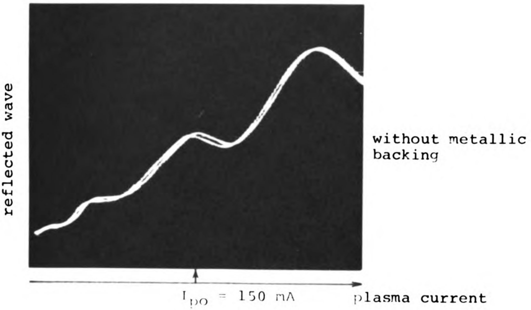

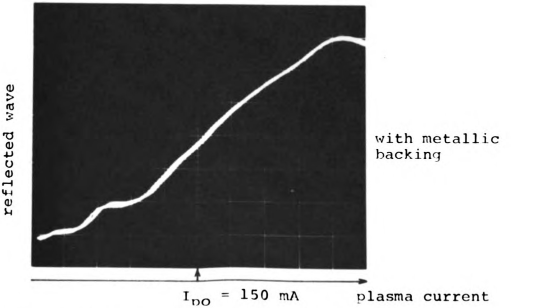

Figure 5.11 Resonance curves observed in the uniform region of a rectangular plasma tube. (f = 2.4 GHz, I_{po} = 150 mA)

plasma tube. This may imply that the second highest peak in the resonance curve observed in a rectangular plasma tube is the dipole resonance.

5.5 Resonances in Single-profile Plasma Column in the Rectangular Tube

As stated before, a single-profile column was fabricated in order to study the reflection behavior of an electroacoustic wave on various boundary surfaces. Before this study was conducted, the plasma density profile of this plasma column was examined by observing the resonance curves created by the electroacoustic probe at different parts of the plasma column.

5.5.1 Glass Reflector Region

We first examined the density profile at three different points in the glass reflector region as shown in Figure 5.12. A large density profile difference was expected to exist between the front and back sides at the neck section of this region. The density profile should become more uniform away from the neck section, so that a small density difference was expected to exist between the front and back sides at the center and tail sections of this region. The electroacoustic probe was placed at different positions along this glass reflector region and the reflection curves were studied.

Figure 5.14 shows that at the neck section, the

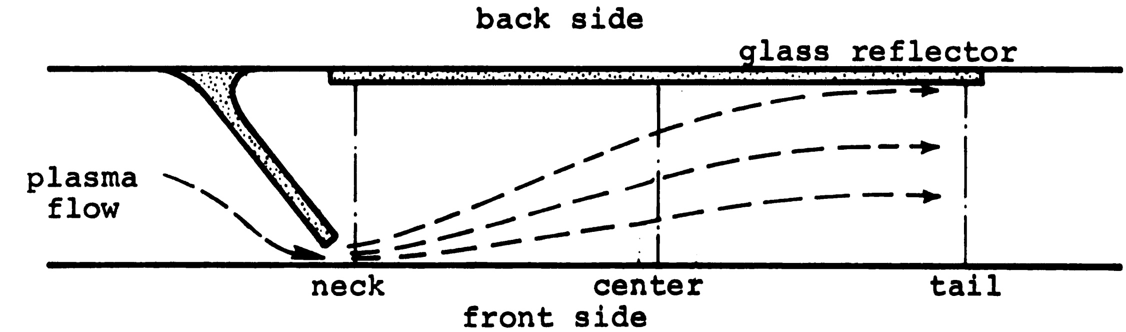

Figure 5.12 Plasma density distribution in the glass reflector region.

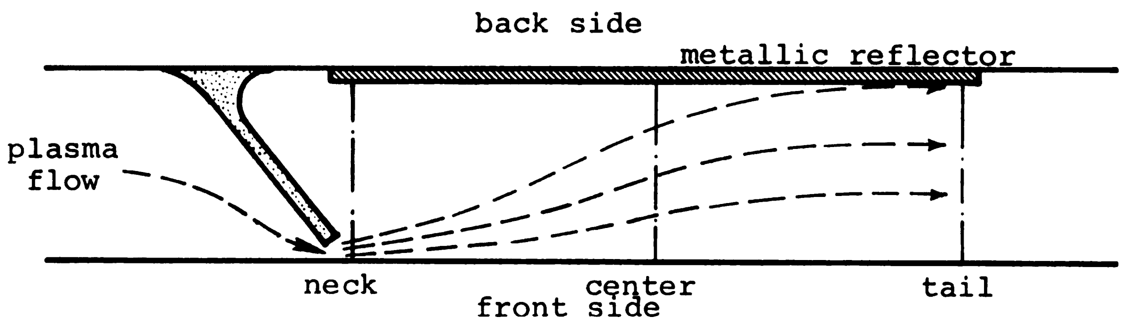

Figure 5.13 Plasma density distribution in the metallic reflector region.

reflection curve from the front side is significantly different from that of the back side implying the existence of a drastic density profile difference between the front and back sides of the tube at this section.

Figures 5.15 and 5.16 show that a relatively small difference exists between the reflection curves from the front and back sides at the central section of the glass reflector region. This will imply the existence of only a small difference in the densities between the front and back sides at this section of the tube. Also in Figure 5.15, the effect due to the metallic backing is indicated. We can see that the second highest peak was altered when the metallic backing was placed on the tube.

Figure 5.17 shows the existence of a small difference in density profile between the front and back sides at the tail section of the glass reflector region. The similar effect due to the metallic backing was also observed in the experiment.

Experimental results shown in Figures 5.14, 5.15, 5.16 and 5.17 confirm that a single-profile was created in this rectangular plasma tube.

5.5.2 Metallic Reflector Region

The density profile in the metallic reflector region of the same tube as shown in Figure 5.13 was studied. Three sections, the neck, center and tail sections, of this region were examined. A series of oscillograms of the reflection

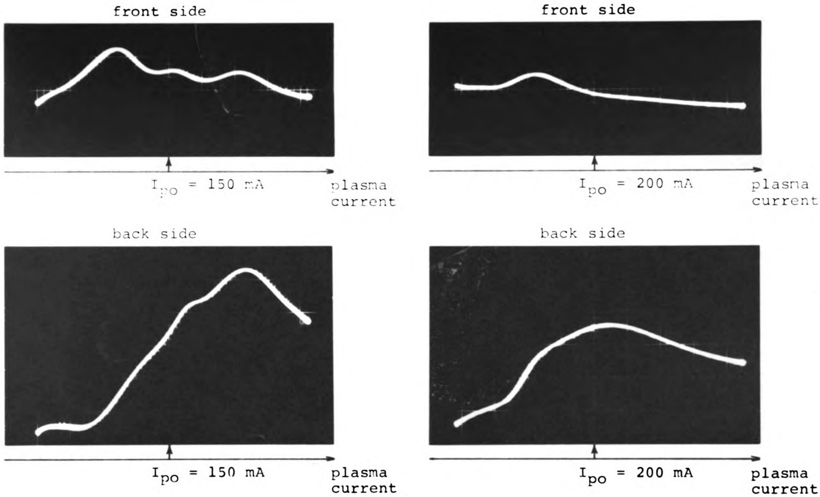

Figure 5.14 Resonance curves observed in the neck section of the glass reflector region of a rectangular plasma tube. (f = 2.4 GHz, I_{po} = 150 mA, I_{po} = 200 mA)

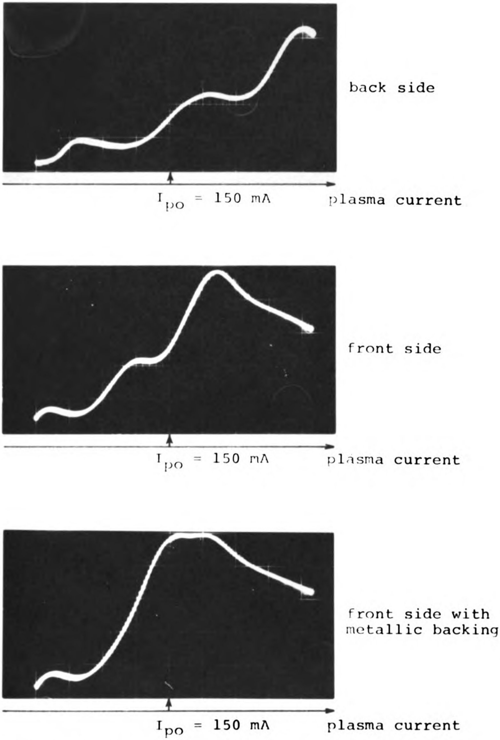

Figure 5.15 Resonance curves observed in the center section of the glass reflector region of a rectangular plasma tube. (f = 2.4 GHz, I_{po} = 150 mA)

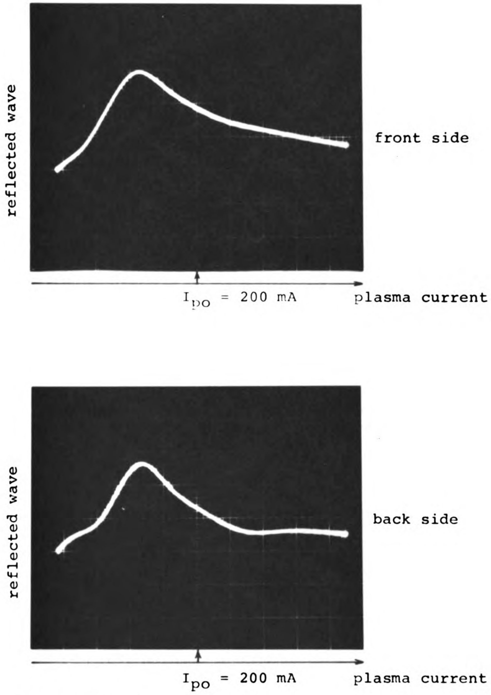

Figure 5.16 Resonance curves observed in the center section of the glass reflector region of a rectangular plasma tube. (f = 2.4 GHz, I_{po} = 200 mA)

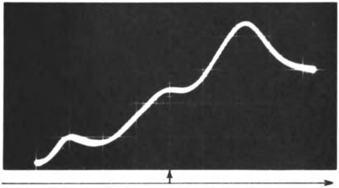

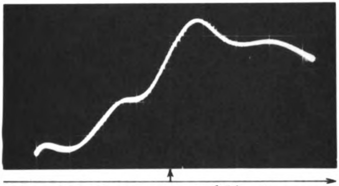

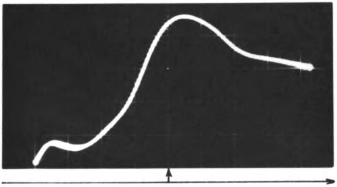

Figure 5.17 Resonance curves observed in the tail section of the glass reflector region of a rectangular plasma tube. (f = 2.4 GHz, I_{po} = 150 mA)

curves were taken during the experiment at the neck, center and tail sections of the metal reflector region under various discharge currents. By grouping these oscillograms together, we obtained three complete curves of the resonance.

Figure 5.18 shows a complete curve of resonance at the neck section. At this section no distinct electroacoustic resonance was observed. It was probably due to the turbulent plasma flow and irregular density distribution in this position.

Figure 5.19 shows a complete curve of resonance at the center section. The electroacoustic and dipole resonances were observed.

Figure 5.20 shows a complete curve of resonance at the tail section. The electroacoustic and dipole resonances were clearly observed at this section.

5.6 Reflection Behavior of Electroacoustic Wave from Metallic and Non-metallic Surfaces

Figure 5.21 shows the reflection curves observed in the uniform, glass reflector and metallic reflector regions of the tube. The reflection curve from the metallic reflector region is different from the other two cases. This appears to imply different reflection behaviors of an electroacoustic wave on metallic and non-metallic surfaces. However, Figure 5.22 shows that the reflection curve observed in the uniform column is affected by an external metallic backing and,

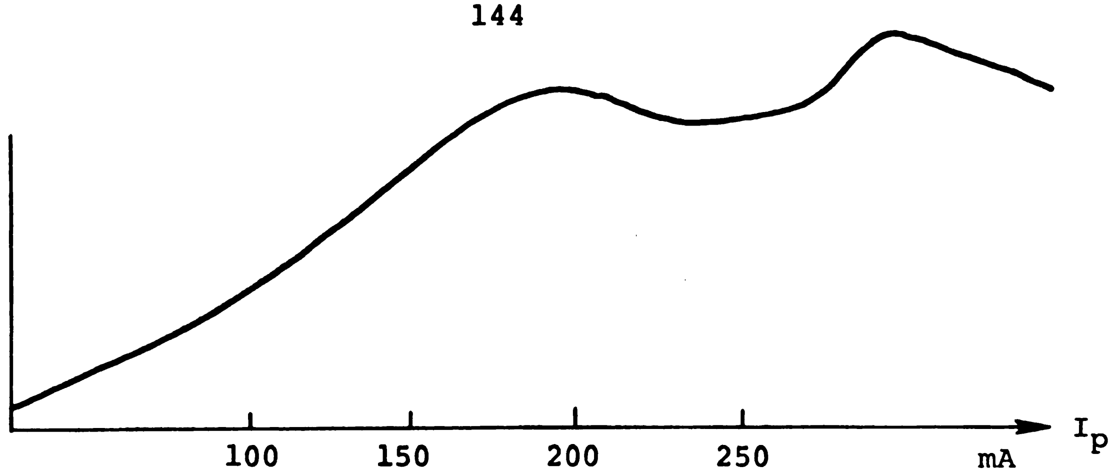

Figure 5.18 Resonance curve observed in the neck section of the metallic reflector region of a rectangular plasma tube. (f = 2.4 GHz)

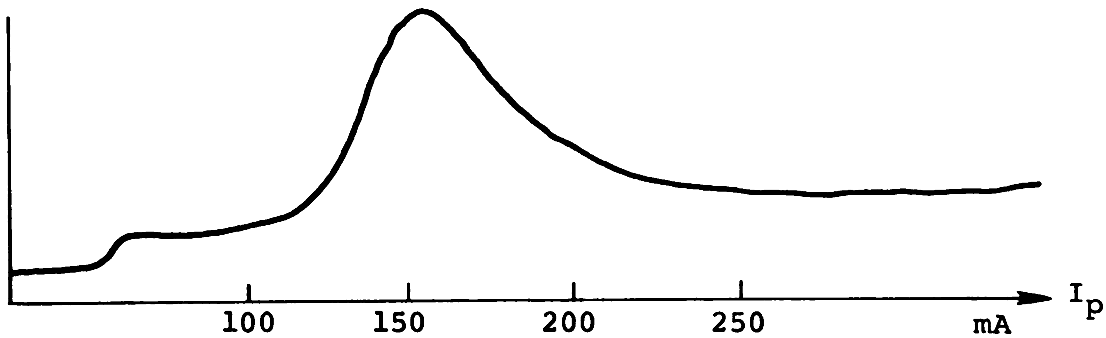

Figure 5.19 Resonance curve observed in the center section of the metallic reflector region of a rectangular plasma tube. (f = 2.4 GHz)

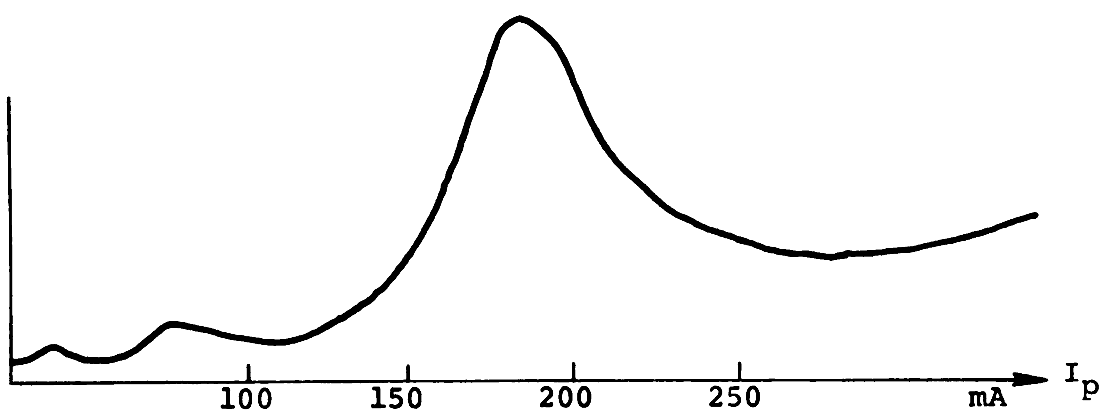

Figure 5.20 Resonance curve observed in the tail section of the metallic reflector region of a rectangular plasma tube. (f = 2.4 GHz)

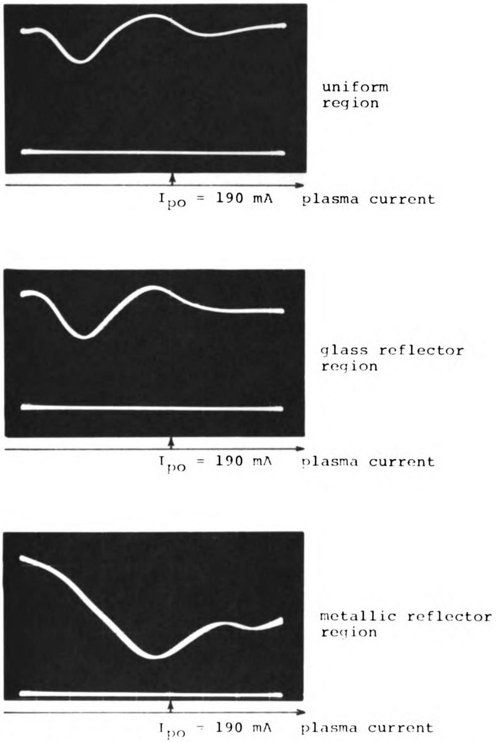

Figure 5.21 Reflection curves observed in uniform, glass reflector and metallic reflector regions of a rectangular plasma tube. (f = 2.33 GHz, I_{po} = 190 mA)

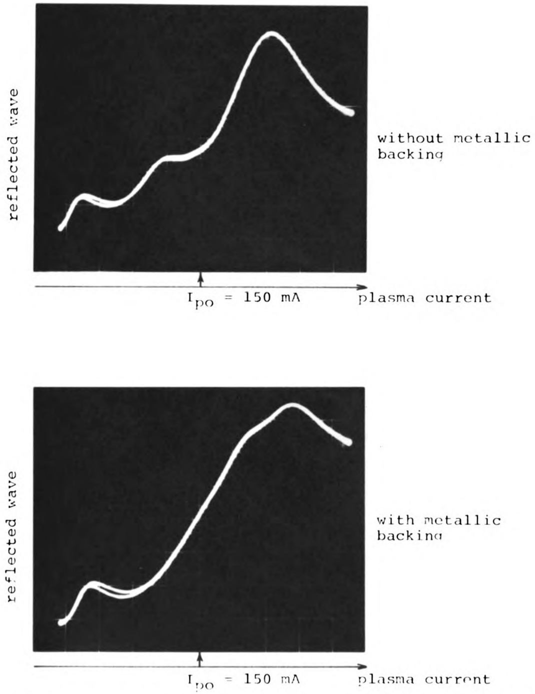

Figure 5.22 Reflection curves observed in the uniform region of a rectangular plasma tube. (f = 2.4 GHz, I_{po} = 150 mA)

furthermore, Figure 5.23 shows that inside and outside metallic backing do not give different reflector curves. Based on the results observed in Figures 5.22 and 5.23, the different reflection curves observed in Figure 5.21 may not be due to the reflecting surface. This may imply that all the electroacoustic resonances were still excited at the front side of the tube directly near the probe. The different reflection curves observed in the glass reflector and metallic reflector regions may be due to the electromagnetic effect of the metallic reflector to the reflected wave.

Our attempt to study the reflection behavior of an electroacoustic wave on metallic and non-metallic surfaces using a single-profile plasma column was proved to be inconclusive. A major disruption in the vacuum system prevented the continuation of this study. It is recommended that with some modifications on the tube construction, but based on the same idea of a single-profile plasma column, the reflection behavior of the electroacoustic wave can be successfully studied.

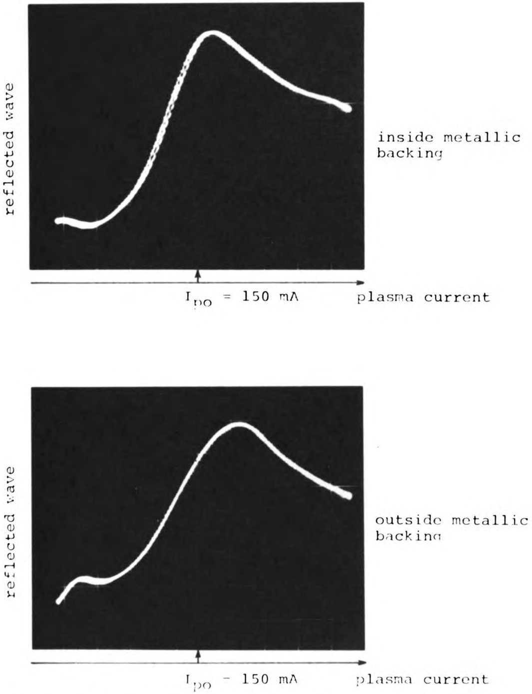

Figure 5.23 Reflection curves observed in a rectangular plasma tube with the inside and outside metallic backing. (f = 2.4 GHz, I_{po} = 150 mA)

APPENDICES

APPENDIX A

NUMERICAL CALCULATION OF R_1, R_2, THE ELECTRON-ION COMPOSITION RATIOS OF THE n_1 WAVE AND THE n_2 WAVE

To determine R_1 and R_2, the electron-ion composition ratios of the n_1 wave and the n_2 wave, for various source frequencies, various collision frequencies and various T_e/T_i by using a computer, we write the following equations in terms of X, Y and Z where

$$X = (\omega_e/\omega)^2 \tag{A-1}$$

$$Y = \gamma_e/\omega \tag{A-2}$$

$$Z = T_e/T_i \quad . \tag{A-3}$$

Equation (2.2.9)

$$\beta_e{}^2 = \frac{\omega^2}{V_e{}^2}\left(1 - \frac{\omega_e{}^2}{\omega^2} - j\,\frac{\gamma_e}{\omega}\right) \tag{A-4}$$

can be written as

$$\beta_e{}^2 = K_2{}^2 A_1 \tag{A-5}$$

where

$$K_2 = \frac{\omega}{V_e} \tag{A-6}$$

$$A_1 = (1 - X - jY) \quad . \tag{A-7}$$

For equation (2.2.13),

$$\beta_i{}^2 = \frac{\omega^2}{V_i{}^2}\left(1 - \frac{\omega_i{}^2}{\omega^2} - j\,\frac{\gamma_i}{\omega}\right) \quad , \tag{A-8}$$

we use equations (2.2.8), (2.2.12), (2.1.11) and (2.1.12) with hydrogen gas plasma assumption, then we have

$$\omega_i{}^2 = (m_e/m_i)\,\omega_e{}^2 \quad ,$$

or

$$\omega_i{}^2 = (1/1836)\,\omega_e{}^2 \quad ; \tag{A-9}$$

$$V_i{}^2 = (m_e/m_i)\,(T_i/T_e)V_e{}^2 \quad ,$$

or

$$V_i{}^2 = V_e{}^2/(1836Z) \quad ; \tag{A-10}$$

assuming

$$(\gamma_i/\gamma_e) = (V_i/V_e) \tag{A-11}$$

and using equation (A-10), we have

$$\gamma_i = \gamma_e/(1836)^{1/2} \quad . \tag{A-12}$$

Equation (A-8) can be written as

$$\beta_i^{\,2} = K_2^{\,2} A_2 \tag{A-13}$$

where

$$A_2 = 1836Z - XZ - jY(1836Z)^{1/2} \quad . \tag{A-14}$$

Similarly, equation (2.3.15)

$$A_o = \left[(\beta_i^{\,2} - \beta_e^{\,2})^2 + 4\left(\frac{\omega^4}{V_e^{\,2} V_i^{\,2}}\right)\left(\frac{\omega_e^{\,2}}{\omega^2}\right)\left(\frac{\omega_i^{\,2}}{\omega^2}\right)\right]^{\frac{1}{2}}$$

can be written as

$$A_o = K_2^{\,2} A_3 \tag{A-15}$$

where

$$A_3 = \left[(A_2 - A_1)^2 + 4ZX^2 \right]^{\frac{1}{2}} \quad . \tag{A-16}$$

Substituting equations (A-5), (A-13), (A-15) into equations (2.4.3), (2.4.5) and using equations (A-1), (A-5) yield

$$R_1 = \frac{1}{2X}(A_1 - A_2 + A_3) \tag{A-17}$$

$$R_2 = \frac{1}{2X}(A_1 - A_2 - A_3) \quad . \tag{A-18}$$

Equations for R_1 and R_2 are functions of X, Y and Z, i.e., functions of $(\omega_e/\omega)^2$, γ_e/ω and T_e/T_i. Therefore, the electron-ion composition ratios of the n_1 wave and the n_2 wave can be determined by assuming various source frequencies, various collision frequencies and various T_e/T_i.

APPENDIX B

NUMERICAL CALCULATION OF k_1, k_2, THE PROPAGATION CONSTANTS OF THE n_1 WAVE AND THE n_2 WAVE

To determine k_1, k_2, the propagation constants of the n_1 wave and the n_2 wave, for various source frequencies, various collision frequencies and various T_e/T_i by using a computer, we rewrite equations (2.5.1) and (2.5.2).

For hydrogen gas plasma, we use equation (A-14) as well as equations (A-5), (A-7), (A-13), (A-15), (A-16) and (A-6). Then equations for k_1 and k_2 can be written as

$$\frac{k_1}{(\omega/V_i)} = \left(\frac{A_1 + A_2 + A_3}{3672Z}\right)^{\frac{1}{2}} \tag{B-1}$$

$$\frac{k_2}{(\omega/V_e)} = \left(\frac{A_1 + A_2 - A_3}{2}\right)^{\frac{1}{2}} \tag{B-2}$$

where

$$A_1 = 1 - X - jY \tag{B-3}$$

$$A_2 = 1836Z - XZ - jY(1836Z)^{1/2} \tag{B-4}$$

$$A_3 = \left[(A_2 - A_1)^2 + 4ZX^2\right]^{1/2} \tag{B-5}$$

$$X = (\omega_e/\omega)^2 \tag{B-6}$$

$$Y = \gamma_e/\omega \tag{B-7}$$

$$Z = T_e/T_i \quad . \tag{B-8}$$

For xenon gas plasma, we use

$$\frac{\omega_i^2}{\omega_e^2} = \frac{m_e}{m_i} = \frac{1}{54 \times 1836} = \frac{1}{99144} \tag{B-9}$$

$$\frac{V_i^2}{V_e^2} = \left(\frac{m_e}{m_i}\right)\left(\frac{T_i}{T_e}\right) = \frac{1}{99144Z} \tag{B-10}$$

$$\frac{\gamma_i}{\gamma_e} = \frac{V_i}{V_e} = \frac{1}{(99144Z)^{1/2}} \quad . \tag{B-11}$$

Equation (A-8) becomes

$$\beta_i^2 = K_2^2 A_2 \tag{B-12}$$

where

$$A_2 = 99144Z - XZ - jY(99144Z)^{1/2} \quad . \tag{B-13}$$

Using equations (B-12), (B-13) as well as equations (A-5), (A-6), (A-7), (A-15), (A-16) in equations (2.5.1) and (2.5.2), we can write

$$\frac{k_1}{(\omega/V_i)} = \left(\frac{A_1 + A_2 + A_3}{198288Z}\right)^{\frac{1}{2}} \tag{B-14}$$

$$\frac{k_2}{(\omega/V_e)} = \left(\frac{A_1 + A_2 - A_3}{2}\right)^{\frac{1}{2}} \tag{B-15}$$

where

$$A_1 = 1 - X - jY \tag{B-16}$$

$$A_2 = 99144Z - XZ - jY(99144Z)^{1/2} \tag{B-17}$$

$$A_3 = \left[(A_2 - A_1)^2 + 4ZX^2\right]^{1/2} \tag{B-18}$$

$$X = (\omega_e/\omega)^2 \tag{B-19}$$

$$Y = \gamma_e/\omega \tag{B-20}$$

$$Z = T_e/T_i \quad . \tag{B-21}$$

Therefore, k_1 and k_2 for various source frequencies, various collision frequencies and various T_e/T_i can be determined. For hydrogen gas plasma, we use equations (B-1) through (B-8). For xenon gas plasma, we use equations (B-14) through (B-21).

Sample Program

```
      PROGRAM PLASMA (OUTPUT)
C
C     **********************************************************
C     THIS PROGRAM CALCULATES
C     (1) THE WAVE NUMBERS AK1K AND AK2K
C     (2) THE RATIOS RN1EI AND RN2EI
C     AS A FUNCTION OF X (X=(WE/W)**2) FOR AN ASSIGNED A
C     (A=COLLISION FREQUENCY/W).
C     THIS CASE (HYDROGEN GAS IS ASSUMED, TE=B*TI WHERE B=100)
C     **********************************************************
C
      REAL MOD1,MOD2
      COMPLEX C,D,AM,AN,ANMX,AK1K,AK2K,RN1EI,RN2EI,P
      DIMENSION A(7),X(15),AM(7,15),AN(7,15),ANMX(7,15),
     1P(7,15),Q(15),AK1K(7,15),AK2K(7,15),
     2RN1EI(7,15),RN2EI(7,15),MOD1(7,15),MOD2(7,15)
      A(1)=0.0
      A(2)=10.E-4
      DO 1 I=3,6
      A(I)=A(I-1)*10.
    1 CONTINUE
      X(1)=10.E-5
      DO 2 J=2,13
      X(J)=X(J-1)*10.
    2 CONTINUE
      B=100.
      C=CMPLX(0.0,1.0)
      E=SQRT(1836.*B)
      D=CMPLX(0.0,E)
      DO 3 I=1,6
      DO 4 J=1,13
      AM(I,J)=1.-X(J)-C*A(I)
      AN(I,J)=1836.*B-B*X(J)-D*A(I)
      P(I,J)=(AN(I,J)-AM(I,J))**2
      Q(J)=4.*B*X(J)**2
      ANMX(I,J)=CSQRT(P(I,J)+Q(J))
C     ----------------------------------------------------------
C     NOTING AT LARGE X, 4BX**2 IS MUCH SMALLER THAN THE
C     RE(AN-AM), SO ANMX SHOULD HAVE THE SIGNS OF (AN-AM).
C     SINCE IM(AN-AM) IS NEGATIVE. WE DEMAND IM(ANMX) NEGATIVE.
C     ----------------------------------------------------------
      IF(AIMAG(ANMX(I,J))-0.0) 20,20,10
   10 ANMX(I,J)=-(ANMX(I,J))
C     ----------------------------------------------------------
C     AK1K MIGHT HAVE 2 SOLUTIONS,ONE IS THE NEGATIVE OF THE
C     OTHER.SINCE IT IS A WAVE NUMBER WHICH HAS TO HAVE
C     POSITIVE REAL PART AND NEGATIVE IMAGINARY PART.SO WE
C     COULD PICK THE REQUIRED SOLUTION BY DOING THE FOLLOWING
```

```
C       STATEMENTS.(SAME FOR AK2K)
C       -----------------------------------------------------------------
   20 AK1K(I,J)=CSQRT((AM(I,J)+AN(I,J)+ANMX(I,J))/(3672.*B))
      IF (REAL(AK1K(I,J))-0.0) 30,30,40
   30 AK1K(I,J)=-(AK1K(I,J))
   40 AK2K(I,J)=CSQRT((AM(I,J)+AN(I,J)-ANMX(I,J))/2.)
      IF (REAL(AK2K(I,J))-0.0) 50,50,60
   50 AK2K(I,J)=-(AK2K(I,J))
   60 RN1EI(I,J)=(AM(I,J)-AN(I,J)+ANMX(I,J))/(2.*X(J))
      RN2EI(I,J)=(AM(I,J)-AN(I,J)-ANMX(I,J))/(2.*X(J))
      MOD1(I,J)=CABS(RN1EI(I,J))
      MOD2(I,J)=CABS(RN2EI(I,J))
    4 CONTINUE
    3 CONTINUE
      PRINT 100
      DO 5 I=1,6
      PRINT 200,I,A(I)
      DO 6 J=1,13
      PRINT 201,J,X(J),AM(I,J),AN(I,J),P(I,J),Q(J),ANMX(I,J)
    6 CONTINUE
    5 CONTINUE
      PRINT 100
      DO 7 I=1,6
      PRINT 200,I,A(I)
      DO 8 J=1,13
      PRINT 300,J,X(J),AK1K(I,J),AK2K(I,J)
    8 CONTINUE
    7 CONTINUE
      DO 9 I=1,6
      PRINT 202,I,A(I)
      DO 11 J=1,13
      PRINT 400,J,X(J),RN1EI(I,J),RN2EI(I,J),MOD1(I,J),MOD2(I,J)
   11 CONTINUE
    9 CONTINUE
  100 FORMAT(*1RESULTS*)
  200 FORMAT(1H0,*A(*,I1,*)=*,F7.3)
  201 FORMAT(3X,*X(*,I2,*)=*,E10.2,3X,*AM=*,E15.7,2X,E15.7,6X,
     1*AN=*,E15.7,2X,E15.7/
     214X,11H(AN-AM)**2=,E15.7,2X,E15.7,2X,7H4BX**2=,E15.7/
     320X,*ANMX=*,E15.7,2X,E15.7)
  202 FORMAT(1H1,*A(*,I1,*)=*,F7.3)
  300 FORMAT(1H ,10X,*X(*,I2,*)=*,E10.2,10X,
     1*AK1K=*,E15.7,2X,E15.7,10X,
     2*AK2K=*,E15.7,2X,E15.7)
  400 FORMAT(1H0,10X,*X(*,I2,*)=*,E10.2,10X,
     1*RN1EI=*,E15.7,2X,E15.7,10X,
     2*RN2EI=*,E15.7,2X,E15.7,/,
     337X,*MOD1 =*,E15.7,27X,*MOD2 =*,E15.7)
      END
```

APPENDIX C

TABLES OF DATA FOR THE CALCULATION OF RADIATION PATTERNS OF THE n_1 WAVE AND THE n_2 WAVE

Notations and constants used in this appendix:

$V_e = (3kT_e/m_e)^{\frac{1}{2}}$, thermal velocity of electrons.

$V_i = (3kT_i/m_i)^{\frac{1}{2}}$, thermal velocity of ions.

$V_A = [3k(T_e + T_i)/m_i]^{\frac{1}{2}}$, phase velocity of the n_1 wave at low frequency range.

$Re[k_1/(\omega/V_i)]$, numerical output of the computer.

$k_1 = \{Re[k_1/(\omega/V_i)]\}(\omega/V_i)$, phase constant of the n_1 wave.

$Re[k_2/(\omega/V_e)]$, numerical output of the computer.

$k_2 = \{Re[k_2/(\omega/V_e)]\}(\omega/V_e)$, phase constant of the n_2 wave.

$k_e \simeq \omega\sqrt{\mu_o\varepsilon_o}(1 - \omega_e^2/\omega^2)^{\frac{1}{2}}$, propagation constant of the electromagnetic wave in the plasma.

f = antenna frequency.

f_p = electron plasma frequency.

$\omega_e = 2\pi f_p$, circular electron plasma frequency.

$L = 2a/(V_{ph}/f)$, normalized antenna length.

$k = 1.38 \times 10^{-23}$ joules/^{0}K , Boltzmann's constant.

$m_e = 9.109 \times 10^{-31}$ kg , electron mass.

$m_i = 9.031 \times 10^{-26}$ kg , xenon ion mass.

Remark: A xenon gas plasma with $(\gamma_e/\omega) = 0$ is assumed for all cases in this appendix.

Table C-1 $k_1 dl$ versus T_e.
(f = 30 kHz, $Re[k_1/(\omega/V_i)]$ = 0.3016 for (T_e/T_i) = 10, dl = 1 cm)

T_e	$\frac{\omega}{V_i}$	k_1	$k_1 dl$
2000°K	623	188	1.88
6000°K	359	108	1.08
10000°K	278	84	0.84

Table C-2 $k_1 dl$ versus T_e/T_i.
(f = 30 kHz, T_e = 6000°K, dl = 1 cm)

$\frac{T_e}{T_i}$	$Re\left[\frac{k_1}{(\omega/V_i)}\right]$	$\frac{\omega}{V_i}$	k_1	$k_1 dl$
1	0.7071	114	80	0.80
10	0.3016	359	108	1.08
100	0.0995	1136	113	1.13
1000	0.0316	3594	114	1.14

Table C-3 $k_1 dl$ versus f.
(T_e = 6000^0K, $Re[k_1/(\omega/V_i)]$ = 0.3016 for (T_e/T_i) = 10, dl = 2.5 cm)

f	$\frac{\omega}{V_i}$	k_1	$k_1 dl$
10 kHz	120	36	0.9
20 kHz	240	72	1.8
30 kHz	360	108	2.7

Table C-4 $k_2 dl$ versus T_e.
(f = 1 GHz, $Re[k_2/(\omega/V_e)]$ = 0.2235 for (ω_e^2/ω^2) = 0.95 and (T_e/T_i) = 1 to 10^4, dl = 1 mm)

T_e	$\frac{\omega}{V_e}$	k_2	$k_2 dl$
2000^0K	2.08×10^4	4650	4.65
6000^0K	1.20×10^4	2690	2.69
10000^0K	9.32×10^3	2080	2.08

Table C-5 $k_2 dl$ versus f.
(T_e = 4000°K, $Re[k_2/(\omega/V_e)]$ = 0.2235 for (ω_e^2/ω^2) = 0.95 and (T_e/T_i) = 1 to 10^4, dl = 1 mm)

f	$\frac{\omega}{V_e}$	k_2	$k_2 dl$
0.5 GHz	7.37×10^3	1650	1.65
1.0 GHz	1.47×10^4	3290	3.29
1.5 GHz	2.21×10^4	4940	4.94

Table C-6 $k_1 a$ versus T_e.
(f = 30 kHz, $Re[k_1/(\omega/V_i)]$ = 0.0995 for (T_e/T_i) = 100, a = 2.25 cm)

T_e	V_A	$\frac{\omega}{V_i}$	k_1	$k_1 a$
2000°K	962	2000	199	4.48
6000°K	1666	1136	113	2.55
10000°K	2150	880	88	1.97

Table C-7 k_1a versus T_e/T_i. (f = 30 kHz, T_e = 2000°K, a = 2.25 cm)

$\frac{T_e}{T_i}$	$Re\left[\frac{k_1}{(\omega/V_i)}\right]$	V_A	$\frac{\omega}{V_i}$	k_1	k_1a
1	0.7071	1354	197	139	3.13
100	0.0995	962	1968	196	4.40
1000	0.0316	958	6225	197	4.43

Table C-9 k_2a versus T_e. (f = 17.5 MHz, λ = 13.1 cm, $Re[k_2/(\omega/V_e)]$ = 0.2235 for (ω_e^2/ω^2) = 0.95 and (T_e/T_i) = 1 to 10^4)

T_e	$\frac{\omega}{V_e}$	k_2	L = 0.6(λ)	L = 1.1(λ)
			k_2a	k_2a
2000°K	365	81.5	3.18	5.87
4000°K	257	57.6	2.25	4.15
6000°K	211	47.0	1.84	3.39

Table C-8 k_1a versus f.
(V_A = 1.05 x 10^3 m/sec, $T_e = T_i \simeq 1200^0$K, Re$[k_1/(\omega/V_i)]$ = 0.7071 for (T_e/T_i) = 1, a = 2.25 cm)

f	L	$\frac{\omega}{V_i}$	k_1	k_1a
16.3 kHz	0.7	138	98	2.2
23.3 kHz	1.0	198	152	3.4
58.3 kHz	2.5	494	349	7.8

Table C-10 k_1a versus T_e.
(f = 30 kHz, Re$[k_1/(\omega/V_i)]$ = 0.3016 for (T_e/T_i) = 10, a = 2.25 cm)

T_e	V_A	$\frac{\omega}{V_i}$	k_1	k_1a
2000^0K	1004	623	188	4.22
6000^0K	1739	359	108	2.44
10000^0K	2245	278	84	1.89

Table C-11 k_1a versus T_e/T_i.
(f = 30 kHz, T_e = 4000°K, a = 2.25 cm)

$\frac{T_e}{T_i}$	$Re\left[\frac{k_1}{(\omega/V_i)}\right]$	$\frac{\omega}{V_i}$	k_1	k_1a
1	0.7071	139	98.4	2.21
10	0.3016	440	133.0	2.99
100	0.0995	139	139.0	3.12

Table C-12 k_1a versus f.
($V_A = 1.05 \times 10^3$ m/sec, $T_e = T_i \approx 1200$°K, $Re[k_1/(\omega/V_i)]$ = 0.7071 for $(T_e/T_i) = 1$, a = 2.25 cm)

f	L	$\frac{\omega}{V_i}$	k_1	k_1a
35.0 kHz	1.5	297	210	4.72
46.6 kHz	2.0	395	279	6.28
93.3 kHz	4.0	790	559	12.60

Table C-13 k_2a versus T_e.
(f = 17.5 MHz, $Re[k_2/(\omega/V_e)] = 0.2235$ for $(\omega_e{}^2/\omega^2) = 0.95$ and $(T_e/T_i) = 1$ to 10^4, a = 7.2 cm)

T_e	$\frac{\omega}{V_e}$	k_2	k_2a
2000 °K	365	81.5	5.87
4000 °K	257	57.6	4.15
8000 °K	182	40.8	2.94

Table C-14 k_2a versus f.
(T_e = 2000 °K, $Re[k_2/(\omega/V_e)] = 0.2235$ for $(\omega_e{}^2/\omega^2) = 0.95$ and $(T_e/T_i) = 1$ to 10^4, a = 7.2 cm)

f	$\frac{\omega}{V_e}$	k_2	k_2a
15.0 MHz	313	69.8	5.03
17.5 MHz	365	81.5	5.87
20.0 MHz	417	93.2	6.71

Table C-15 k_1h versus T_e.
(f = 30 kHz, $Re[k_1/(\omega/V_i)] = 0.3016$ for $(T_e/T_i) = 10$)

T_e	$\frac{\omega}{V_i}$	k_1	k_1h	
			h = 2.5 cm	h = 5 cm
2000°K	623	188	4.7	9.4
6000°K	359	108	2.7	5.4
10000°K	278	84	2.1	4.2

Table C-17 k_1h versus f.
(T_e = 6000°K, $Re[k_1/(\omega/V_i)] = 0.3016$ for $(T_e/T_i) = 10$,
h = 5 cm)

f	$\frac{\omega}{V_i}$	k_1	k_1h
10 kHz	120	36	1.8
20 kHz	240	72	3.6
30 kHz	360	108	5.4

Table C-16 k_1h versus T_e/T_i. ($f = 30$ kHz, $T_e = 6000^{\circ}$K)

$\frac{T_e}{T_i}$	$\mathrm{Re}\left[\frac{k_1}{(\omega/V_i)}\right]$	$\frac{\omega}{V_i}$	k_1	k_1h	
				h = 2.5 cm	h = 5 cm
1	0.7071	114	80	2.0	4.0
10	0.3016	359	108	2.7	5.4

Table C-18 k_2h and k_e/k_2 versus T_e.
($f = 5.5$ MHz, $f_p = 4.5$ MHz, $(T_e/T_i) = 1$ to 10^4, $Re[k_2/(\omega/V_e)] \simeq 0.57$ and $k_e \simeq 0.066$ for $(\omega_e^2/\omega^2) = 0.67$, $h = 6$ cm)

T_e	$\frac{\omega}{V_e}$	k_2	$\frac{k_e}{k_2}$	k_2h
4000°K	81.0	46.1	0.00143	2.70
6000°K	66.2	37.7	0.00176	2.26
8000°K	57.3	32.6	0.00203	1.95

Table C-21 k_eh versus f.
($f_p = 4.5$ MHz, $h = 8.5$ cm)

f	$\frac{\omega_e^2}{\omega^2}$	k_e	k_eh
5.0 MHz	0.81	0.046	0.0039
5.5 MHz	0.67	0.066	0.0056
7.0 MHz	0.41	0.113	0.0096

Table C-19 k_2h and k_e/k_2 versus f. ($T_e = 6000^0$K, $(T_e/T_i) = 1$ to 10^4, $f_p = 4.5$ MHz, h = 8.5 cm)

f	$\frac{\omega_e^2}{\omega^2}$	$\mathrm{Re}\left[\frac{k_2}{(\omega/V_e)}\right]$	$\frac{\omega}{V_e}$	k_e	k_2	$\frac{k_e}{k_2}$	k_2h
5.0 MHz	0.81	0.43	60.1	0.04564	25.8	0.00177	2.19
5.5 MHz	0.67	0.57	66.2	0.06617	37.7	0.00176	3.20
7.0 MHz	0.41	0.76	84.2	0.11260	63.9	0.00176	5.44

Table C-20 k_2h and k_e/k_2 versus f. ($T_e = 5150^0$K, $(T_e/T_i) = 1$ to 10^4, $f_p = 4.5$ MHz)

f	$\mathrm{Re}\left[\frac{k_2}{(\omega/V_e)}\right]$	$\frac{\omega}{V_e}$	k_e	k_2	$\frac{k_e}{k_2}$	k_2h	
						h = 6 cm	h = 8.5 cm
5.5 MHz	0.57	71.4	0.06617	40.7	0.00163	2.44	3.46
7.0 MHz	0.76	90.9	0.11260	69.1	0.00163	—	5.87

Sample Program

```
      PROGRAM PLASMA (OUTPUT)
C
C     ******************************************************
C     THIS PROGRAM CALCULATES THE RADIATION PATTERNS OF THE
C     N2 WAVE EXCITED BY A CYLINDRICAL ANTENNA.
C     RADPAT=COS(THETAR)*(COS(K2*H*COS(THETAR))-COS(KE*H))/
C     ((COS(THETAR))**2-(KE/K2)**2)
C      WE LET P=K2*H, B=KE*H, C=KE/K2.
C     ******************************************************
C
      DIMENSION THETA(20),THETAR(20),P(5),A(5),B(5),C(5)
      P(1)=1.95
      P(2)=2.26
      P(3)=2.70
      P(4)=3.20
      B(1)=0.00396
      B(2)=0.00388
      B(3)=B(1)
      B(4)=0.00562
      C(1)=0.00203
      C(2)=0.00176
      C(3)=0.00143
      C(4)=C(2)
      PI=3.14159265
      DO 2 J=1,4
      PRINT 100
      PRINT 101,J,P(J)
      DO 1 I=1,19
      THETA(I)=-100.+10.*I
      PRINT 200,I,THETA(I)
      THETAR(I)=(PI/180.)*THETA(I)
      A(J)=P(J)*COS(THETAR(I))
      RADPAT=COS(THETAR(I))*(COS(A(J))-COS(B(J)))/
     1((COS(THETAR(I)))**2-C(J)**2)
      PRINT 300,RADPAT
    1 CONTINUE
    2 CONTINUE
  100 FORMAT(*1RESULTS*)
  101 FORMAT(*0*,5X,*CASE(*,I2,*)*,2X,6HK2*H =,E15.7)
  200 FORMAT(* *,5X,*THETA(*,I2,*)=*,F6.1,* DEGREE*)
  300 FORMAT(*+*,33X,*RADPAT=*,E15.7)
      END
```

REFERENCES

REFERENCES

1. M. H. Cohen, "Radiation in a plasma, III, metal boundaries," Phys. Rev., Vol. 126, 2, 398, (1962).

2. A. Hessel and J. Shmoys, "Excitation of plasma waves by a dipole in a homogeneous isotropic plasma," Proceedings of the Symposium on Electromagnetics and Fluid Dynamics of Gaseous Plasma, Interscience, 173, (1961).

3. H. H. Kuehl, "Excitation of waves in a warm plasma by a current source," Phys. Fluids, Vol. 6, 10, 1465, (1963).

4. P. J. Barrett and P. F. Little, "Externally excited waves in low-pressure plasma columns," Phys. Rev. Letters, Vol. 14, 356, (1965).

5. W. D. Jones and I. Alexeff, "A study of the properties of ionic sound waves," Proc. Seventh Int. Conf. Phenomena in Ioniz. Gases, Vol. 2, 330, (1965).

6. I. Alexeff and W. D. Jones, "Collisionless ion-wave propagation and the determination of the compression coefficient of plasma electrons," Phys. Rev. Letters, Vol. 15, 7, 286, (1965).

7. J. H. Malmberg and C. B. Wharton, "Dispersion of electron plasma wave," Phys. Rev. Letters, Vol. 17, 175, (1966).

8. K. M. Chen, H. Judson and C. C. Lin, "Experimental study of an electroacoustic wave excited by an antenna in a hot plasma," Proc. IEEE Vol. 55, 1656, (1967).

9. H. Doucet, "Propagation d'ondes ioniques excitées en impulsion dans des gaz rares ionisés," J. Phys. Vol. 28, 973, (1967).

10. I. Alexeff, W. D. Jones and K. Lonngren, "Excitation of pseudowaves in a plasma via a grid," Phys. Rev. Letters, Vol. 21, 13, 878, (1968).

11. I. Alexeff, W. D. Jones and D. Montgomery, "Effects of electron-temperature variation on ionacoustic waves," Phys. Fluids, Vol. 11, 1, 167, (1968).

12. Y. Nakamura, M. Nakamura and T. Itoh, "Reception characteristics of monopole antennas for electron plasma waves," IEEE Trans. Plasma Sci., Vol. PS-1, 100, (1973).

13. T. Ishizone, K. Sawaya, S. Adachi and Y. Mushiake, "Measurements of the transmitting and the receiving patterns of a dipole antenna for an electron plasma wave," Private communication, to be published in IEEE Trans. on Ants. and Prop.

14. K. Shen, S. Aksornkitti, H. C. S. Hsuan and K. E. Lonngren, "Radiation characteristics of longitudinal waves from an antenna in a plasma," Radio Sci. (New Series), Vol. 5, 611, (1970).

15. S. K. Majumdar, "Electrodynamics of a charged particle moving through a plasma without magnetic field," Proc. Phys. Soc. (London), Vol. 76, 657, (1960).

16. S. R. Seshadri, "Excitation of plasma waves in an unbounded homogeneous plasma by a line source," IEEE Trans. on Microwave Theory and Techniques, Vol. MTT-11, 39, (1963).

17. S. R. Seshadri, "Radiation from electromagnetic sources in a plasma," IEEE PGAP, Vol. 13, 79, (1965).

18. G. Maxam and K. M. Chen, "Effects of pseudosonic and electroacoustic waves on the radiation of a plasma-coated spherical antenna," Radio Science, Vol. 7, 979, (1972).

19. L. Tonks and I. Langmuir, "Oscillations in ionized gases," Phys. Rev., Vol. 33, 2, 195, (1929).

20. A. Dattner, "Resonance densities in a cylindrical plasma column," Phys. Rev. Letters, Vol. 10, 205, (1963).

21. F. W. Crowford, "Internal resonances of a discharge column," J. Appl. Phys., Vol. 35, 5, 1365, (1964).

22. J. V. Parker, J. C. Niçkel and R. W. Gould, "Resonance oscillations in a hot non-uniform plasma," Phys. Fluids, Vol. 7, 1489, (1964).

23. P. E. Vandenplas, "Electron waves and resonances in bounded plasmas," Interscience Publishers, New York, (1968).

24. M. Tutter, "Transmission measurements of electrostatic plasma waves in the GHz frequency range," Plasma Physics Vol. 10, 775, (1968).

25. G. Van Hoven, "Observation of plasma oscillations," Phys. Rev. Letters, Vol. 17, 4, 169, (1966).

26. H. Derfler and T. C. Simonen, "Landau waves: an experimental fact," Phys. Rev. Letters, Vol. 17, 4, 172, (1966).

27. P. P. Golddan and E. J. Yadlowsky, "Plasma resonance and standing longitudinal electron waves," Phys. Fluids, Vol. 14, 9, 1990, (1971).

28. D. E. Baldwin, "Kinetic model of Tonk-Dattner resonances in plasma columns," Phys. Fluids, Vol. 12, 279, (1969).

29. K. J. Parbhakar and B. C. Gregory, "Direct measurements of dipole radial electric fields in a resonating plasma column," Phys. Fluids, Vol. 14, 9, 1984, (1971).

30. S. R. Seshadri, "Propagation coefficients for the current distribution along a cylindrical antenna immersed in a warm plasma," Proceedings of IEEE (London), Vol. 112, 877, (1965).

31. A. D. Wunsch, "Current distribution on a dipole antenna in a warm plasma," Electronics Letters, Vol. 3, 320, (1967).

32. H. Judson and K. M. Chen, "Measurement of antenna current distribution in a hot plasma," Proceedings of IEEE, Vol. 56, 4, 753, (1968).

33. H. Judson, K. M. Chen and R. Lundquist, "Measurement of the current distribution on monopoles in a large volume of hot plasma," Electronics Letters, Vol. 4, 14, 289, (1968).

34. T. Ishizone, K. Taira, S. Adachi and Y. Mushiake, "Sheath effects on the current distribution along an antenna in a plasma," IEEE Trans. Ants. and Prop.(Commun.), Vol. AP-17, 398, (1968).